UiT The Arctic University of Norway

**Department of Arctic and Marine Biology**

# Turbid Arctic Coastal Waters: Potential Hotspots for Primary Productivity

Riverine Influence on Microbial Productivity in high Arctic Fjords

**Sebastian D.J. Andersen**

**Master's thesis, BIO-3950, May 2022**

*Cover photo: The river plume in Adventfjorden, Svalbard, during August of 2021. The plume can be seen as a highly turbid, brown watermass. A mixing zone of  greenish water is bordering the plume.*

# Turbid Arctic Coastal Waters
# Potential Hotspots for Primary Productivity

*Riverine Influence on Microbial Productivity in high Arctic Fjords*

**Master's thesis in Arctic Marine Ecology and Resource Biology**
**by**
**Sebastian David Junker Andersen**

**Supervisors**

**Amanda Poste**[1,2]
**Rolf R. Gradinger**[1]
**Janne E. Søreide**[3]
**Tobias R. Vonnahme**[4]

Advisors

Johnna M. Holding[5]
Eva Falck[6]

Collaborators

Maeve McGorvern[1,2]
Eleanor R. Handler[1,3]

Associations
[1] Institute for Arctic and Marine Biology, UiT – The Arctic University of Norway, Tromsø, Norway
[2] Norwegian Institute of Water Research (NIVA), Oslo, Norway
[3] Department of Arctic Biology, The University Centre in Svalbard (UNIS), Svalbard, Norway
[4] Department of Greenland Climate Research Centre, Greenland Institute of Natural resources, Nuuk, Greenland
[5] Arctic Research Centre, Aarhus University, Aarhus, Denmark
[6] Department of Arctic Geophysics, The University Centre in Svalbard (UNIS), Svalbard, Norway

# Acknowledgements

The first and greatest gratitude goes to my team of supervisors. Thank you, Amanda Poste, for giving me the opportunity to write this thesis and for the endless supervision and support you've provided through chaos, and calm. Thank you, Rolf Gradinger, for being there in times of need and for orchestrating this master(s)piece. Thank you, Janne Søreide, for always being there when rope hit the propeller (metaphorically and literally). Thank you, Tobias Vonnahme, for your invaluable teachings and for your radiating drive.

Thanks also to Johnna Holding for sharing advice, experience and thoughts on the main methodologies used in this thesis, and to Eva Falck, for training me and lending me equipment for everything Winkler-related. Your help and support have been crucial.

This thesis would also not have been possible without the preceding work done by Maeve McGovern which truly paved the way for this project.

And of course: immense gratitude goes to Ellie Handler. Thank you for joining me on this marathon (one year sprint), for dragging me out of (and into) the mud, and for being a wonderful partner in crime through long days in field, late nights in the lab and deep R pits of despair. I wouldn't have made it without you.

A long list of people helped to pull off this thesis, and some deserve extra gratitude:

First, cheers to the absolute killer team of field and lab assistants: Lady Florina Roana Schalamon Hillesheim of Glencoe, Marjolein Gievers, Astrid Vikingstad, Ymke Lathouwers, Juha Sørensen, Nil Rodés, and of course to Maria Dance for last second help with thesis revision. You helped to lay the foundation for the results in this thesis.

Secondly, eternal gratitude to Erwin Kers for salvaging and dealing with the sample chaos that landed on his desk – you are a savior.

A huge thanks also goes to Stuart Thomson, lab technician at UNIS, for helping with setup of instruments, preparing chemicals, sorting lab infrastructure, ordering consumables and always being available when needed.

In addition, thanks to the boat operator team and engineers at tech and logistics at UNIS for making field work possible and for constructing essential parts of the incubation rigs used in this project, and to the HIDEX team for providing hardware, software and crucial support for analyses.

Last, thanks to family and friends, and especially Laura Madsen, for supporting me all the way through a much longer and more difficult journey than expected.

Of course, many more people have provided valuable tips and advice and shared ideas and thoughts, and to all who have had a role to play, whether mayor or minor, I thank you deeply.

This research was supported with funding by the Fram Center Flagship "Fjord and Coast" grant (FreshFate; project number 132019), the Norwegian Research Council, (TerrACE; project number: 268458) and the Svalbard Science Forum's Arctic Field Grant (RIS number: 11392).

# Abbreviations

| | |
|---|---|
| BP | Bacterial Production |
| Chl *a* | Chlorophyll *a* |
| CR | Community Respiration |
| DOC | Dissolved Organic Carbon |
| DOM | Dissolved Organic Matter |
| DPM | Disintegrations Per Minute |
| GCP | Gross Community Production |
| LSC | Liquid Scintillation Counter/C |
| MB | Metabolic Balance, given as GCP:CR (oxygen production:respiration) |
| NCP | Net Community Production |
| NPP | Net Primary Production |
| NPP:BP | Autotrophic:Bacterial production ratio (in biomass carbon) |
| $NPP_B$ | Biomass specific NPP, as NPP / Chl *a* |
| PP | Primary Production |
| SPM | Suspended Particulate Matter |
| TDCR | Triple-Double Coincidence Ratio |

# Table of Contents

# 1. Abstract

The coastal domain of the Arctic is in rapid change with shifts in discharge phenology and catchment characteristics. Riverine discharge shapes hydrography, under water light climate, and nutrient dynamics during the brief melt season. Nutrients transported from catchment to coast can stimulate primary productivity, yet light attenuation caused by high surface turbidity is considered a limiting factor. This in turn affects the relative role of bacterial growth, with subsequent changes to carbon and metabolic balances. However, the effect of nutrient versus light availability on microbial growth remains understudied.

The main goal of this master's thesis was to **assess the impact of riverine inputs on bacterial and primary production in a High Arctic Fjord Estuary.** A full melt season study (May to September) was conducted in Adventfjorden, Svalbard, with samples collected across horizontal and vertical salinity and turbidity gradients. Microbial productivity was measured using *in vitro* incubations for net primary productivity (NPP) and bacterial production (BP), using the $^{14}$C-bicarbonate and $^{3}$H-methyl-thymidine incorporation essay methods. I paired this with *in situ* estimations of system metabolic balance (gross community production (GCP) versus community respiration (CR)) over a 24h incubation period.

I found that NPP had the potential of exceeding BP by 100 to ~2800 times in freshwater influenced fjord waters, which was up to 3 times higher than the saline fjord max. Light had a strong impact on system metabolic balance, yet the system was net autotrophic even under low light conditions.

River influenced areas in Arctic fjords are potential hotspots for high, sustained primary productivity during the melt season, challenging previous consensus. This has implications for our general understanding of nutrient cycling and carbon balances in the Arctic.

# 2. Introduction

## 2.1 Coastal Domains in a Changing World

The coastal domain is one of the most dynamic environments on Earth. It is the boundary of land-ocean interactions, forming a system of complex hydrological, biogeochemical and ecological interactions that affects global carbon cycles from the tropics to the poles (Rachold et al., 2005; Deininger & Friegstad, 2019). Coasts support life across all trophic levels and are important regions for human civilizations from large cities to indigenous communities (Martínez et al., 2007; Meredith et al., 2019). However, they are also at the heart of global changes, as they are directly affected by increased anthropogenic activities, climate changes, and ecological restructuring both at sea and on land. Yet, coastal systems remain poorly understood but have become of increasing interest as their role in global carbon cycling has been elucidated over the past decades. (Bauer et al. 2013, Ward. 2017, Duarte 2020).

## 2.2 The Impact of Freshwater in the Arctic

The Arctic Ocean (AO) is one of the areas in the world most extremely influenced by its surrounding coasts. It is bordered by ~1/3 of the world's coastline and receives approximately 11% of the world's freshwater discharge. Yet, it is a quite small ocean, containing only 1% of the global ocean volume (Lantuit et al., 2012; Carmack et al., 2016; Wassman et al., 2020).

Freshwater input to the Artic is highly seasonally regulated, being confined mainly to the Arctic half year of light from April-September. During the melt season, freshwater is shaping hydrological, biogeochemical, and ecological processes across the land-ocean continuum of the AO (Wrona et al., 2016; Bianchi et al., 2020).

Freshwater discharge causes strong stratification upon contact with marine water. This creates conservative mixing, keeping the freshwater inputs suspended in the top water masses. Sustained discharge will drive estuarine circulation, which brings in saline waters from outer and deeper water masses (Bianchi et al., 2020). This causes freshwater plumes to form, which can be very heterogenous across both space and time, changing in thickness and extend (Osadchiev et al., 2020, McGovern et al., 2020). In addition, the associated large amount of terrestrial matter in the surface, causes high surface turbidity regions extending from the discharge endpoint. These turbid waters absorb heat, causing the plume to often be several degrees warmer than the surrounding saline waters (Mulligan & Perrie, 2019). In addition to regulating plume extend, displacement of opposing water masses, tidal forcing, and wind stress causes shearing between the water masses forming zones of brackish mixing layers around the plume. (Scully et al., 2005; McClelland et al., 2012).

However, the most striking effect of these freshwater plumes is the profound impact on light availability that can cause partial or full shading of the water column. This in turn affects the primary producers at the base of the food web, in both the pelagic and benthic environment, which has led to a (not unreasonable) consensus that areas of high surface turbidity are areas of low primary productivity (Carmack et al. 2016; Halbach et al., 2019; Bauer et al., 2013; Lund-Hansen et al., 2010; Bhatia et al., 2021, Pavlov et al., 2019). However, discharge from land is not only bringing darkness, but can also be a source of particulate and dissolved inorganic and organic nutrients that can become available for pelagic and benthic microbial production (Vonnahme et al., 2021; Ward et al., 2017; Nowak & Hodson., 2015; McGovern et al., 2020; Paulsen et al., 2017; Deininger & Friedstad 2019).

On the way from catchment to coast both dissolved and particulate matter can be altered through biogeochemical processing (Cole et al. 2007), flocculation (Meslard et al., 2018), and photochemical degradation (Smith & Benner 2005), which affects the final quantity and quality (bioavailability) of nutrients available for the marine system (Carmack et al., 2016). In addition to the nutrients supplied by the freshwater discharge, estuarine circulation can cause upwelling of benthic matter, resupplying the pelagic system with settled matter, as well as bring in biota from the marine environment (Wainright, 1990; Bianchi et al., 2020).

This forms a complex and dynamic environment where nutrients, hydrology and light can have local effects on the microbial community, which in turn affects the whole marine ecosystem.

### 2.3 The Importance of Smaller Freshwater Systems

Of the total freshwater delivered to the AO, ~60% is supplied by the "Big 6" riverine systems: Mackenzie, Lena, Yenisey, Ob, Yukon, and Kolyma (Carmack 2000). However, this leaves ~40% of the remaining discharge to be covered by larger and smaller freshwater systems. These systems are diverse and include ice and tidewater glacial melt, riverine systems fed by land terminating glaciers and permafrost, the annual melt of snow and ice and summer precipitation (Lique et al., 2016; Hansen-Bauer et al., 2019; Carmack et al., 2016) (Fig. 1). These are some of the most vulnerable systems in a warming climate, yet also some of the most understudied in terms of their role in regulating microbial processes and carbon balances. Understanding these smaller systems and their role in biogeochemical cycling and

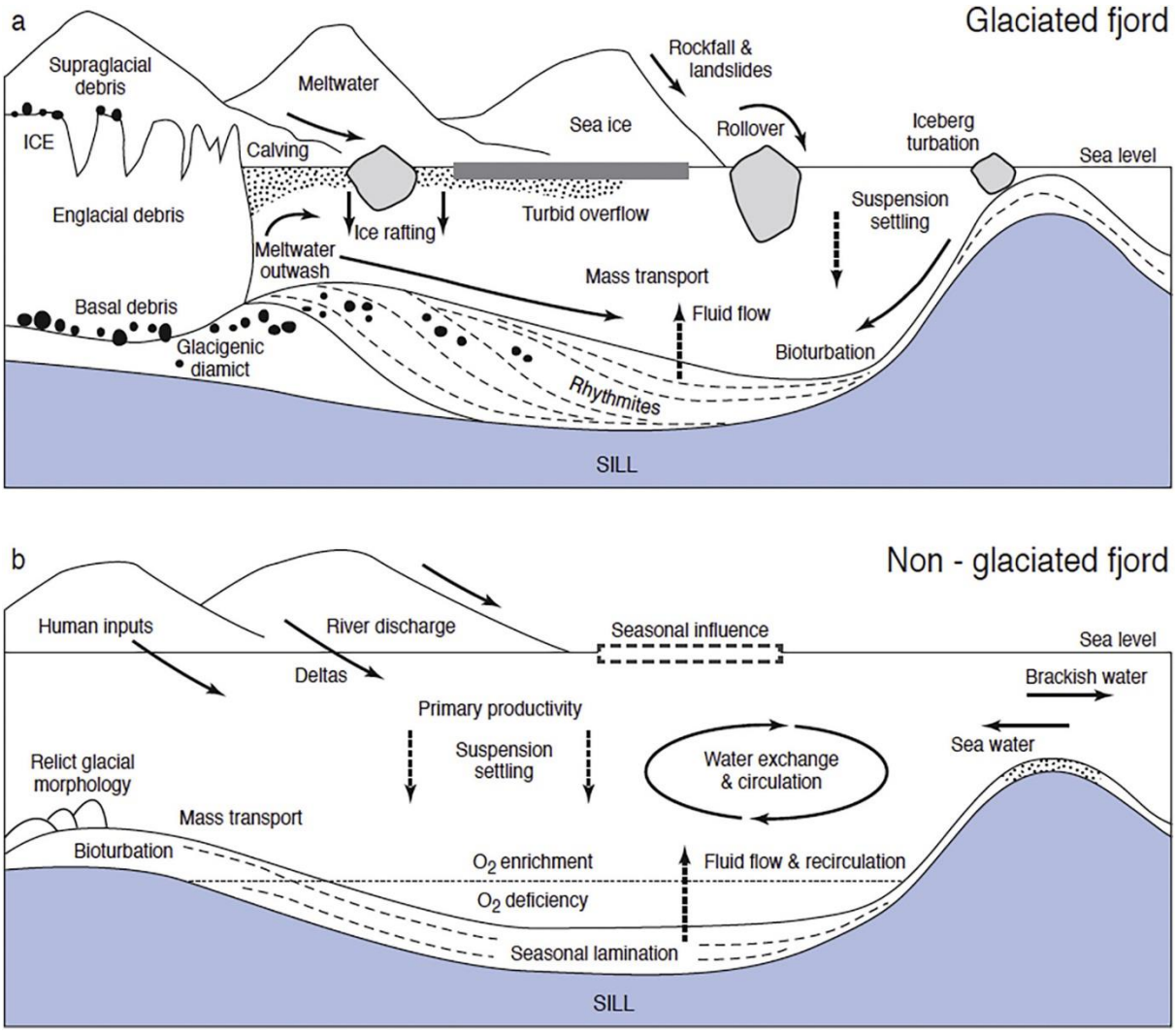


**Fig. 1:** A conceptual illustration of two common land-discharge systems (in fjords) and the hydrological and sedimentary processes taking place during the melt season. **a)** a glaciated fjord, and **b**) a non-glaciated sword. Estuarine circulation. (*source: Bianchi et al. 2020*)

how they affect food web structures, are therefore crucial if we want to understand how changes to freshwater sources and dynamics in a changing climate will affect coastal productivity of the Arctic.

One area of the Arctic dominated by smaller freshwater systems is Svalbard, Norway. Svalbard is undergoing rapid changes due to Atlantification, glacier and sea ice loss, permafrost melt and changes in annual precipitation patterns (Hanssen-Bauer et al. 2019).

Freshwater discharge in Svalbard is confined to the summer months from June – September (Hodson et al., 2016; McGovern et al., 2020; Dunse et al., 2022) where plumes can be observed from satellite imagery along the coast of the entire Svalbard archipelago (Søreide et al. 2021). The high latitude constrains overall seasonal light availability due to changes in sun angle, which can be limited even further by the shading from the surrounding topography (Bianchi et al. 2020).

Recent progress has been made by McGovern et al. 2020, in trying to characterize the input and fate of terrestrially derived matter in western Svalbard fjords (Isfjorden and associated estuaries). They observed strong seasonal changes in discharge dynamic related to the main melt source (Fig 2). High amounts of cDOM (colored dissolved organic matter), SPM (suspended particulate matter) and DOC (dissolved organic carbon) was characteristic for the early season associated with snow melt. This shifted to a late season system characterized by high concentrations of inorganic nutrients from glacial melt.

High DOC concentrations and land-ocean fluxes have been observed for several Arctic systems (Giesler et al., 2014; Osterholz et al., 2014; Csank et al., 2019; Kaste et al., 2022) as has the importance of glacial discharge for supplying inorganic nutrients and trace metals, (Hodson et al., 2016; Vonnahme et al., 2021).

In conjunction with impacts of freshwater inputs to Isfjorden's coastal waters observed by McGovern, it was found by  Delpech et al. (2021) that the bacterial community of the pelagic also changed temporally and spatially related to freshwater influence.

However, little effort has been made in trying to understand the fate of this transported matter on microbial production in Svalbard, and a remaining question is to which extend matter transported from land to sea is affecting microbial production. McGovern et al. (2020) hypothesized, that the light attenuation and warmer, fresher waters could give bacteria a competitive advantage for nutrients, causing areas of high surface turbidity to be heterotrophic. Yet, they also theorized, that in areas where light is adequate (i.e., the plume fronts) the high supply of nutrients could be stimulating primary production.

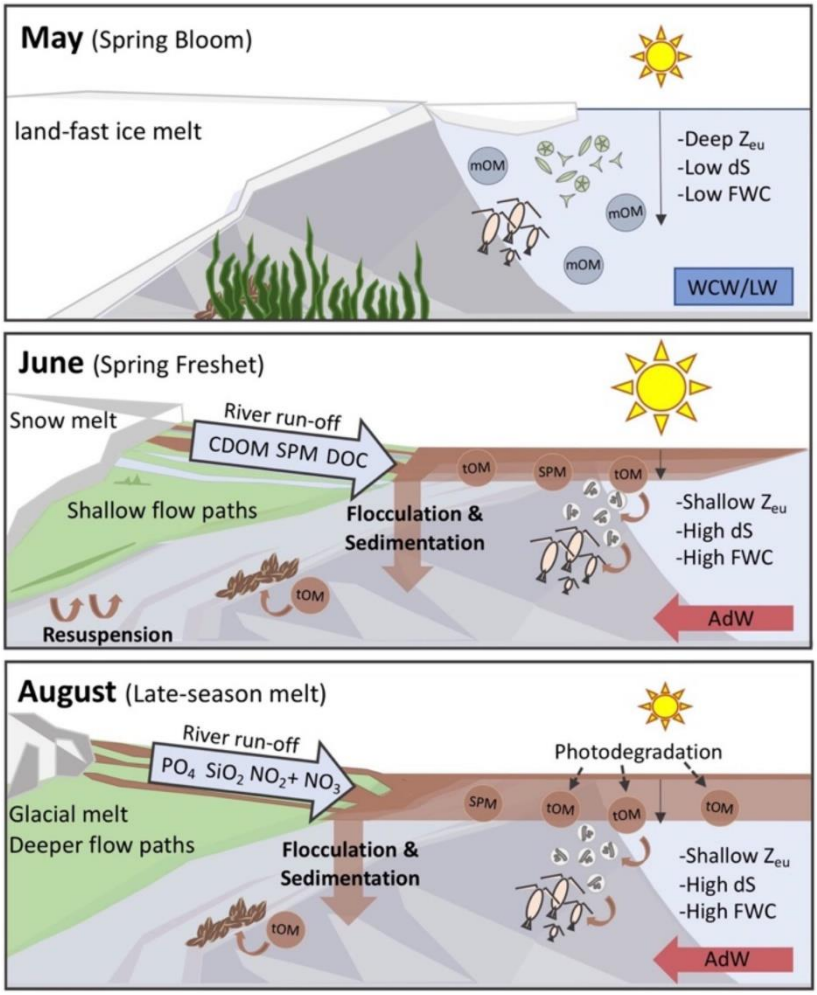


**Fig. 2:** Illustration of the seasonal development in the discharge system of a coastal catchment based on results from Mcgovern et al. 2020. In May, the inner fjord and land is covered in snow and ice, with the fjord showing high marine OM (mOM) due to the spring bloom, and a deep photic zone ($Z_{eu}$). During the freshet (June), large amounts of DOC, cDOM and SPM is flushed into the marine system, causing a strong stratification (dS) and a substantial plume with subsequent low photic zone depth and high freshwater content (FWC). In the late season of August, High inorganic nutrietns are supplied to the fjord, and the plume is rich in terrestrial OM (tOM). (*source: McGovern et al., 2020*).

## 2.4 Microbial Productivity in Pelagic Systems

Primary production (PP) rates in the Arctic varies greatly between environment, season and area, ranging from <1 to >450mgC $m^{-2}$ $d^{-1}$ in sea ice during under ice blooms, (Leu et al., 2015), to 42.6mgC $m^{-2}$ $d^{-1}$ at glacial terminus (Vonnahme et al., 2021), to 30 – 1850mgC $m^{-2}$ $d^{-1}$ during spring bloom in Kongsfjorden, Svalbard (Hodal et al., 2012), up to 2078mgC $m^{-2}$ $d^{-1}$ during summer in Hornsund, Svalbard (Smola el al., 2017), to >500mgC $m^{-2}$ $d^{-1}$ just after ice melt in the Beufort sea (Lavoie et al., 2009), to 50-200mgC $m^{-2}$ $d^{-1}$ during summer in Young Sound, Greenland (Holding et al., 2019). Spring blooms are dominated by Diatoms, but communities shifts towards different groups of flagellates towards summer (Leu et al. 2015). In general, primary production in the Arctic are constrained by macronutrients, often nitrate and silicate (Randelhoff et al., 2020), and light (Leu et al., 2015).

Bacterial production (BP) is generally lower than PP, but is not limited to growth during the light season. In Franklin Bay, Canada, bacterial production has been estimated to be 1 – 80mgC $m^{-2}$ $d^{-1}$ (Garneau et al, 2008), in the open Arctic Ocean 0.1 – 250mgC $m^{-2}$ $d^{-1}$ (Rich et al 1997), 0.8-130mgC $m^{-2}$ $d^{-1}$ in sea ice (Søgaard et al, 2010; Piontek et al. 2021) and 16 – 151mgC $m^{-2}$ $d^{-1}$ along a freshwater to marine gradient in the Mckenzie system (Vallières et al., 2008).

The ratio between bacterial production (BP) and primary production (PP) can be used as an estimate for system carbon balance (Ameryk et al. 2005). PP is the amount of new, autotrophically generated carbon (dissolved inorganic carbon (DIC) incorporated to particulate organic carbon (POC)), and BP is the amount of heterotrophically regenerated carbon (transformation of organic carbon (OC), generating DIC). PP:BP ratio informs about

the relative new versus regenerated growth, where a system with a PP:BP > 1 will be net autotrophic and act as a carbon sink (Holding et al., 2017).

A well-established method for measuring microbial productivity (amount of carbon assimilated into biomass) is to measure the uptake of low-energy radioactively labelled substrates during growth experiments (Blum & Mills, 2012). Two of the most common tracer substrates are $^{3}$H-methyl-thymidine (used only by prokaryotes during growth) and $^{14}$C-bicarbonate (taken up by photoautotrophs during photosynthesis), (Hodal 2012; Leu et al 2015; Holding et al., 2019). $^{3}$H-methyl-thymidine, (although also used by archaea) is used to estimate bacterial production (BP) and $^{14}$C-bicarbonate is used to measure primary production (PP).

In addition to carbon balance, system metabolic balance (oxygen production versus respiration) can also be used to assess whether a system community is net autotrophic (inorganic carbon sink through photosynthesis) or heterotrophic (inorganic carbon source through respiration) (Testa et al., 2012). The method can be used to compare net community oxygen production (NCP, net oxygen production after respiration) (in light bottles), and community respiration (CR, respiration only) (in dark bottles). Assuming equal respiration in light and dark treatments, gross community production (GCP, the total oxygen produced) can be inferred as NCP + CR, which can then be used to calculate the system metabolic balance (MB) as the ration between $O_2$ production and respiration (MB = GCP/CR) (Holding et al. 2013). A system with MB > 1 is net autotrophic, while a system with MB < 1 is net heterotrophic. System metabolic balance can vary substantially across space and time, and a previous study by Cottrell et al. 2006 (a quite comprehensive study for the Arctic Ocean)

suggested that metabolic balance is controlled by localized areas of net production, whereas respiration is more uniform.

Combined, carbon production and metabolic balance get at two different but related questions: what is the balance between primary and bacterial production (is PP:BP > 1)? And is the system an overall carbon sink MB (> 1) or source (MB < 1)?

Due to the nature of the tracers used in estimating PP and BP being radioactive, *in situ* experiments are problematic and *in vitro* or *in situ-like* incubations are therefore commonly used. Consequently, the measurements indicate the *potential* productivity in the inherent sample environment when subjected to the incubation conditions. In short, this method is *targeted*, and *tests inherent potential productivity* in an *artificial environment*.

Production measured through metabolic balance is well suited for *in situ* incubations and gives insights into *realized* productivity dynamics given changes in the surrounding environment. However, it is hard to target specific groups of organisms and *in situ* incubations can be logistically challenging. In addition, the results gathered can be hard to compare due to the natural variation in the incubation environment and changes to the community composition. In summary, this method is *general and unspecific,* but *tests the realized environmental effect on productivity dynamics.*

## 2.5 Project goals

In this project, my main goal was to **assess the impact of riverine inputs on bacterial and primary production in a High Arctic Fjord Estuary.**

This was achieved by collecting samples from a river to fjord gradient across multiple depths, to cover salinity and light gradients. Samples were collected monthly from May through September to cover the pre-melt conditions and full melt season. In addition, I acquired high frequency data on the development of physicochemical conditions of the river system to better understand the impact of freshwater inputs on the marine endpoint.
I hypothesized that:

1) River inputs are associated with net heterotrophy, especially in the inner fjord where light is strongly limiting,

and, that:

2) where sufficient light is available, riverine nutrients can have a positive effect on coastal PP

# 3. Materials and Methods

## 3.1. Study Site

Sampling took place from May through September 2021 in Adventfjorden and Adventelva on Svalbard (78.23'N;15.70'E). Adventfjorden is a smaller sub-fjord estuary in the larger Isfjorden complex on the western side of Spitsbergen (Fig. 3 A). The depth of the fjord ranges from < 1m in the tidal flats to 100-150m in the outer fjord (Fig. 3 B). Freshwater is delivered to the fjord via two main rivers (Adventelva and Longyearelva), but the fjord is also influenced by the nearby Bjørndalselva (Fig. 3 A). The catchment of the largest river, Adventelva, is ~694km$^{-2}$ and fed mostly by land terminating glaciers (Zajaczkowski & Wlodarska-Kowlczhuk, 2007; Weslawski et al., 2011). In addition, Adventfjorden is the location of Longyearbyen, the largest settlement in Svalbard and has a high human impact influenced by active and inactive mining sites, ship traffic, dog yards and general anthropogenic activities.

Three fjord stations (A2, A4 and IsA) and one river station in Adventelva (River) were sampled during the main campaign (11$^{th}$ of May, 14$^{th}$ of June, 14$^{th}$ of July, 16$^{th}$ of August, 13$^{th}$ of September) (Fig. 3 C). The stations were chosen from earlier studies in order to achieve a gradient in surface water salinity and turbidity (McGovern et al 2020). Samples were taken at three depths at fjord stations (0m (all stations); 15m (all fjord stations); 50m (IsA only)) and at the surface at the river station.

In addition to the main campaigns, the river was sampled on a weekly to biweekly basis (designated "*River Monitoring*") to capture high resolution seasonal changes of the riverine discharge.

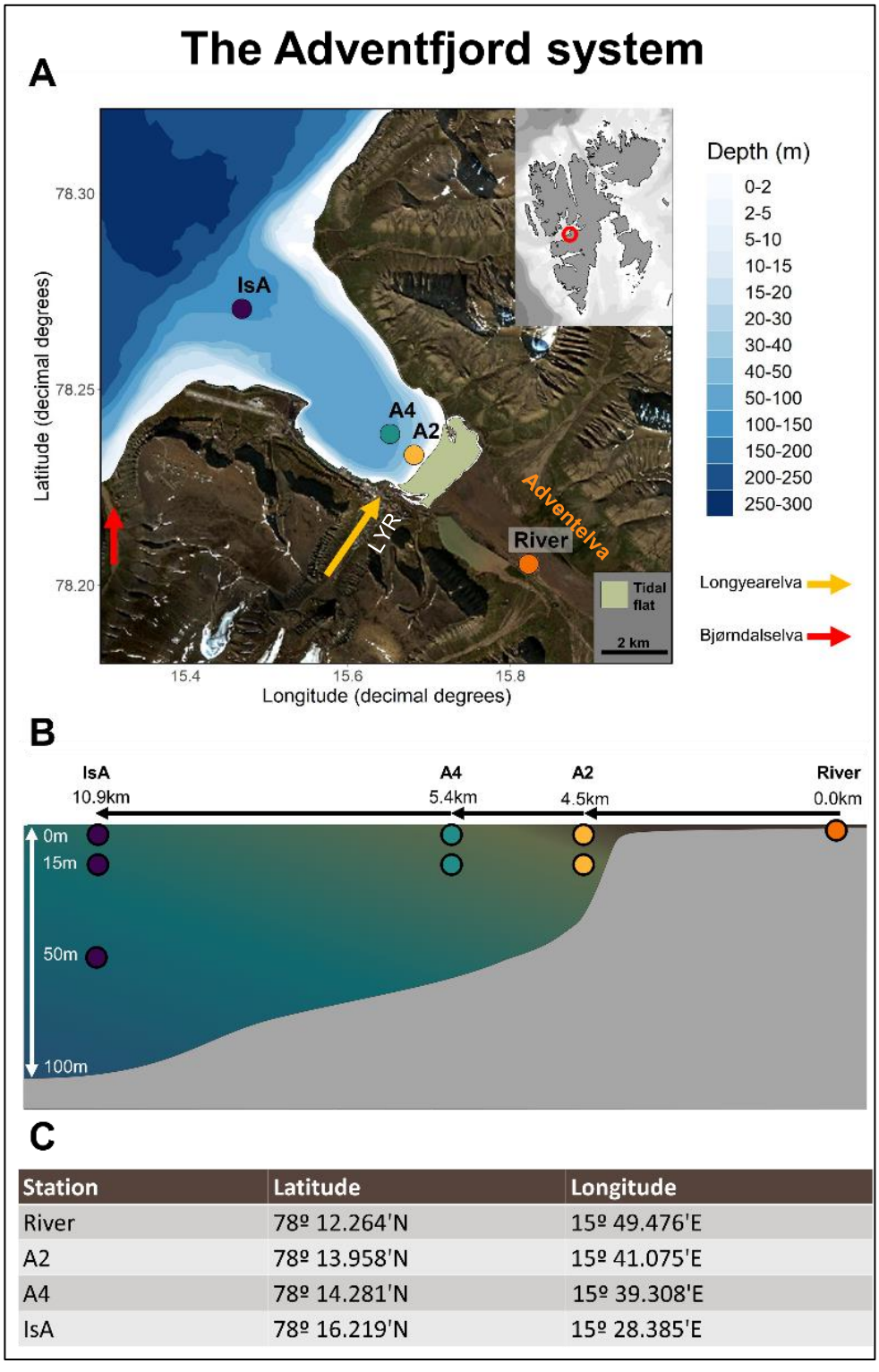


C

| Station | Latitude | Longitude |
|---|---|---|
| River | 78º 12.264'N | 15º 49.476'E |
| A2 | 78º 13.958'N | 15º 41.075'E |
| A4 | 78º 14.281'N | 15º 39.308'E |
| IsA | 78º 16.219'N | 15º 28.385'E |

**Fig. 3:** Map of the Adventfjord system and sampling sites. **A)** Area map with marked out stations and main adjacent river systems. LYR = Longyearbyen. Bathymetry and Svalbard map generated using R package "PlotSvalbard" (Vihtakari, 2020) and superimposed on top of satellite imagery from the Sentinel II mission (*ESA, 10/08/2021*). **B)** Cross section of the fjord with marked sampling depths and distance between stations. Bathymetry interpreted from Zajaczkowski & Wlodarska-Kowlczhuk (2007), **C)** Table with station target coordinates, based on McGovern et al. (2020).

## 3.2. River Sampling (Main Campaign and River Monitoring)

The River station was reached by foot. Water for physicochemistry was collected using a bucket. The water was pre-filtered with a 200µm Nitex mesh and transferred to an acid washed and sample rinsed 5L carboy (0.4M HCl solution for >8h). Water temperature was recorded in the field using an analog thermometer. The carboy was kept dark and transported back to UNIS where it was kept in a fridge until further processing (max 3 hours). During sampling campaigns, water was collected by field assistants trained in the methodology during river monitoring prior to the sampling campaigns.

## 3.3. Fjord Sampling (Main Campaign)

Fjord stations were reached with Polarcirkel boats (Unis Kolga/Sila).

### 3.3.1. Water column CTD and Light Profiling

CTD profiles (Conductivity, Temperature, Depth, Turbidity, Chlorophyll *a* Fluorescence) profiles were made using a SAIV model SD595 (SAIV A/S, Bergen, Norway). The CTD was submerged for 1 min at the surface before profiling began. The CTD was lowered slowly (<0.25m/s) through the top meters (~5m) of water column to ensure robust data of the surface water structure. For the deeper water column it was lowered by ~1m/s. In May and June the SAIV 595 CTD was deployed together with other CTD's (SAIV model SD612 in May, SAIV model SD208 in June (SAIV A/S, Bergen, Norway)). Due to concerns about the depth sensor of the SAIV 595. In the cases of daisy chained CTD's, the SAIV 595 was at the bottom to not disturb the water column before measurements of salinity and temperature. I encountered no

problems but the uppermost water column data (<0.5m) from May and June are merged from the SAIV SD612 and SD208 respectively.

Light profiles were made using LiCor PAR-sensors (LI-COR Biosciences UK Ltd, Cambridge, UK). PAR (photosynthetically active radiation (400-700nm) measured as µmol photons $m^{-2}$ $s^{-1}$) measurements were taken by manual lowering of a weighted LI-192 (in-water sensor) and a stationary LI-190R (in-air sensor placed on boat, unshaded). Logging was done manually on a LI-1400 (May-July) or LI-COR LI-1500 (August-September). The ratio between in-air and in-water measurements were used to calculate the relative light attenuation, later used to infer attenuation coefficients by exponential regression. In addition, a Secchi dish was used to measure approximate photic zone depth.

I accessed data from NIVA's research infrastructure including seasonally deployed *in situ* sensors in the Adventelva river (78º 12.169'N; 15º 50.010'E), and a seasonally deployed buoy in inner Adventfjord (78º 13.392'N; 15º 37.386'E) (A. Poste, unpublished data). At the river station, temperature, turbidity, conductivity, pH and water level was measured just below the surface, and at the fjord buoy, temperature, salinity, turbidity, chlorophyll *a* fluorescence, dissolved oxygen and oxygen saturation was measured at 2m depth. These data are used to conceptualize the gathered data in a broader seasonal perspective.

### **3.3.2.** Water Collection

Water was collected using a 10L Niskin bottle (KC Denmark A/S, Silkeborg, Denmark). Water for physiochemical analysis and incubations was pre-screened using 200µm Nitex mesh to remove large grazers. The water was collected in acid washed 5L containers and 500ml acid washed Nalgene bottles respectively (0.4M HCl solution for >8h). All water samples were stored dark in a cooler until further processing in the lab (up to 7 hours).

### **3.3.3.** Deployment of *in situ* incubations.

A custom incubation rig (a steel bar cage with attachment points for 10 Winkler bottles) was constructed for *in situ* incubation of Winkler bottles, used to determine the changes in dissolved $O_2$ over a 24h incubation period (Fig 4). 10 Winkler bottles were incubated at 2m depth below an anchor float of the mooring system of the SIOS/NIVA buoy at A2. This depth corresponded to the buoy sensor depth. Distance from buoy to float was ~30m. From June onwards, HOBO loggers (Onset HOBO UA-002-64, Bourne, MA, USA) measuring temperature (°C) and irradiance (LUX) were attached to the incubation rig (2m) and anchor float (surface, above water).

Water for the incubation was collected at A2 at 0m depth using the 10L Niskin bottle. 15 Winkler bottles were flushed with 2-3x flask volume and filled air-free with water using the Niskin bottle faucet. All flask necks and stoppers were wrapped with parafilm. Five random bottles were designated for T0 $dO_2$ measurement and stored dark and in a cooler immediately. Of the remaining 10 bottles, five were wrapped in aluminum foil, and five remained unwrapped (dark and light incubations respectively). The 10 light and dark bottles were mounted to the incubation rig and incubation was started as the rig was deployed.

The five T0 bottles were brought to the lab for immediate fixation, while the incubated bottles were collected after ~24h (incubation end point) whereafter they too were brought to the lab for fixation.

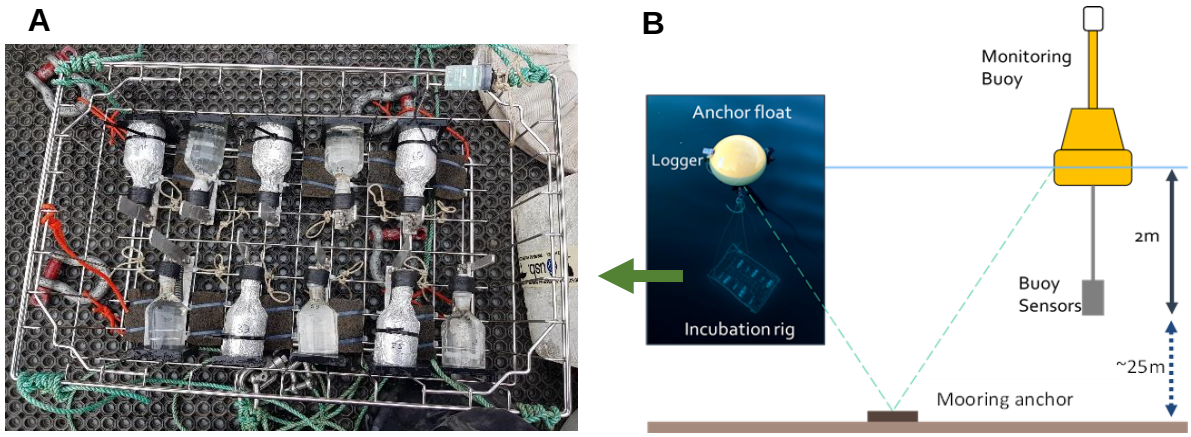


**Fig. 4:** Overview of the *in situ* incubation setup. **A)** Photo of the incubation rig ready for deployment, with mounted sample bottles and a HOBO-logger attached (seen in the top right corner). **B)** An illustration of the monitoring buoy mooring setup. 4 anchors were attached to the buoy, each with their own anchor float where the rig could be suspended from. The picture in B shows the rig suspended below the anchor float during deployment in September. A swivel at the attachment point ensured the ropes remained untangled, and weights at each of the bottom corners of the rig kept it level and suspended at the right depth.

### 3.4. Laboratory analysis of sampled water chemistry

Acid washing of all glass and plastic containers (including carboys and containers used in the field), and filtration apparatus for collecting water for chemical analysis was done by submersion in a 0.4M HCl solution for a minimum of 8h. After the bath the equipment was thoroughly rinsed with DI water and excess water was shaken out by hand. All rinsed equipment was stored capped in clean zip lock bags.

Pre-combustion of glass fiber filters and glass bottles for sample collection was done by burning at 450°C for 4.5 hours in a Nabertherm Muffle Furnace (Nabertherm GmbH, Lilienthal, Germany). Bottles were free standing while filters were placed in an acid washed glass jar. After burning the bottles were capped with acid washed plastic caps and stored clean. Filters were covered with pre-combusted aluminum foil and capped with the jar lid (acid washed).

### 3.4.1. Sensor Based Measurements and Nutrient Analysis.

Salinity, conductivity and pH of sampled water was measured using a HI98194 Multiparameter Meter (Hanna Instruments, Woonsocket RI, USA) in the lab as soon as possible after returning from the field. Turbidity was measured as triplicate measurements using a TN-100 handheld turbidity meter (Thermo Scientific Eutech, USA).

Filtrate for analysis of inorganic nutrients (Nitrite+Nitrate ($NO_2$+$NO_3$), Phosphate ($PO_4$), Silicate ($SiO_2$), ammonia ($NH_4$) and DOC was collected using pre-combusted 47mm GF/F filters (Whatman plc, Maidstone UK). Filtrate for inorganic nutrients and $NH_4$ was collected in acid washed 100ml HDPE bottles and stored at -20°C. They were analyzed using inductively coupled plasma mass spectrometry using standard and accredited methods (see Kaste et al., 2022) at the Norwegian Institute of Water Research (Oslo, Norway).

DOC samples were collected in acid washed and pre-combusted 100ml amber glass bottles and acidified by adding 1% v/v of 4N $H_2SO_4$ (May and first half of June River Monitoring samples) or 1% v/v 8N $H_2SO_4$ (remaining samples). The use of 8N was an error and the final goal was 1% v/v 4N $H_2SO_4$. The acidified samples were stored dark and at 4ºC until further processing. DOC was measured at UNIS using a Sievers M5310 C TOC analyzer (SUEZ Water Technologies, USA). The samples were mixed well and transferred to acid washed and pre-combusted 30ml Dram glasses for use with an in-line autosampler. The analysis template was determined using acidification and oxidation rates specified by the manual for an expected Total Organic Parbon (TOC) < 5ppm. All samples were measured in triplicate. Any samples exceeding 5 ppm were re-run using the same method, but with rates of acid and oxidizer specified for 5-10ppm by the manual. Blanks were measured and the collection syringe was flushed per $11^{th}$ sample using Milli-Q water. TOC was calculated as the difference between total carbon (TC) and inorganic carbon (IC).

### **3.4.2.** Chlorophyll *a*

50-300ml homogenized sampled water (depending on particle load) was filtered through a GF/F filter using a vacuum pump (Whatman plc, Maidstone UK). The filter was stored dark in a glass vial at -20°C until further processing. Chlorophyll *a* (Chl *a*) and phaeopigment concentrations were determined fluorometrically following methanol extraction (Parsons et al. 1984a; Marquart 2016). The extract was measured using a Turner 10-AU fluorometer (Turner Designs, USA), calibrated in 2019 using a 1mg standard (Sigma-Aldrich, Product no. C6144). Chlorophyll *a* concentrations and phaeopigments were calculated (Parsons et a. 1984a,b) as

$$\text{(Eq. 1) Chl } a \left[\mu\text{g L}^{-1}\right] = (\text{Rb} - \text{Ra}) * \tau * \text{Fd} * \text{D} * \left(\frac{V_{methanol}}{V_{sample}}\right)$$

$$\text{(Eq. 2) Phaeopigment } \left[\mu\text{g L}^{-1}\right] = \left(\left(\frac{Rb}{Ra} * \text{Ra}\right) - \text{Rb}\right) * \tau * \text{Fd} * \text{D} * \left(\frac{V_{methanol}}{V_{sample}}\right)$$

Where Rb is the fluorometer readout before acidification, Ra is the fluorometer readout after addition of 2 drops 5% HCl (1.2M), $\tau$ is an acidification correction factor (= 1.68), Fd is the calibration factor (= 0.87), D is the dilution factor, *V* is volume (mL), and $\frac{Rb}{Ra}$ is a correction factor for natural occurrence of phaeopigment in the standard (= 2.52).

### **3.4.3.** Suspended Particulate Matter

Between 200-2000 ml of water (depending on particle load) was filtered through pre-combusted and a pre-weighed GF/F filter and the filter was stored cold and dark in a plastic petri dish at -20ºC until further processing.

Suspended particulate matter (SPM) was determined as the gravimetrical change in weight of the filter after drying at 105°C in a Thermo Scientific OMH 180 Drying and Heating Oven (Thermo Scientific, Waltham, MA, USA). Each batch was initially dried for 1h and

determined dry when a subset of 5 random filters had a weight loss of <0.5mg after subsequent cycles of 30 min drying times. The particulate organic matter ($SPM_{org}$) content was determined as the mass loss of the dried SPM filters after burning at 450°C for 1h using Nabertherm Muffle Furnace (Nabertherm GmbH, Lilienthal, Germany), **(**Sutherland 1998, Wang et al. 2011**).**

### 3.5. Determination of *in vitro* Bacterial and Primary Productivity

Bacterial Production (BP) and Net Primary Production (NPP) were determined using measured incorporation of radioactively labelled substrates in the form of $^{3}$H-methyl-thymidine and $^{14}$C-bicarbonate respectively (Fuhrman & Azam, 1982; Steemann NE., 1952).

The protocol for measuring BP (Table 1) was based on results from a pilot study in 2019 conducted in the Adventfjord system (data not shown) and finalized with advice and inputs from T. Vonnahme and J. Holding (personal communication).

The incubation protocol (Table 1) for NPP was adapted from the Nansen legacy protocol with

**Table 1:** Overview of the incubation protocol parameters for NPP and BP.

| | **Protocol overview for carbon production incubations** | |
|---|---|---|
| **Measured** | Net Primary Production | Bacterial Production |
| **Tracer used** | $^{14}$C-Bicarbonate | $^{3}$H-Methyl-Thymidine |
| **Specific activity at manufacturing date** | 56.6mCi/mmol | 80.5Ci/mmol (May-Aug)<br>83.2Ci/mmol (Sept) |
| **Lot:** | 2520165 | 201907 (May-Aug)<br>202107 (Sept) |
| **Incubation container** | 50 ml culture flask | 15ml centrifuge tube |
| **Sample volume** | 45ml | 3ml |
| **Final tracer activity/concentration** | 0.1µCi/ml | 20nM (5nM, 10nM and 50nM) |
| **Replicate setup pr. sample** | 5 Live (3 Light, 2 Dark)<br>1 Kill control | 3 Live<br>2 Kill control |
| **Illuminated** | Yes (for Light) | No |
| **Incubation period** | 24h | 8h |
| **Temperature** | ~10*C | |
| **Fixation** | 2% v/v hexamine buffered formalin | |
| **Storage** | Cold and dark (in fridge) | |

modifications made for smaller sample volumes, by increased replication. A fixation step was added, making it necessary to leave a ~5ml headspace in the bottles as the samples were not filtered immediately after end incubation, (The Nansen Legacy, Sampling protocol V7, chapter 7.26).

A custom incubator setup was constructed for the incubation itself (Fig. 5A). A Stuart Linear Shaker SSL2 table was used for constant stirring (Cole-Parmer, Staffordshire, UK). A Grant LTD6G closed-loop temperature regulator was connected to the tub for a target temperature of 10°C (Grant Instruments, Cambridgeshire, UK). The tub was filled with ~7L of DI water and left to acclimatize for 24h prior to incubation. For BP the samples were placed in a metal cage in an aluminum foil bag (darkened) fully submerged in the incubator water. For NPP, the samples were placed standing upright in the incubator using a plastic rack on top of a metal cage (Fig. 5B). A Sanolux moodlight with two F15W/T8 02244 light tubes (Sanolux AS, Hundhamaran, Norway) was placed on top of the incubator, providing an average of 50µmol photons $m^{-2}$ $s^{-1}$ PAR at the position of the NPP samples (measured

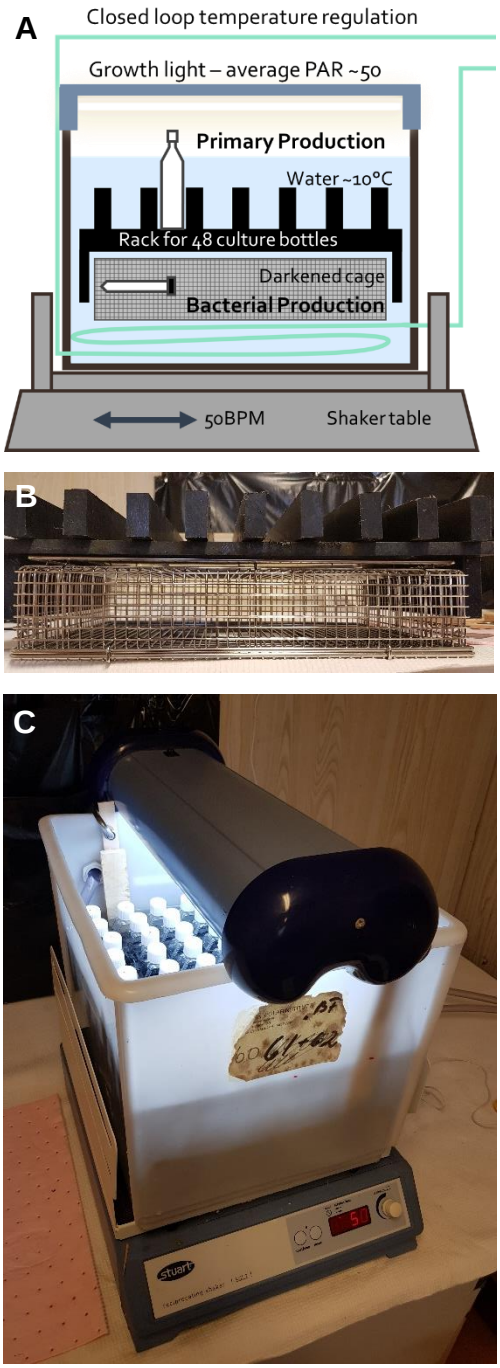


**Fig. 5:** Overview of the *in vitro* incubation setup. **A)** Illustration of the incubation setup with sample placement; **B)** The rack for $^{14}$C-spiked bottles placed on top of the $^{3}$H-spiked sample cage; C) A test setup with mounted samples. The circulation unit is off to the right and a connecting tube can be seen at the back of the tub.

using the same LiCor PAR sensor as for in-air field measurements). Digital thermometers were placed at two points within the incubator to record the temperature for start and end point measurements.

To prepare samples for incubation, sampled water was mixed well and transferred to 15ml centrifuge tubes (BP) and 50ml culture flasks (PP), respectively, and kill controls were fixed using 20% hexamine buffered formaldehyde for a final concentration of 2% v/v.

For BP, $^{3}$H-methyl-Thymidine tracer (NET027Z, PerkinElmer inc., USA) was added to a final concentration of 20nM, using a 1:5 tracer:milliQ working solution. All flasks were incubated dark for 8h at 10±1°C. Tracer saturation was determined using additional incubations from River 0m and IsA 0m in each month, with final tracer concentrations of 5nM, 10nM and 50nM. After the incubations the samples were fixed with formaldehyde as described for the killed controls. Tracer activity at the time of use were adjusted on natural decay rates of $^{3}$H from the specific activity at the manufactured date.

For NPP, tracer (NEC086H, PerkinElmer inc., USA) was added for a final activity of 0.1µCi/ml $^{14}$C-bicarbonate using a 1:13 sodium carbonate buffered working solution (prepared according to NOAA, 1999a). Darkened bottles (wrapped in black electric tape prior to incubation) and light bottles were all incubated for 24h at 10±1°C. After incubation the samples were fixed in formaldehyde. Three subsamples from a random light treatment NPP sample were taken each month immediately after spiking, for tracer activity determination (50µl spiked sample in 10ml scintillation Ecolume scintillation cocktail (MP Biomedicals, Germany) buffered with 50µL ethanolamine).

All samples were stored dark and cold until further processing.

BP samples were filtered onto 0.2µm cellulose acetate filters (Sartorius AG, Germany) not exceeding 300mbar, and unincorporated tracer was removed during four washing steps, first with 2x5ml 5% ice cold TCA and then with 2x5ml 80% ethanol. The filters were stored in 20ml HDPE scintillation vials (WHEATON®, Germany) at room temperature.

NPP samples were filtered onto GF/F filters (Whatman plc, UK), not exceeding 300mbar, and transferred to 10ml HDPE scintillation vials. Unincorporated tracer was removed by adding 750µl concentrated HCl and leaving the samples uncapped to dry. The samples were then capped and stored at room temperature.

Sample activity (tracer uptake) was measured using liquid scintillation counting (LSC) and determined as disintegrations per minute (DPM) using the Triple-Double Coincidence Ratio (TDCR) correction method (Broda, 2003). 10ml of Ecolume scintillation cocktail was added to each vial, with BP samples being dissolved beforehand in 500µl ethyl acetate. Activity was measured using a Hidex 300 sl liquid scintillation counter using measurement templates developed in corporation with Hidex MicroWin LSC Software (Hidex, Finland). For more detail, see Table A1.

Final BP rates (as µgC $L^{-1}$ $d^{-1}$) were calculated (NOAA, 1999b) as

$$\text{(Eq. 3) BP } (\mu gC/L/d) = F * \text{ uptake rate} * 24 * C$$

Where *F* is the conversion factor for production of bacterial cells $mole^{-1}$ 3H-thymidine ($2*10^{18}$ cells $mole^{-1}$), and *C* is the carbon content pr. bacterial cell 20fgC $cell^{-1}$ (Fukuda 1998; NOAA, 1999b).

The uptake rate (also by NOAA, 1999b) is given as

(Eq. 4) [methyl-$^{3}$H-thymidine]pmol kg$^{-1}$ h$^{-1}$ = $\frac{DPM-DPM_{kill.control}}{2200} * \frac{1000}{V} * \frac{1}{SA*(1+CF)} * \frac{60}{T}$

Where *DPM* is blank and TDCR corrected, *V* is the sample volume (mL), *SA* is the specific activity of the tracer at the time of use (Ci/mmol), *CF* is a correction factor calculated as the relative change in the tracer activity between use and measurement, and *T* is the incubation time in minutes.

Final NPP rates (as µgC L$^{-1}$ d$^{-1}$) were calculated as

(Eq. 5) $NPP = PP_{Light} - PP_{Dark}$

Where PP from either treatment is calculated (based on The Nansen Legacy Sampling Protocol v. 7, chapter 7.26, 2021) as:

(Eq. 6) $PP$ (µgC/L/d) = $\left(\frac{(DPM_{sample}-DPM_{kill.control})*DIC*U_C*d}{DPM_{added\ pr\ sample}}\right) * \frac{T_h}{24}$

Where *DPM* is blank, TDCR and chemiluminescence corrected; *DIC* (µmolC/L) was estimated based on sample salinity as $DIC = 52.1 * S + 339$ (Ericson, Y., 2019, eq 5), $U_C$ is the atomic weight of carbon (12u), *d* is a discrimination factor for $^{14}$C (=1.05), and *T* is the incubation time in hours.

The carbon balance between primary and bacterial production in the system was calculated as the ratio between NPP and BP.

### 3.6. Metabolic Balance based on *in situ* Incubations

Pelagic metabolic balance (Holding et al., 2013) was measured as changes in dissolved oxygen concentrations using the Winkler titration method with visual detection of the titration end point (Winkler, 1888; Codisputi 1988; Carpenter 1965). Sample fixation, analysis and subsequent calculations were carried out using a protocol from of E. Falck (2007), (not published, see appendix for Winkler Titration Protocol**).** Samples were fixed within 2h of sampling and left to settle overnight at room temperature. Samples were analyzed within 24h of collection by manual titration. Oxygen concentrations were calculated as

$$\text{(Eq. 7) } O_2 \text{ (mgO}_2\text{/L/d)} = \frac{V_{tit} * F}{V_{flask} - 2} * \frac{24}{T} * 1.429 * 10^3 mg/L$$

Where $V_{tit}$ is the volume of titration solution used (mL), *F* is the calibration factor of the thiosulfate solution used for the titration calculated as $F = \frac{3358.8}{Vol_{tit}}$, $V_{flask}$ is the flask volume (mL), T is the incubation time (h), and the constant of 1.429 is converting $O_2$ in $mlO_2/ml_{water}$ to mg/ml (OGSL 2014; USGS 2011). *F* was measured each month within 24h of sampling as the average of the 2-3 closest calibration tests with an accepted variation of 2%.

Metabolic balance of the system ($O_2$ production vs. $O_2$ uptake) was calculated as

$$\text{(Eq. 8) Metabolic Balance (MB)} = \frac{\text{GCP}}{\text{CR}}$$

Where GCP and CR are solved as mass balance equations (Holding et al., 2013) both measured in $mgO_2\ L^{-1}\ d^{-1}$, based on the mean $dO_2$ values of the different treatments given as

$$\text{(Eq. 9) Net Community Production (NCP)} = \mu_{Light} - \mu_{T0}$$

$$\text{(Eq. 10) Community Respiration (CR)} = \mu_{T0} - \mu_{Dark}$$

(Eq. 11) Gross Community $O_2$ Production (GCP) = NCP + CR

With all variables in Eq. 8-10 being in $mgO_2\ L^{-1}\ d^{-1}$.

## 3.7. Data Processing of Data Generated in This Study

### 3.7.1. Core Dataset Processing

Outliers from the BP dataset were identified as points that would make the average DPM of the kill controls be higher than all three measured live replicates of the same sample. This was only necessary for one datapoint. This was done with the assumption, that the kill control average should not exceed all (but could exceed some) live replicate measurements.

No outliers were removed from the PP dataset, but samples with high chemiluminescence counts (found mostly in September) resulted in underestimation of TDCR of samples with low actual activity. This led to artificially low DPM. In cases where TDCR was less than 0.25, the average TDCR from the other samples within the replicate was used, assuming even quenching. The samples with artificially low TDCR were either dark samples or kill controls.

For the measurements of dissolved oxygen, a 2% error rate was used to distinguish outliers, similar to the accepted error from the calibration test. The 2% cutoff resulted in the removal of two datapoints. The 2% cutoff was more discriminative than 3xSD. High variability was found across all August samples, therefore no datapoints were removed even if they met the 2% error criteria.

### 3.7.2. Additional Data Processing (Calculations, Statistics, Plotting, Mapping)

Data processing, (calculations, plotting) was done using R (R Core Team, 2021, v. 1.14.1717) using The R packages, “ggplot2” (Wickham, 2016), “ggpmisc” (Aphalo, 2021)

and “cowplot” (Wilke, 2020) for general data plotting; “tidyverse” (Wickham et al., 2019) and “lubridate” (Grolemund & Wickham, 2011) for data handling.

Maps of Svalbard with stations were created using the R package “PlotSvalbard” (Vihtakari, 2020). The same package was used for constructing T/S plots with water mass definitions from Nielsen et al. (2008).

CTD data was extracted using MiniSoft SD200W v. 3.22.19.254 (SAIV A/S, Bergen, Norway. The R packages “oce” (Kelley & Richards, 2022), “reshape2” (Wickham, 2007), “MBA” (Finley et al., 2017) and ”mgcv” (Wood, 2017) were used to create the extrapolation for contour plots.

HOBO logger light and temperature data was extracted using HOBOware v 3.7.23 (Onset Bourne, MA, USA). Conversion from LUX to estimated PAR was done using a conversion constant of 54 (from Thimijan & Heis (1983), table 3).

Calculations of standard deviation and coefficients of variance for propagated errors (added, subtracted and ratios of means) were based on Holmes & Buhr (2007).

Exponential regressions analysis for coefficients was conducted using the R package “broom” (Robinson et al., 2022) and “ggpmisc” (Aphalo, 2021).

Correlation matrixes and corresponding regression analysis were done using the R packages “corrplot” (Wei & Simko (2021), “Hmisc” (Harrell Jr, 2021) and “PerformanceAnalytics” (Peterson & Carl, 2020). A Spearman ranking test with Bonferroni adjustment of the calculated p-values was used to perform the analysis.

Multivariate statistics (Principle Component Analysis, PCA) were done using R packages “PCAtools” (Blighe & Lun, 2021) and “vegan” (Oksanen et al., 2020).

# 4. Results

## 4.1. Seasonal System Development

High spatial and temporal differences were observed in the physicochemical environment of the system due to freshwater inputs. Salinity and turbidity showed an inverse relationship, coupled to high turbidity freshwater inputs (Fig. 6). $NO_2$+$NO_3$, $SiO_2$ and $PO_4$ were linked to the salinity/turbidity relation. DOC, ammonium, Chl *a* and temperature were more seasonally and regionally dynamic. Three time periods were identified in the PCA performed: *Pre-Melt* (May), *Melt* (June-August), *Post-melt* (September) and three groups across space, based on freshwater influence: *River* (high), *Fjord Surface* (medium), *Fjord Deep* (low). A detailed overview of measured and calculated environmental variables can be found in Table A1.

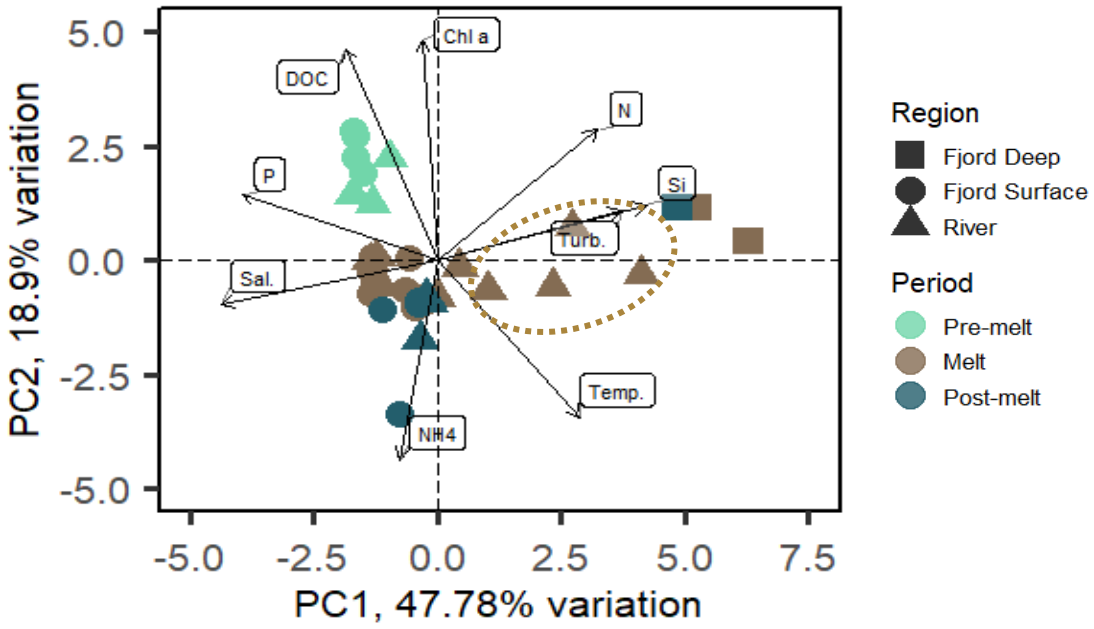


**Fig. 6:** Principal component analysis (PCA) mapping samples based on environmental areas. All values were scaled to the mean. The region groups are shown by symbol shape, and the period by color. The dotted ring is superimposed on top, marking the four identified plume samples. The first axis explains 47.8% of the data variation and can be linked to salinity (Sal., in PSU) and turbidity (Turb. In NTU). Chl a (µg/L), $NO_2$+$NO_3$ (N, in µM), P (P, in µM), Si ($SiO_2$, in µM), DOC (µM), $NH_4$ (µM) and temperature (Temp, in °C) were also used as explanatory variables.

Further, four distinct river plume samples were identified, based on a combination of relatively low salinity and high turbidity (1<S<34 PSU ; >10 NTU): A2 0m and A4 0m in both July and August (encircled in Fig. 6).

During May (*Pre-melt*) the river was frozen, and the fjord was well-mixed, saline and cold (Fig. A1). All recorded temperatures were between 0 and -0.5°C. Turbidity was low (<2) and the phytoplankton spring bloom was detected by high fluorescence signal at all stations and depths.

The *melt* season started with the first recorded freshet from the river on the 30$^{th}$ of May as part of river monitoring, and by the 1$^{st}$ of June the river had opened. Within a few days a turbid plume had formed in the fjord (Fig. 7).

The river showed gradual but clear seasonal evolution of the physical and chemical environment (Fig 8). The highest water temperatures were found in July (5.8 ± 1.7°C) peaking at 10.4°C. Average turbidity was highest in August (887 ± 595 NTU) and peaked at 3461 NTU. Conductivity increased towards the end of the *melt* period from a general low in


**Fig. 7:** Satellite images of the Adventfjorden system on the 28th of May 2021 (Left, Post-melt) and the 6th of June 2021 (Right, Freshet) showing the transition into the melt season, (*source: Sentinel II, ESA*).

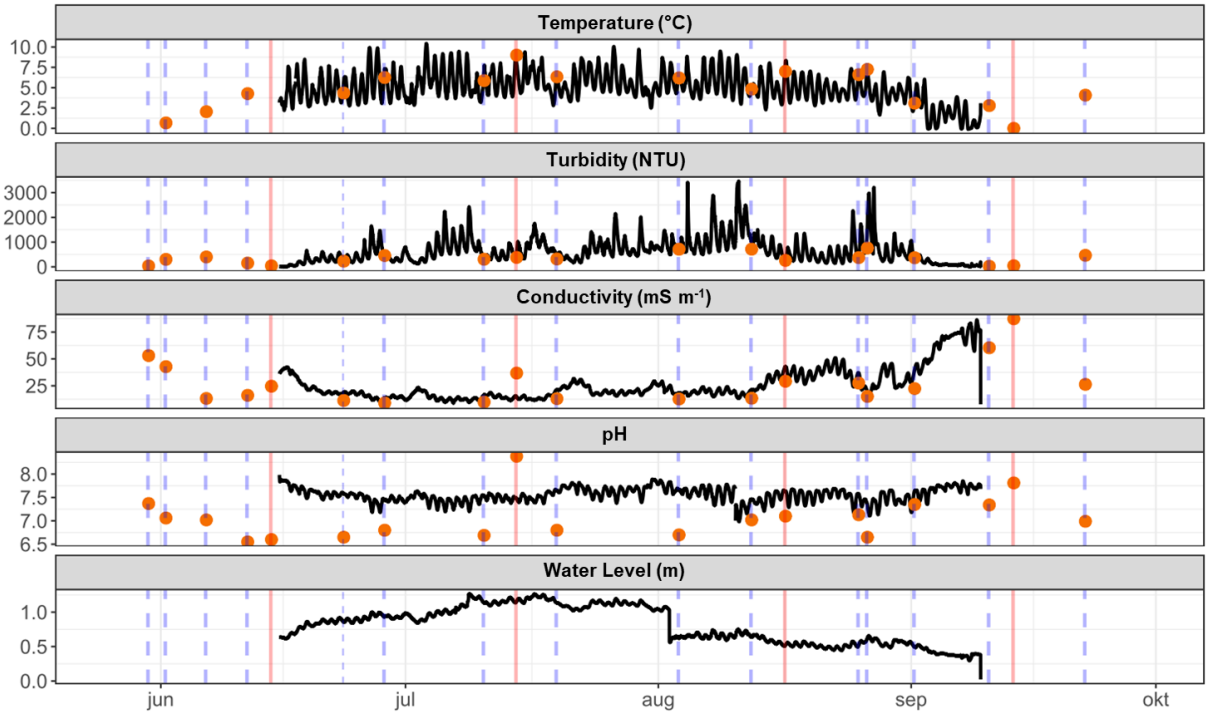


**Fig. 1:** River data with sample data values (orange points) and monitor station data (black line). Logging interval of the logger was set to every half hour. Blue vertical lines signify river monitoring samples, red lines signify main campaigns. The dip in water in August level was due to rearrangement of the mooring as it was being covered in sediments. The dip in pH was due to a recalibration. Monitor and data values match better after recalibration of monitor sensor.

July (~9mS $m^{-1}$) to *post-melt* values of >86.4mS $m^{-1}$. In general, all sampling campaigns (red vertical lines in Fig. 8) fell on periods with rather low turbidity. Both temperature and turbidity exhibitied clear diurnal cycles. Periods of high turbidity (discharge events) generally correlated with periods of warming (Fig A1).

In the fjord, the plume was present as a shallow turbid and freshened lens from June through August. While less than 2m in depth on sampling days the fjord buoy sensor detected the plume multiple times during the season as a decrease in salinity, generally tied to warmer water temperature and increased turbidity (Fig A3),.

There were  distinct coupling between salinity, turbidity, and temperature in the *fjord surface*, relating to riverine inputs (Fig 9). The plume was most pronounced in the inner fjord at A2 but was also detected further out at A4 (July and August) and IsA (August). In the CTD data the plume extension was defined by strong, near-surface pycnoclines, mainly caused by

salinity gradients (Fig. 9). A brackish mixing layer (10-30 PSU) developed in proximity of the plume and increased in depth with the progression of the season.

Towards the end of the melt season the freshwater input had caused freshening (~31 PSU) of the upper 30m of the water column (Fig. A4). In addition, the upper 30m warmed to >4°C, while the remaining water column remained cold (<2°C). The changes in *fjord deep* waters were more gradual and less extreme than the hydrographic changes observed in the surface waters.

During the melt season Chl *a* fluorescence peaks were found across salinity gradients and depths but peaked in the surface at A4 in July.

The *Post-melt* period was initialized by a period of cold weather in early September when air temperatures went below 5°C with periods of negative degrees (Fig. A1). As a consequence, the river started to freeze up which caused the river flow to subside substantially and the plume to disappear. This gave rise to a distinct fjord system, characterized by overall low turbidity (<15 FTU). The upper 30m remained relatively warm and freshened. A late season increase in chlorophyll fluorescence was observed at all stations in the warmer and freshened waters with peaks at the surface (<2m).

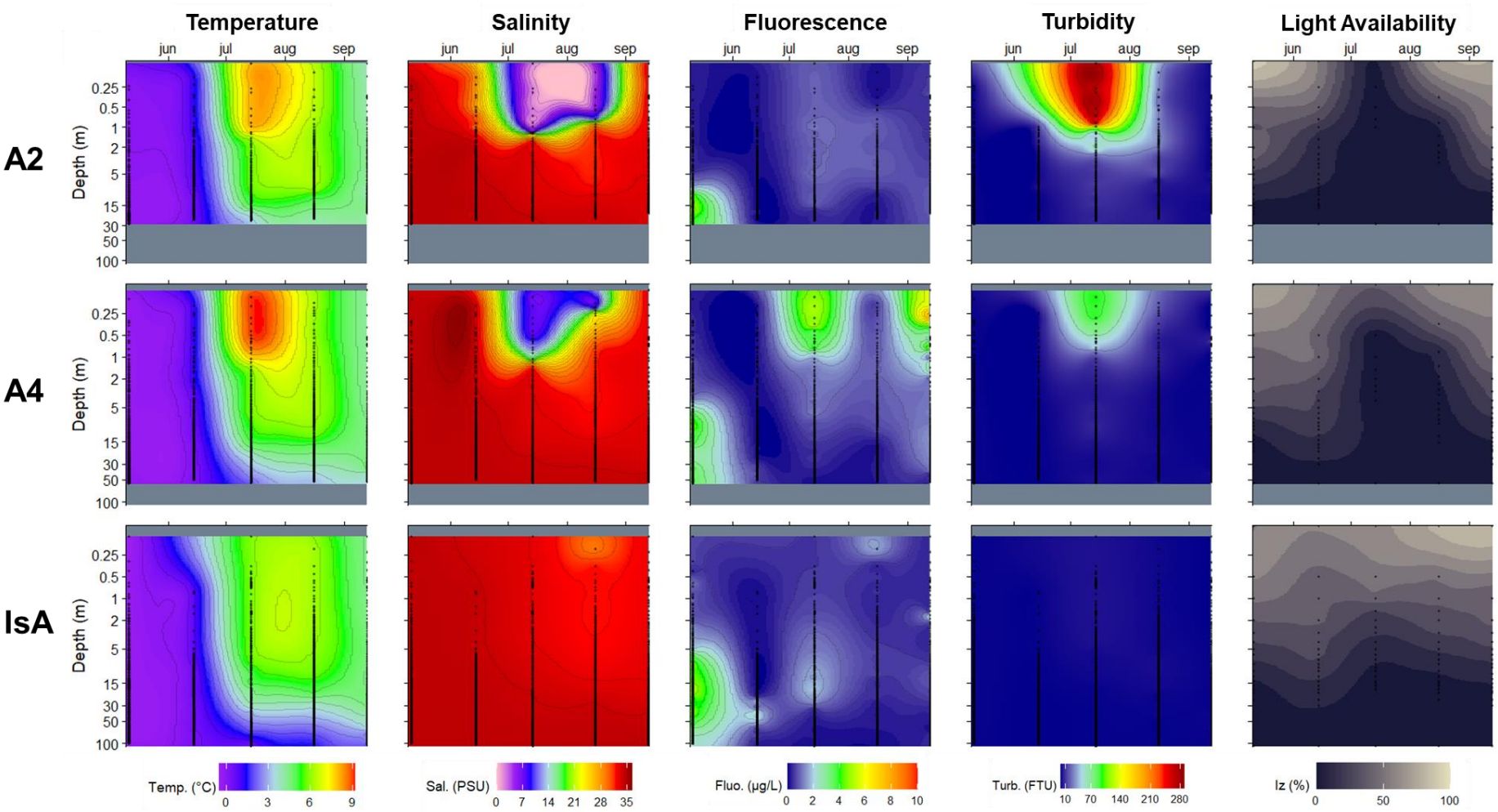


**Fig. 2:** Modelled contour plots based on monthly CTD and LiCor data (black dots) from fjord stations. Y-scale is log-transformed to emphasize the plume structure at the surface. Top row: A2, mid row: A4, bottom row: IsA. Fluorescence is measured as chlorophyll *a* fluorescence. Light availability (Iz) is measured in % PAR (µmol photons $m^{-2}s^{-1}$)

Light attenuation was strongly associated with surface turbidity (Table 2). Highly turbid surface waters (>10 NTU) were associated with the river plume and resulted in high light attenuation at 0.36 - 10.5$m^{-1}$. At stations with less turbid surface waters light attenuation was lower with all attenuation coefficients being < 0.30$m^{-1}$. Subsequently the euphotic zone depth (1% incoming PAR) was less than half at turbid stations (0.24 - 7.3m) than at clear stations (all stations > 15m). In August, the shallow plume caused an initial sharp increase in light attenuation, followed by a weaker light attenuation in the mixed and more clear waters below.

Incoming solar radiation followed seasonal changes in sun angle and local weather conditions, causing a decreasing trend in radiation towards the end of the season and high inter-daily variation. (Fig A5).

Table 2: Light climate data based on measurements with LiCor and secchi dish, with surface turbidity for reference. PAR is in µmol photons $m^{-2}$ $s^{-1}$, and the attenuation coefficient is in $m^{-1}$.

| Month | Station | Surface turbidity (NTU) | Secchi Depth (m) | Surface Irradiance (PAR) | Attenuation coefficient (α) | $R^2$ of (α) | Photic zone Depth (m) |
|---|---|---|---|---|---|---|---|
| May | A2 | 2.07 | 7.60 | 786.88 | 0.237 | 0.977 | 18.09 |
| | A4 | 1.59 | 8.75 | 513.28 | 0.230 | 0.988 | 18.47 |
| | IsA | 1.12 | 7.65 | 591.65 | 0.204 | 0.992 | 20.21 |
| June | River | 40.5 | -- | -- | -- | -- | -- |
| | A2 | 5.58 | 1.00 | 197.27 | 0.208 | 0.857 | 16.05 |
| | A4 | 1.23 | 17.1 | 176.20 | 0.086 | 0.926 | 43.80 |
| | IsA | 1.00 | 15.00 | 411.00 | 0.076 | 0.919 | 49.99 |
| July | River | 379.00 | -- | -- | -- | -- | -- |
| | A2 | 193.67 | 0.15 | 562.66 | 10.505 | 0.968 | 0.24 |
| | A4 | 76.17 | 0.42 | 541.67 | 1.800 | 0.713 | 1.10 |
| | IsA | 2.53 | 2.30 | 336.85 | 0.239 | 0.965 | 15.41 |
| August | River | 258.00 | -- | -- | -- | -- | -- |
| | A2 | 12.74 | 0.3 | 1287.33 | 2.084 | 0.945 | 1.87 |
| | A4 | 14.58 | 0.7 | 698.92 | 0.363 | 0.790 | 7.32 |
| | IsA | 1.62 | 6.0 | 640.75 | 0.210 | 0.973 | 18.92 |
| September | River | 43.66 | -- | -- | -- | -- | -- |
| | A2 | 1.97 | 9.20 | 423.50 | 0.258 | 0.972 | 16.57 |
| | A4 | 1.57 | 11.50 | 500.69 | 0.152 | 0.965 | 25.31 |
| | IsA | 0.69 | 11.00 | 450.15 | 0.148 | 0.969 | 26.63 |

## 4.2 Sampled water chemistry

### 4.2.1 River Chemistry

Particulate water chemistry generally followed patterns aasociated with air and water temperature, while the dissolved nutrients showed changes with general seasonal progression (Fig. 10). Notably, the early freshet contained the highest concentrations of $NO_2$+$NO_3$ (19.6µM), $PO_4$ (2.4µM), $NH_4$ (77.4µM), DOC (485µM) and $SPM_{org}$ (11.8%) measured across all collected samples.

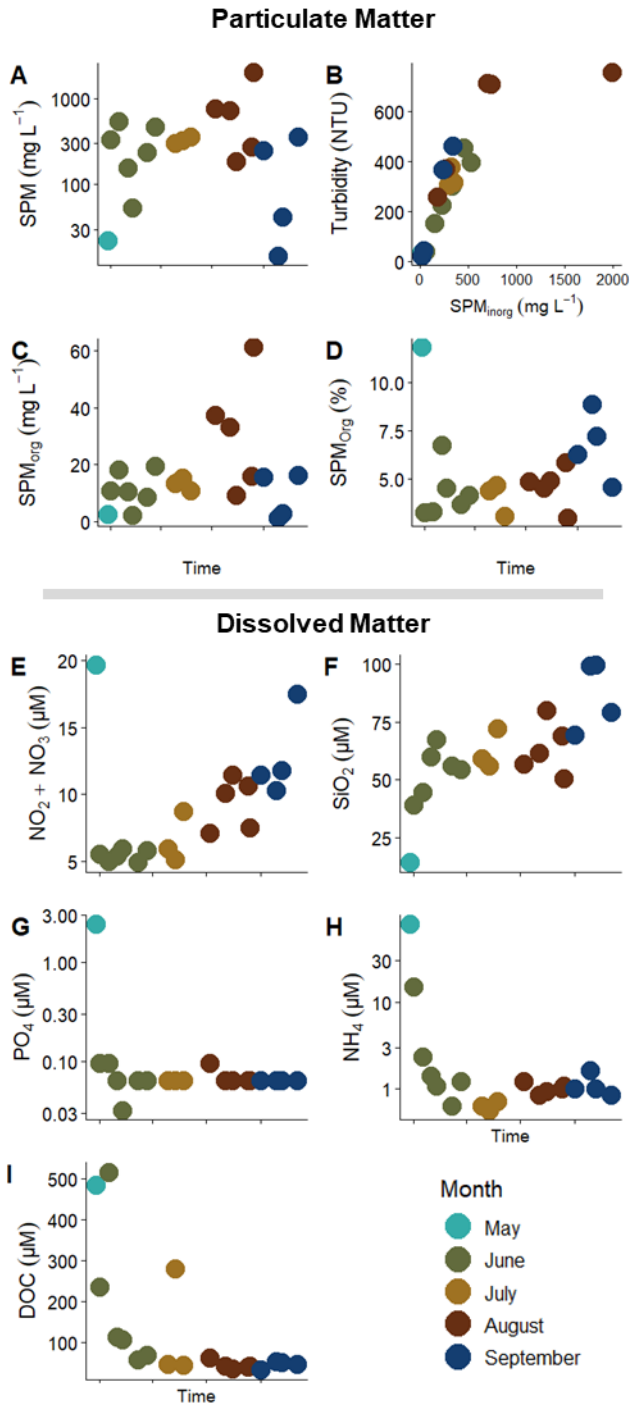


**Fig. 10:** River water environmental data from sampling rounds and river monitoring, showing particulate matter (A-D) and Dissolved Matter (E-I) development over time.

SPM was high throughout the season, ranging from a minimum of 14mg/L during the September freeze up, to a maximum of 2049mg/L during a warming period in August. Average SPM across all samples were 394 ± 455mg/L. The fraction of $SPM_{org}$ varied between 3 – 8.8% (not including freshet).

The concentrations of $NO_2$+$NO_3$ and $SiO_2$ showed an increase with seasonal progression, with concentrations more than doubling from early to late season (4.9 -

17.5µM $NO_2$+$NO_3$; 39.2 - 99.7µM $SiO_2$). DOC showed a quick decline from June to July after the freshet (516 – 70µM C), followed by relative stable values during the remaining season (34 – 70µM C) apart from a July peak (280µM C). $NH_4$ and $PO_4$ showed a sharp decrease after the initial freshet, with values after the initial decline varying from 0.6 to 2.4µM $NH_4$ and 0.03-0.1 µM $PO_4$.

### **4.2.2** Fjord Chemistry

Adventfjorden showed strong temporal and spatial heterogeneity in particulate and dissolved matter, with clear responses to riverine inputs in the surface waters of the fjord during the melt period (Fig. 11).

During *Pre-melt*, the fjord was overall homogenous with the lowest average SPM (8.79 ± 10.58mg/L), consisting of high $SPM_{org}$ (34.45 ± 14.7%), associated with the spring phytoplankton bloom. $NO_2$+$NO_3$ and $SiO_2$ concentrations were similar (2.47 ± 0.10µM $NO_2$+$NO_3$; 2.01 ± 1.31µM $SiO_2$ respectively) and ~10 times greater than $PO_4$ (0.28 ± 0.05µM $PO_4$). DOC was relatively high and even across regions (255.5 ± 61 µM C). $NH_4$ was the only nutrient showing strong vertical gradients, with *Fjord Surface* having higher concentrations (6.04 ± 11µM $NH_4$) compared to *Fjord Deep* (0.37 ± 0.06µM $NH_4$).

During *melt*, *Fjord Surface* values showed high temporal and spatial variability in response to riverine inflow and changes in plume extent. In general, high SPM, $NO_2$+$NO_3$ and $SiO_2$ were found in fresher water, while high $PO_4$, $NH_4$ and DOC were found in more saline water. SPM varied from 14.4 to 135.8mg/L with an average of 41.6 ± 38.9mg/L. The fraction of $SPM_{org}$ followed the same pattern as seen in the river, with low $SPM_{org}$ but high total $SPM_{org}$ due to high total particle load (4.7 - 19%, averaging at 14 ± 4.8%).

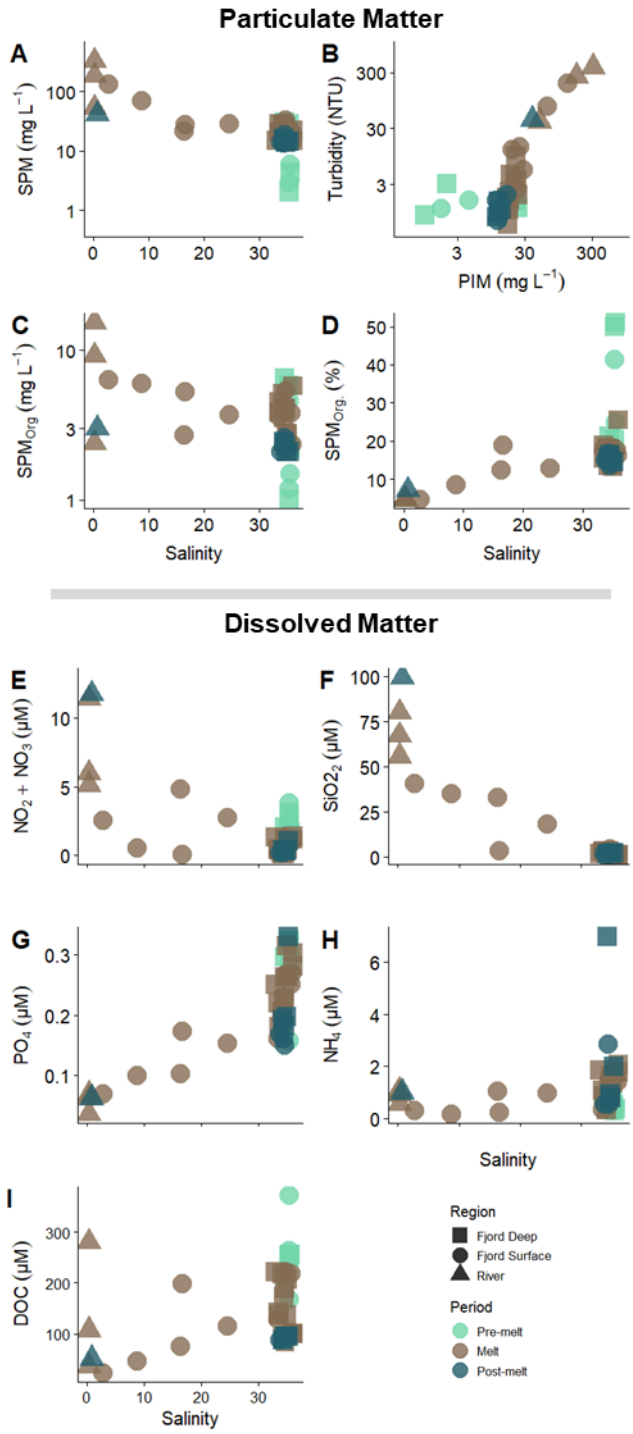


**Fig. 11**: Sampling campaign environmental data in relation to sample salinity, showing particulate matter (A-D) and Dissolved Matter (E-I). See table A2 for more detail.

The highest heterogeneity in inorganic nutrient concentrations were in $NO_2$+$NO_3$ (0.04 - 4.9µM)$_3$ and $SiO_2$ (1.1 - 40.9 µM) with averages of 1.6 ± 1.6µM and 15.7 ± 16.5µM respectively. DOC showed similar high variability (126 ± 74µM C, ranging from 23µM C to 222 µM C). $PO_4$ and $NH_4$ were less heterogenic, (0.169 ± 0.07µM and 0.88 ± 0.6µM) and generally lower than in the deeper fjord.

Compared to the surface waters, *Fjord Deep* was a relatively stable environment during the *Melt* period with low SPM (21.7 ± 4.95mg/L, of which 16.9 ± 3.4% was organic). In general, the deeper waters of the fjord were nutrient poor compared to the *Pre-melt* conditions (0.65 ± 0.51µM $NO_2$+$NO_3$, 1.94 ± 0.82µM $SiO_2$, 0.25 ± 0.4µM $PO_4$, 1.24 ± 0.53µM $NH_4$, 150 ± 51µM DOC).

*Post-melt* conditions were relatively homogenous across all samples. SPM fell in between that of *Pre-Melt* and *Melt* conditions. SPM varied little at 15.1 ± 1.9µg/L, with an organic

fraction of 15.2 ± 1.2%. $SiO_2$ had returned to approximate *Pre-melt* concentrations (1.83 ± 0.33µM $SiO_2$), while $NO_2$+$NO_3$, $PO_4$, and DOC concentrations remained similar to that of the deeper fjord in the *Melt* period, (0.37 ± 0.21µM $NO_2$+$NO_3$; 0.19 ± 0.06µM $PO_4$; 93.5 ± 3.65µM DOC). $NH_4$ increased on average, with local peaks leading to an average of 2.68 ± 29µM $NH_4$ in the deeper waters, and 1.33 ± 1.32µM $NH_4$ in the surface, but with a total range of 0.571 - 7.00µM $NH_4$ across the system.

### **4.2.3** Chlorophyll *a*

Chl *a* concentrations were generally higher in the fjord, (0.1 - 10µg/L Chl *a*) than in the river (0.1 - 0.5µg/L Chl *a*) (Fig. 12). The highest concentrations of Chl *a* were measured during the spring bloom in May (5.0 ± 1.2µg/L Chl *a*, ranging 2.1 – 8.1 µg/L Chl *a*), and in freshwater influenced fjord samples during *Melt* (0.7 – 10.0 µg/L Chl). These samples also had the lowest percent phaeopigments (Table A2). The highest Chl *a* was measured at the river plume edge in July (A4 0m, 10.0µg/L Chl *a*), exceeding values from the spring bloom

During *Melt*, surface waters of the fjord had the highest variability (0.1 – 10.0µg/L Chl *a*), whereas the deeper fjord had lower values overall (0.5 ± 0.6µg/L Chl *a*). The fjord had evenly distributed Chl *a* concentrations during *Post-melt*, (0.8 ± 0.3µg/L Chl *a*).

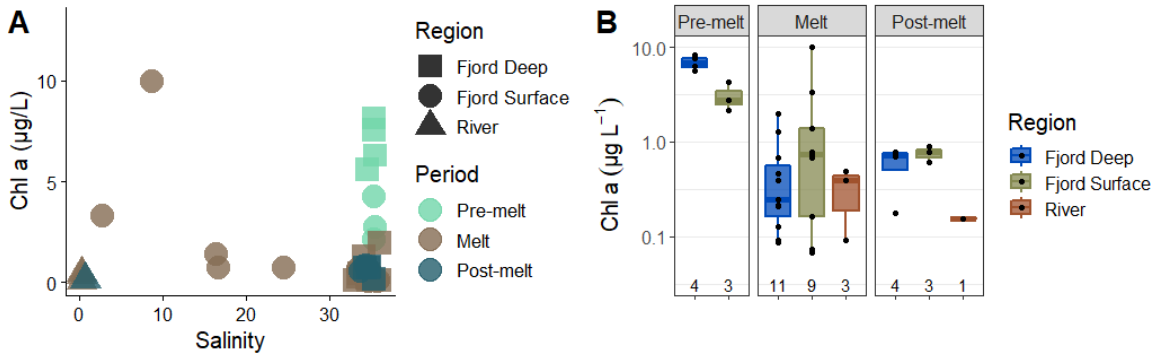


**Fig. 12:** Sampling campaign Chl *a* data, showing **A)** Relation to sample salinity and **B)** Summarized across region and period as boxplots, with Chl *a*. measurement as black dots. The number at the bottom denotes number of measurements. In the associated box.

## 4.3 Incubation results

### 4.3.1 *In vitro* Primary and Bacterial Production

NPP was overall much higher than BP throughout the whole season, yet both rates were seasonally and spatially heterogenous, varying by up to three orders of magnitude (0.1 – 299.4 µgC $L^{-1}$ $d^{-1}$ and 0.007 – 1.15 µgC $L^{-1}$ $d^{-1}$ respectively) (Fig. 13). See Table A3 for details.

BP was generally lower in all fjord waters during *Pre-melt* (0.13 ± 0.06 µgC $L^{-1}$ $d^{-1}$) and *Melt* (0.09 ± 0.08 µgC $L^{-1}$ $d^{-1}$) but increased during *Post-melt* in both *Fjord Deep* (0.47 ± 0.22 µgC $L^{-1}$ $d^{-1}$) and *Fjord Surface* (0.85 ± 0.27 ugC $L^{-1}$ $d^{-1}$). Bacterial production in the river was higher than in the fjord, with a peak in August (0.52 µgC $L^{-1}$ $d^{-1}$) and relatively constant productivity across the remaining samples from *Melt* and *Post-melt* (0.28 ± 0.11 µgC $L^{-1}$ $d^{-1}$). Saturation experiments showed that 20nM tracer did not result in saturation, but did reveal binding of tracer to sediments (as high kill uptake) (Fig A6).

Net primary productivity varied more in space than time, with both the lowest and highest measurements found in fjord surface waters during *Melt* (0.1 - 299.4 µgC $L^{-1}$ $d^{-1}$). Five samples had NPP > 10.0 µgC $L^{-1}$ $d^{-1}$ included the four plume samples (92.4 ± 139.0 µgC $L^{-1}$

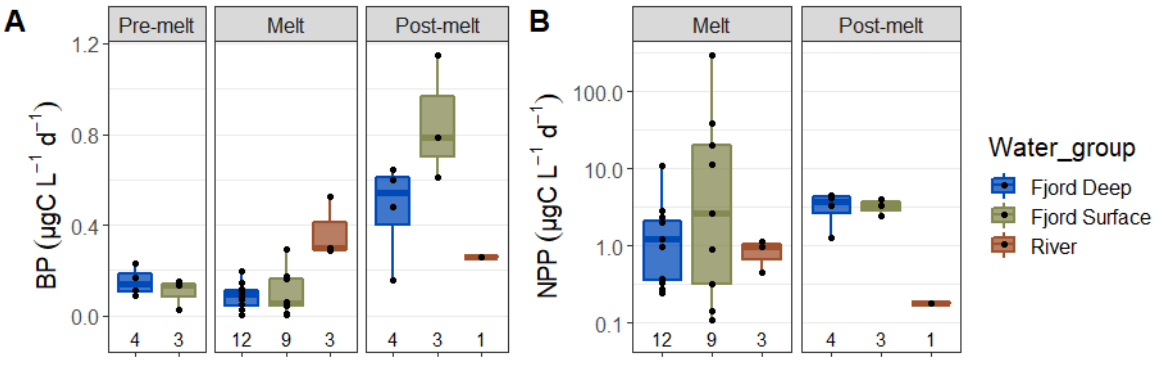


**Fig 13:** Boxplots of *in vitro* incubation data with datapoints, summarized across region and period. **A)** Bacterial production and **B)** Net primary production. Notice difference in y-scale. The number at the bottom denotes number of measurements. In the associated box. See Fig. A7 and Table A3 for more detailed.

$d^{-1}$) and a deep chlorophyll max in June (11.1 µgC $L^{-1}$ $d^{-1}$). All remaining fjord samples during *Melt* had values NPP < 3 µgC $L^{-1}$ $d^{-1}$ (average 1.1 ± 0.9 µgC $L^{-1}$ $d^{-1}$). During *Post Melt*, NPP was less variable and relatively even across all fjord samples (3.31 ± 1.14 µgC $L^{-1}$ $d^{-1}$). The river showed low NPP throughout the season (0.52 ± 0.35 µgC $L^{-1}$ $d^{-1}$).

Chl *a* concentrations and NPP were positively correlated (t-test, p < 0.001, r2 = 0.88) (Fig. 14). The sample specific growth response to environmental conditions ($NPP_B$ = NPP/Chl *a*) was highly variable across samples (1.2 - 29.9 µgC $d^{-1}$ µg Chl $a^{-1}$) but was ~5 times higher in freshwater influenced fjord samples, (17.1 ± 8.2 µgC $d^{-1}$ µg Chl $a^{-1}$) compared to more saline fjord samples (3.7 ± 1.8 µgC $d^{-1}$ µg Chl $a^{-1}$).

Overall, $NPP_B$, showing high variability of biomass specific growth response. When excluding the plume values, $NPP_B$ was on average higher in the fjord during *Post-melt* (4.7 ± 1.8 µgC $d^{-1}$ µg Chl $a^{-1}$) than *Melt* (3.3 ± 1.7 µgC $d^{-1}$ µg Chl $a^{-1}$). $NPP_B$ was higher in the river during *Melt* than *Post-melt*.

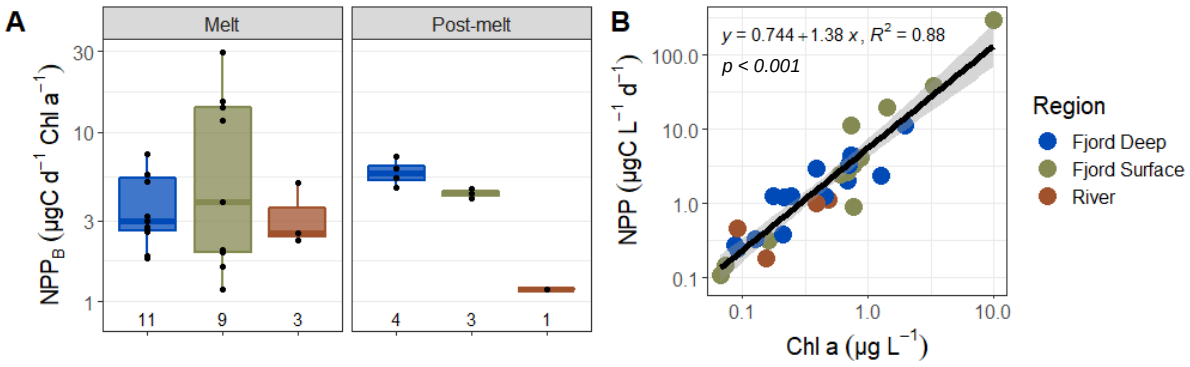


**Fig. 14: A)** Showing biomass specific NPP summarized over period and region. **B)** Showing the relation between total NPP and Chl a. Numbers at the bottom of A) designates number of datapoints in the group. See Fig. A7 & Table A3 for more detail.

### 4.3.2 *In situ* Oxygen Production and Respiration

GCP and CR showed high monthly variation (Fig. 15), with GCP generally being higher than CR. GCP ranged from 35.8 – 483 $mgO_2$ $L^{-1}$ $d^{-1}$ (average 220 ± 227 $mgO_2$ $L^{-1}$ $d^{-1}$), and CR ranged from -85.2 - 204 $mgO_2$ $L^{-1}$ $d^{-1}$ (average of 45 ± 105 $mgO_2$ $L^{-1}$ $d^{-1}$).

The negative CR value was due to July showing net oxygen production in all dark treatment flasks (11.4 ± 0.06 $mgO_2$ $L^{-1}$) (Fig. A8). This gave rise to lower GCP than NPP for July. NPP is therefore also presented in Fig. 16 as a better estimate of GCP.

Unusually high variability between measurements were found in August (GCP = 483 ± 347 $mgO_2$ $L^{-1}$ $d^{-1}$, CR = 204 ± 447 $mgO_2$ $L^{-1}$ $d^{-1}$) which matched sampling of a shallow freshwater lens with deeper, more saline water, (Fig A8 B).

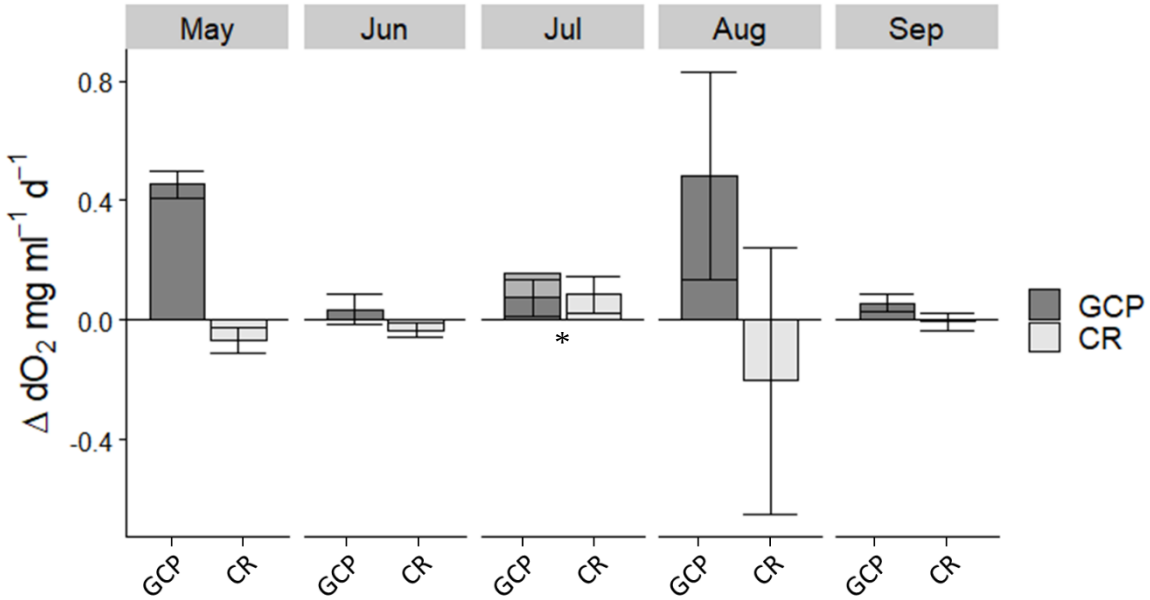


**Fig. 15:** Changes in dissolved oxygen after *in situ* incubation, showing GCP and CR across months. Errorbars shows standard deviation. Light grey bar on GCP July shows NCP, with asterix denoting known uncertainty of these values.

Temperature had no obvious effect on either GCP or CR, while relative light availability (PAR measured at the rig relative to surface PAR, ($PAR_W/PAR_A$)) and Chlorophyll *a* concentration had a profound effect on GCP (Table 3).

Unfortunately, light data from May (in-air and in-water) and June (in-air) is not available, but on-shore light sensor stations showed that ambient radiation was relatively high in May and low in June (Fig A5). Additionally, environmental data (and the fact that the river was frozen) showed that turbidity in May was likely low during incubation.

With this in mind, I observed that high Chl *a* (potential) and low attenuation gave rise to higher GCP in May. Most notably is July which had the highest Chlorophyll *a* but the lowest light levels at the incubator, leading to low GCP (and NPP) compared to May, even when accounting for the dark oxygen production. A mixed effect of low chlorophyll *a* and low light in June and September resulted in generally low GCP, while mid-range chlorophyll *a* but quite low light resulted in higher production in August (albeit with high error).

**Table 3:** Metabolic variables and metabolic balance (with coefficient of variance, CV) in relation to data from HOBO-loggers and Chl a. Avg.Temp is the average temperature measured from the in-water logger over the incubation period. $PAR_W$ is PAR from in-water sensor, while $PAR_A$ is from in-air sensor. Par values are estimated from measured LUX based on conversion constant of 54 (from Thimijan & Heis (1983) and given as median (min – max).

| **Month** | *Avg.Temp* ℃ | *$PAR_W$* µmol phot. $m^{-2}$ $s^{-1}$ | *$PAR_A$* µmol phot. $m^{-2}$ | *$PAR_W/PAR_A$* (of median) | *Chl a* µg/L | **GCP** **$mgO_2/L/d$** | **CR** **$mgO_2/L/d$** | **MB** | **$CV_{MB}$** |
|---|---|---|---|---|---|---|---|---|---|
| ***May*** | NA | NA | NA | NA | 2.13 | 454.2 | 66.4 | 6.8 | 1.0 |
| ***Jun*** | 1.1 | 3.5 (0 - 96) | NA | NA | 0.07 | 35.8 | 33.9 | 1.1 | 2.0 |
| ***Jul*** | 5.9 | 0.0 (0 - 0.4) | 191 (18 – 1122) | 0 | 3.30 | 73.7 | -85.2 | -0.9 | 1.5 |
| ***Aug*** | 6.5 | 5.6 (0 - 27) | 382 (3 – 1122) | 0.02 | 1.40 | 483.5 | 204.2 | 2.4 | 2.4 |
| ***Sep*** | 4.7 | 7.4 (0 - 99) | 41 (0 – 484) | 0.18 | 0.77 | 55.3 | 5.7 | 9.7 | 2.7 |

## 4.4 Carbon and Metabolic Balance

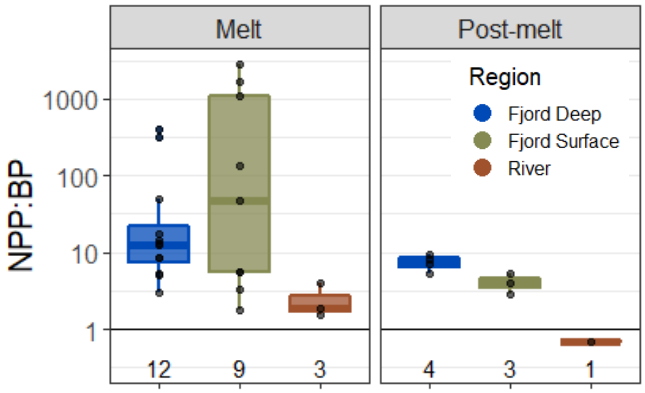


**Fig 16:** Carbon balance as NPP:BP summarized across region and period. Numbers at the bottom designates number of datapoints in each boxplot. See Fig. A7 & Table A3 for more detail.

The potential carbon balance showed the system to be a net carbon sink (NPP:BP > 1) (Fig 16). The ratio of NPP:BP ranged from 0.7 to 2810.1 with only River in September being < 1.

During *Melt*, the highest variability was found in *Fjord Surface* (1.8 - 2810.1), with higher values associated with freshwater influenced samples. Variation was also high in *Fjord Deep* (2.93 – 408.17) with higher values associated with high Chl *a* concentrations and/or very low BP values (leading to ratio inflation). NPP:BP was generally lower during *Post-melt*, with higher ratios in *Fjord Deep* (7.42 ± 1.75) than *Fjord Surface* (4.03+1.14). Across all groups, River NPP:BP was consistently lowest (2.36 ± 1.14).

Realized metabolic balance (MB, as GCP:CR) was on average > 1, showing the system to bet net autotrophic (Table 3). MB varied from 1.06 to 9.67, when ignoring the July datapoint. High MB in September was mainly a result of low CR.

In summary, the system has a potential to be a net carbon sink under ample light, with NPP exceeding BP up to ~3000 times. When looking at *in situ* values the balance is similar but much less extreme, showing a net autotrophic system even under low light conditions.

### 4.5 Correlation Analysis for NPP, BP and Environmental Variables

Spearman ranking analyses, (with p-values adjusted using Bonferroni correction) across periods was used to infer correlations between NPP, BP and NPP:BP to environmental variables (Fig. 17 A). In agreement with previous presented data, I found strong correlations between NPP and Chl *a* when looking at the data overall, and also when looking separately into *Fjord Deep* and *Fjord Surface*.

The analysis showed no strong drivers of BP, but BP was weakly positively correlated with $NH_4$ and Temperature.

Chl *a* concentrations were correlated with DOC in Fjord Deep, but not in surface waters.

Patterns in surface waters related to temperature, salinity, $NO_2$+$NO_3$ and $SiO_2$, and turbidity are corresponding with the observed patterns in freshwater influence.

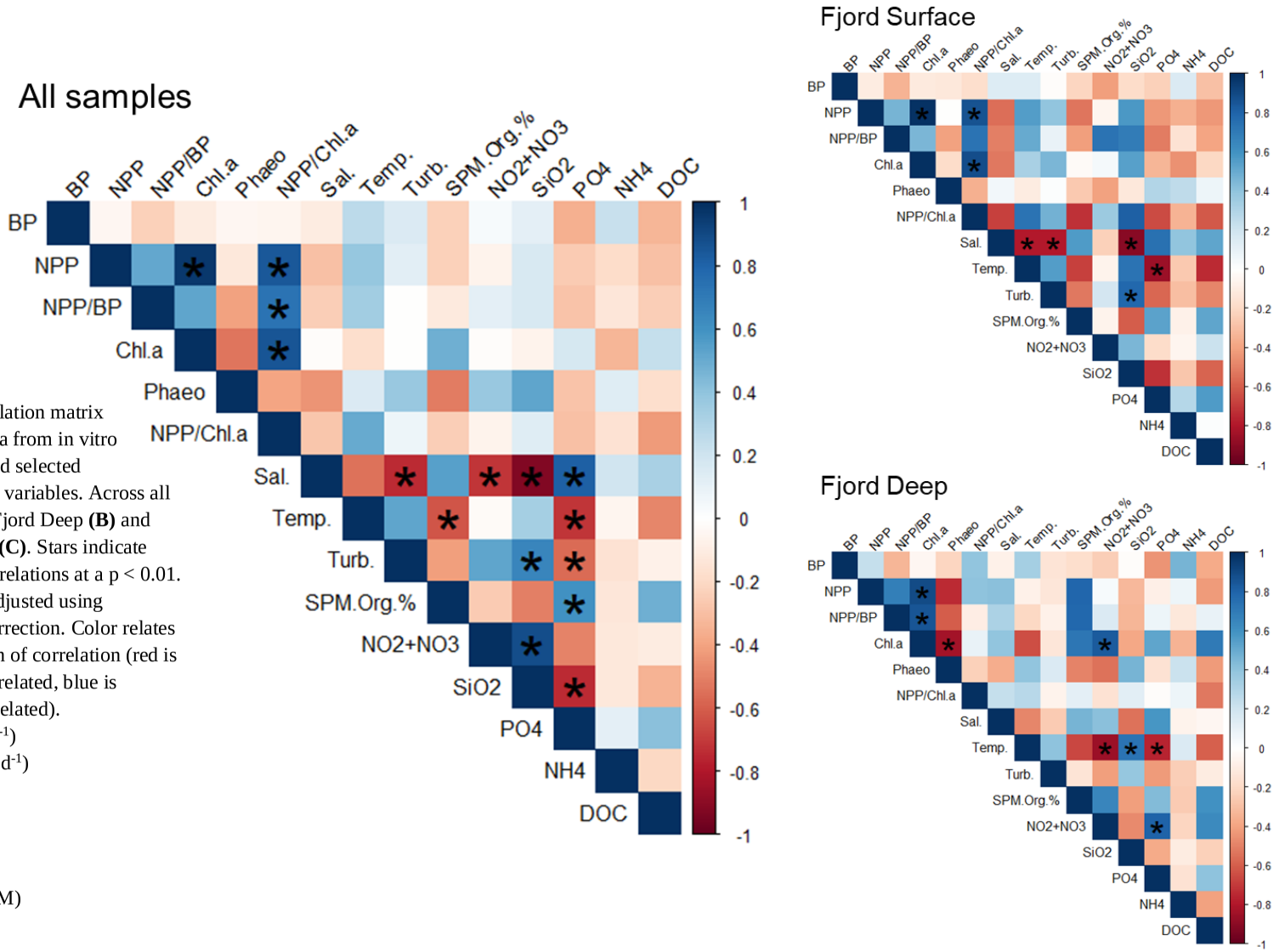


**Fig. 17:** Correlation matrix comparing data from in vitro incubations and selected environmental variables. Across all samples **(A)**, Fjord Deep **(B)** and Fjord Surface **(C)**. Stars indicate significant correlations at a $p < 0.01$. p-values are adjusted using Bonferroni-correction. Color relates to the direction of correlation (red is negatively correlated, blue is positively correlated).

BP (µgC $L^{-1}$ $d^{-1}$)
NPP (µgC $L^{-1}$ $d^{-1}$)
Chl *a* (µg $L^{-1}$)
Sal (PSU)
Temp (°C)
Turb (NTU)
NO2+NO3 (µM)
SiO2 (µM)
PO4 (µM)
NH4 (µM)
DOC (µM)

# 5. Discussion

The goal of the thesis was to *assess the impact of riverine inputs on bacterial and primary production in a High Arctic Fjord Estuary*, with the hypotheses that freshwater influenced areas (especially in the inner fjord) would be associated with heterotrophy, and that freshwater inputs could have a positive effect on primary production when sufficient light is available.

I found that freshwater influenced waters have a strong positive effect on primary production when light is available, shown as total NPP and high $NPP_B$ in *in vitro* incubations, confirming the second hypothesis.

While MB was clearly affected by light conditions, even low light could stimulate primary production to an extent where GPP could exceeded CR. This indicates that even the inner fjord can be surprisingly autotrophic and not necessarily always heterotrophic.

I found that freshwater inputs had little to no impact on bacterial production. BP remained low (compared to primary productivity) throughout the whole system but increased towards the later season suggesting seasonal responses rather than local conditions.

### 5.1 The River as a Source of Limiting Nutrients and Light-Attenuating Particles

The findings presented here support hypotheses by McGovern et al. 2020: that the high amount of inorganic nutrients from the riverine system can support high primary production during summer. This challenges the general paradigm that Arctic high turbid regions are areas of low primary productivity.

I find the river to be a source of $NO_2$+$NO_3$ and $SiO_2$ to the fjord throughout the entire melt season, with values and patterns matching that found by McGovern et al., 2020. $NO_2$+$NO_3$, $PO_4$ and $SiO_2$ values in the fjord are similar to that found in Kongsfjorden during summer (Hegseth et al., 2019), but is higher than that found in Young Sound, Greenland, where the river system is also not a source of inorganic nitrate (Paulsen et al., 2018).

The relative concentrations of $NO_2$+$NO_3$ and $SiO_2$ in the river increased from early to late season by ~2 to >5 times ($NO_2$+$NO_3$) and ~10 to >100 times ($SiO_2$) the concentrations of that of the fjord, while DOC remained comparable to or lower than that of the marine system, except for during early snow melt. Upon entering the marine system $NO_2$+$NO_3$ and $SiO_2$ were generally confined to the plume and was not detectable in the saline fjord.

The high frequency river monitoring shed light on the changes in river water chemistry. The initial melt is a short pulse event that supplies very high concentrations of all measured inorganic nutrients (except $SiO_2$) (Fig 10). This very quickly transitions into an early, less nutrient rich system in June, with gradual decrease of DOC, stable $NO_2$+$NO_3$ and increasing $SiO_2$. From there, the system gradually evolves into a system of high $NO_2$+$NO_3$ and $SiO_2$ towards the end of the season, which matches a shift towards glacial dominated melt (McGovern et al 2020; Nowak & Hodson, 2015).

While the suspended particles were mostly inorganic, the total particulate load led to high total $SPM_{org}$ (POM). POM is a potential source of nutrients to the pelagic system, but studies have shown that this pool is rapidly lost to the benthic or transformed by the heterotrophic community into higher quality POM, which then sinks out (Zajączkowski, M. et al 2010). While particles can be a microcosm for bacterial productivity (Garneau et al., 2009) the high sinking rate likely means that these nutrients are not a major source for the pelagic nutrient

pool (Maerz et al. 2019; Zajączkowski, M. et. al 2010; Zajączkowski, M. & Włodarska-Kowalczuk 2008). Supporting this, we did not observe a clear increase in BP with SPM, indicating that POM is not an important nutrient source for the pelagic in this system.

### 5.2 Freshwater Influenced Fjord Waters – Potential Primary Productivity Hotspots

The high discharge formed stratified and spatially heterogenous plume regions throughout the season, stretching from inner to outer fjord, and from less than one to several meters in depth, which is similar to the general trend in the system (Weslawski et al., 2011; McGovern et al., 2020; Szeligowska et al., 2021; Klein et al., 2021) (Fig. 9).

High surface particle loads associated with riverine inputs were an important regulator of light attenuation in the water column, as has previously been found in discharge systems (McGovern et al., 2020; Klein et al., 2021; Pavlov et al. 2019; Holding et al., 2019). However, I also found that in cases of shallow plumes (August A2 and A4), a sharp initial decrease in light attenuation was limited to this thin layer, followed by a more graduate decrease in the less turbid waters below (seen as lower R2 values in Table 2).This suggests that surface turbidity

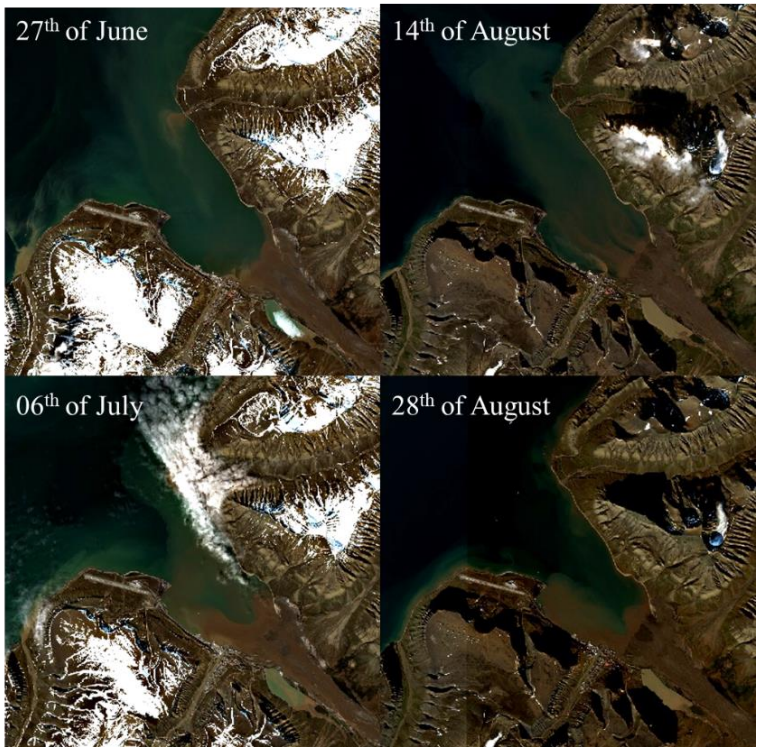


**Fig. 3:** Satellite imagery of Adventfjorden 2021, showing the strong spatial heterogeneity of the river plume (*source: Sentinel II (ESA)*).

can be misleading for water column light availability if the freshwater lens is narrow. Seasonality and weather also played a role on light climate, with the persistent summer cloud cover making the summer months darker on average than the spring. This coupled with the rapid sun angle decline after June max had a clearly visible effect on light levels in the surface of the fjord.

The light and nutrient regulation of the river had profound effects on microbial productivity. In the deeper parts and saline surface of the fjord, where the river influence was negligible, both bacterial and primary production was low throughout the melt season. In the mixed waters at either season end point, microbial productivity increased, with primary production in the spring and bacterial production in the autumn.

However, in stark contrast, high biomass and *in vitro* primary productivity was clearly associated with freshwater influence during summer. Chlorophyll *a* concentrations in the freshwater influenced samples in July matched that of the spring bloom. The measured concnetrations were similar to concentrations found in the spring bloom in Kongsfjorden, but much higher than the concentrations found in Kongsfjorden during summer (Hegseth et al., 2019). Consequently, I saw high total NPP peaking at 300µgC $L^{-1}$ $d^{-1}$, which are higher than spring bloom measured in Kongsfjorden, Svalbard (15 - 93.2µgC $L^{-1}$ $d^{-1}$, Hodal et al., 2012), the marginal ice zone (11 – 178µgC $L^{-1}$ $d^{-1}$, Hodal & Kristiansen, 2008), Young Sound, (peaking at 12µgC $L^{-1}$ $d^{-1}$, Rysgaard et al., 1999) and under ice blooms (peaking at 185µgC $L^{-1}$ $d^{-1}$, Mock & Gradinger, 1999). The results are likely an overestimation due to the artificial light conditions, but it shows the potential for high primary productivity. This is supported by $NPP_B$ which was 60 - 300 times higher in freshwater influenced samples compared to the highest rates found in saline fjord samples. The physicochemical changes to the environment

caused by freshwater influence are therefore highly stimulating primary productivity. The coupling with high chlorophyll *a*, low phaeopigments (comparable to that of the spring bloom) and low local $NO_2$+$NO_3$ suggests high production of new biomass in the freshwater influenced regions of the fjord, fueled by the river.

Nitrate is considered the limiting macronutrient for primary production in marine systems (Randelhoff et al. 2020), and land-derived nitrate have been shown to have an important role in driving primary production Arctic Ocean (Terhaar et al., 2021). It is therefore not surprising that the high concentrations transported from the river is stimulating high primary production.

The effect of light attenuation from sediments was important in shaping MB but I observed that even low light levels led to oxygen production. Holding et al., (2019) measured saturation irradiance for primary productivity in the summer, to be 5.8 – 67µmol photons $m^{-2}$ $s^{-1}$, showing low light adaptation in the photosynthesizing community. The low range of saturation matches with the median values measured during August and September *in situ*, (where the system showed net $O_2$ production) and is slightly higher than the median for June ($O_2$ equilibrium), suggesting that the Adventfjord community is also adapted to low light levels. Yet, no light (as in July) does indeed limit production, although this is obscured by the dark oxygen production. The reason for the dark $O_2$ production remains unknown but could be a result of redox reactions of $Fe^{3+}$ and iodine, which is used in the Winkler method for determining oxygen concentrations during titration.

The high saturation range of 67 µmol photons $m^{-2}$ $s^{-1}$ measured by Holding et al. (2019) also indicates that the incubator irradiance of 50µmol photons $m^{-2}$ $s^{-1}$ is reasonable for

measuring productivity without photoinhibition. The measurement of P/I curves would be valuable in further studies to assess the light adaptation of the primary production community.

Community respiration did not show signs of being affected by freshwater influence and remained low, suggesting that metabolic balance is regulated more by the activity/inactivity of photosynthesis than by respiration. This is similar to what was suggested by Cottrell et al., 2006.

### 5.3 Bacterial Production – A Pulse Regulated Ecological Mechanism?

The measured values of BP match that of other areas of the Arctic (Vallieres et al 2008; Middelboe et al., 2012; Garneau et al., 2008; Engel et al., 2013).

Contrary to primary productivity, riverine inputs had little to no influence on bacterial productivity. I hypothesized that the dark conditions (allowing for nutrient competition with eukaryotes) and higher temperature in the plume would be beneficial for bacterial production. However, BP in freshwater influenced samples remained similar to BP in the colder marine environment. Yet, it has been shown that bacterial production rates increase with increasing temperature. (Kritzberg et al., 2010, Kirchman et al, 2005). While the incubator was 10°C warmer than the collected water in May, BP remained the same as the rest of the season where collected water and incubator temperature was more similar.

DOM is known to be important for bacterial productivity (Kaiser et al., 2017). Previous studies have observed an increase in bacterial production linked to spring blooms and algal DOM production, (Middelboe et al., 2012; Rich et al., 1997). However, I did not observe enhanced bacterial activity during the spring bloom, although DOC concentrations during the bloom were in some cases the highest observed in the system during the season.

BP has been observed to increase with early season freshet derived DOM (Gareis et al., 2018) but this is a very short and pulsated event in the Adventfjord system. The freshet is known to be a source of highly concentrated, bioavailable DOM (Kaiser et al., 2017), but it is possible that a response in BP to the freshet pulse was not caught since sampling took place two weeks after the freshet flush. Yet, land derived matter have been observed to be a nutrient source for BP, as fertilization experiments have shown that bacterial growth increases with the addition of permafrost derived DOC. However, growth increased after a lag phase of a few days (Müller et al., 2018; Paulsen et al., 2017).

The late season increase in BP was surprising. A theory could be that higher water temperatures and indications of a late season algal bloom (as increase in Chl *a* in surface waters) could lead to a late season supply of algal DOM and POM and higher BP in the warmer system. However, methodological challenges at this time could have caused high estimates as an artefact. I found high chemiluminescence in $^{14}C$ LSC measurements in many late season samples, which is detected in the same region as $^{3}H$ signals. While this was corrected in the $^{14}C$ sampling approach, this chemiluminescence could lead to an overestimation in the bacterial production estimates. While I did not find a close relation between high chemiluminescence in $^{14}C$ samples and bacterial production estimates, this factor should be evaluated carefully in future studies.

### 5.4 System Balance – Comparing Potential and Realized Productivity.

The presented data suggests that freshwater influenced areas, where limiting inorganic nutrients are supplied by the freshwater discharge, can sustain high local primary production in regions where sufficient light availability. The fact that NPP from freshwater influenced samples is up to 3 times higher than the highest measurement saline samples, and that $NPP_B$ is

2-10 times higher in the freshwater influenced samples, shows that the environment can support high growth rates for new primary biomass.

Even under low light conditions, the system can be net autotrophic. This was also due to low, average community respiration, which in cases resulted in GCP being up to 10 times higher than CR. Yet the system was generally net autotrophic.

However, we must consider the scale (vertical and horizontal) at which primary production can take place at high rates. Plumes are highly heterogenous across space and time, governed by the dynamics of estuarine hydrography and, local weather patterns (Bianci et al., 2020). Whether the high regional primary productivity is enough to outweigh the bacterial and heterotrophic production of the integrated water column is a question that needs more careful study. Small-scale differences in growth conditions across the freshwater/marine continuum, should be targeted in future studies to get a clearer picture of the impact of freshwater inputs on the productivity of the full water column.

While the chosen methodologies for assessing microbial productivity and system metabolic balance were not entirely comparable, they were successful in addressing the patterns of *potential* productivity based on inherent environmental conditions (*in vitro* data), and *realized* productivity based on a changing environment (*in situ* data). A comparison between *in situ* oxygen production and *in vitro* oxygen production (by incubation of Winkler bottles under *in vitro* conditions) would have been helpful in assessing the effect of temperature, light, relationship between C and O production. Albeit they have their inherent limitations and strengths, (as mentioned in paragraph 2.4) each method provided good insights into the role of freshwater inputs to the system, and together worked well in elucidating the role of water physicochemistry versus light availability.

## 5.5 Outlook

The current consensus is that smaller estuarine systems with high surface turbidity, are heterotrophic and not a source of primary productivity (Carmack et al. 2016; Bauer et al., 2013). These findings challenge this idea, suggesting that if limiting nutrients are supplied to the system by the catchment, the areas of sufficient light can be hotspots for primary productivity.

Considering that roughly half of the freshwater in the Arctic Ocean is supplied by smaller discharge systems (Carmack 2000) it is important to consider the specific system dynamics when trying to estimate their impact on the Arctic carbon cycle on large. Remote sensing (satellite and/or aircraft) and continuous, local monitoring of plume depth (i.e. by stationary monitoring buoys and the use of AUV's) could be an important tool for improving modelling of the effect of terrestrial runoff on microbial productivity on a large scale. High chlorophyll concentrations at plume edges have been found previously in large discharge systems (Huang et al., 2013) and continuous improvement of remote sensing modelling (Klein et al., 2021) could provide capabilities for mapping potential biological processes remotely in the future.

In the face of climate change, artic coastal systems are expected to undergo drastic changes (Meredith et al., 2019; Hanssen-Bauer et al. 2019). Disappearing sea ice, loss of glaciers, increased permafrost thaw and changing precipitation patterns coupled with an expected change in melt season phenology during summer  can potentially drive changes in carbon cycling and food web structure (Bianchi et al., 2020; McGovern et al., 2020). This could mean higher plume associated primary production but come at the cost of other classical Arctic primary productive systems that support the current food webs. However, continuous summer productivity, although highly local, could be an important source of primary production in the future Arctic.

# 6 Conclusion

In this study I set out to investigate the productivity dynamics related to the meltwater season in the Advenfjord system. Potential productivity from *in vitro* incubations showed potential high NPP:BP ratios indicating that if ample light is supplied, NPP can exceed BP by more than 1000 times. While not as extreme, *in situ* incubations shows the same trend, with GCP being up to 10 times higher than CR.

I identify the plume as a heterogenous system providing local hotspots for high NPP during the meltwater season. The river supplies large amounts of inorganic nutrients to a nutrient limited fjord system. However, the high sediment load also limits light availability. This creates a marginal zone for high NPP in narrow bands at the plume front and associated mixing layers, where sufficient light is available.

In contrast, the plume seems to have little to no effect on bacterial productivity, pulse discharges of DOC during the melt season and freshet could be of importance, yet targeted sampling could be a challenge due to potential growth response delay. However, while low, BP is unconstrained by light availability and could be a significant factor on an integrated scale.

My findings challenge the general paradigm that freshwater discharge from land terminating glaciers are only a limiting factor for primary productivity. Instead, while very local, primary productivity can remain high throughout the melt water season. Diversity among smaller plume systems should therefore be considered when addressing the role of climate change on microbial productivity in present and future Arctic coastal systems.

# 7 References


Ameryk, A., Podgorska, B., & Witek, Z. (2005). The dependence between bacterial production and environmental conditions in the Gulf of Gdańsk. *Oceanologia, 47*(1).

Aphalo, P. J. (2021). ggpmisc: Miscellaneous Extensions to 'ggplot2'. R package version 0.4.5. Retrieved from https://CRAN.R-project.org/package=ggpmisc

Bauer, J. E., Cai, W.-J., Raymond, P. A., Bianchi, T. S., Hopkinson, C. S., & Regnier, P. A. G. (2013). The changing carbon cycle of the coastal ocean. *Nature, 504*(7478), 61-70. doi:10.1038/nature12857

Bhatia, M. P., Waterman, S., Burgess, D. O., Williams, P. L., Bundy, R. M., Mellett, T., . . . Bertrand, E. M. (2021). Glaciers and Nutrients in the Canadian Arctic Archipelago Marine System. *Global Biogeochemical Cycles, 35*(8), e2021GB006976. doi:https://doi.org/10.1029/2021GB006976

Bianchi, T. S., Arndt, S., Austin, W. E. N., Benn, D. I., Bertrand, S., Cui, X., . . . Syvitski, J. (2020). Fjords as Aquatic Critical Zones (ACZs). *Earth-Science Reviews, 203*, 103145. doi:https://doi.org/10.1016/j.earscirev.2020.103145

Blighe, K., & Lun, A. (2021). PCAtools: PCAtools: Everything Principal Components Analysis. R package version 2.6.0.

Blum, L. K., & Mills, A. L. (2012). Estuarine Microbial Ecology. In *Estuarine Ecology* (pp. 235-261).

Broda, R. (2003). A review of the triple-to-double coincidence ratio (TDCR) method for standardizing radionuclides. *Applied Radiation and Isotopes, 58*(5), 585-594. doi:https://doi.org/10.1016/S0969-8043(03)00056-3

Carmack, E. C. (2000). The Arctic Ocean's Freshwater Budget: Sources, Storage and Export. In E. L. Lewis, E. P. Jones, P. Lemke, T. D. Prowse, & P. Wadhams (Eds.), *The Freshwater Budget of the Arctic Ocean* (pp. 91-126). Dordrecht: Springer Netherlands.

Carmack, E. C., Yamamoto-Kawai, M., Haine, T. W. N., Bacon, S., Bluhm, B. A., Lique, C., . . . Williams, W. J. (2016). Freshwater and its role in the Arctic Marine System: Sources, disposition, storage, export, and physical and biogeochemical consequences in the Arctic and global oceans. *Journal of Geophysical Research: Biogeosciences, 121*(3), 675-717. doi:https://doi.org/10.1002/2015JG003140

Carpenter, J. H. (1965). THE ACCURACY OF THE WINKLER METHOD FOR DISSOLVED OXYGEN ANALYSIS1. *Limnology and Oceanography, 10*(1), 135-140. doi:https://doi.org/10.4319/lo.1965.10.1.0135

Codispoti, L. (1988). One Man's Advice on the Determination of Dissolved Oxygen in Seawater. *University of Washington*, 1-11.

Cole, J. J., Prairie, Y. T., Caraco, N. F., McDowell, W. H., Tranvik, L. J., Striegl, R. G., . . . Melack, J. (2007). Plumbing the Global Carbon Cycle: Integrating Inland Waters into the Terrestrial Carbon Budget. *Ecosystems, 10*(1), 172-185. doi:10.1007/s10021-006-9013-8

Cottrell, M. T., Malmstrom, R. R., Hill, V., Parker, A. E., & Kirchman, D. L. (2006). The metabolic balance between autotrophy and heterotrophy in the western Arctic Ocean. *Deep Sea Research Part I: Oceanographic Research Papers, 53*(11), 1831-1844. doi:https://doi.org/10.1016/j.dsr.2006.08.010

Csank, A. Z., Czimczik, C. I., Xu, X., & Welker, J. M. (2019). Seasonal Patterns of Riverine Carbon Sources and Export in NW Greenland. *Journal of Geophysical Research: Biogeosciences, 124*(4), 840-856. doi:https://doi.org/10.1029/2018JG004895

Deininger, A., & Frigstad, H. (2019). Reevaluating the Role of Organic Matter Sources for Coastal Eutrophication, Oligotrophication, and Ecosystem Health. *Frontiers in Marine Science, 6*. Retrieved from https://www.frontiersin.org/article/10.3389/fmars.2019.00210

Delpech, L.-M., Vonnahme, T. R., McGovern, M., Gradinger, R., Præbel, K., & Poste, A. E. (2021). Terrestrial Inputs Shape Coastal Bacterial and Archaeal Communities in a High Arctic Fjord (Isfjorden, Svalbard). *Frontiers in Microbiology, 12*. Retrieved from https://www.frontiersin.org/article/10.3389/fmicb.2021.614634

Duarte, C. M., Agusti, S., Barbier, E., Britten, G. L., Castilla, J. C., Gattuso, J.-P., . . . Worm, B. (2020). Rebuilding marine life. *Nature, 580*(7801), 39-51. doi:10.1038/s41586-020-2146-7

Dunse, T., Dong, K., Aas, K. S., & Stige, L. C. (2022). Regional-scale phytoplankton dynamics and their association with glacier meltwater runoff in Svalbard. *Biogeosciences, 19*(2), 271-294. doi:10.5194/bg-19-271-2022

Engel, A., Borchard, C., Piontek, J., Schulz, K. G., Riebesell, U., & Bellerby, R. (2013). $CO_2$ increases $^{14}C$ primary production in an Arctic plankton community. *Biogeosciences, 10*(3), 1291-1308. doi:10.5194/bg-10-1291-2013

Ericson, Y., Chierici, M., Falck, E., Fransson, A., Jones, E., & Kristiansen, S. (2019). Seasonal dynamics of the marine CO<sub>2</sub> system in Adventfjorden, a west Spitsbergen fjord. *Polar Research, 38*(0). doi:10.33265/polar.v38.3345

Finley, A., Banerjee, S., & Hjelle, Ø. (2017). MBA: Multilevel B-Spline Approximation. R package version 0.0-9. Retrieved from https://CRAN.R-project.org/package=MBA

Fuhrman, J. A., & Azam, F. (1982). Thymidine incorporation as a measure of heterotrophic bacterioplankton production in marine surface waters: Evaluation and field results. *Marine Biology, 66*(2), 109-120. doi:10.1007/BF00397184

Fukuda, R., Ogawa, H., Nagata, T., & Koike, I. (1998). Direct Determination of Carbon and Nitrogen Contents of Natural Bacterial Assemblages in Marine Environments. *Applied and Environmental Microbiology, 64*(9), 3352-3358. doi:doi:10.1128/AEM.64.9.3352-3358.1998

Garcia, H. E., & Gordon, L. I. (1992). Oxygen solubility in seawater: Better fitting equations. *Limnology and Oceanography, 37*(6), 1307-1312. doi:https://doi.org/10.4319/lo.1992.37.6.1307

Gareis, J. A. L., & Lesack, L. F. W. (2018). Photodegraded dissolved organic matter from peak freshet river discharge as a substrate for bacterial production in a lake-rich great Arctic delta. *Arctic Science, 4*(4), 557-583. doi:10.1139/as-2017-0055

Garneau, M.-È., Roy, S., Lovejoy, C., Gratton, Y., & Vincent, W. F. (2008). Seasonal dynamics of bacterial biomass and production in a coastal arctic ecosystem: Franklin Bay, western Canadian Arctic. *Journal of Geophysical Research: Oceans, 113*(C7). doi:https://doi.org/10.1029/2007JC004281

Garneau, M.-È., Vincent, W. F., Terrado, R., & Lovejoy, C. (2009). Importance of particle-associated bacterial heterotrophy in a coastal Arctic ecosystem. *Journal of Marine Systems, 75*(1), 185-197. doi:https://doi.org/10.1016/j.jmarsys.2008.09.002

Giesler, R., Lyon, S. W., Mörth, C. M., Karlsson, J., Karlsson, E. M., Jantze, E. J., . . . Humborg, C. (2014). Catchment-scale dissolved carbon concentrations and export estimates across six subarctic streams in northern Sweden. *Biogeosciences, 11*(2), 525-537. doi:10.5194/bg-11-525-2014

Grolemund, G., & Wickham, H. (2011). Dates and Times Made Easy with lubridate. *Journal of Statistical Software, 40(3)*, 1-25. Retrieved from https://www.jstatsoft.org/v40/i03/

Halbach, L., Vihtakari, M., Duarte, P., Everett, A., Granskog, M. A., Hop, H., . . . Assmy, P. (2019). Tidewater Glaciers and Bedrock Characteristics Control the Phytoplankton Growth Environment in a Fjord in the Arctic. *Frontiers in Marine Science, 6*. doi:10.3389/fmars.2019.00254

Hanssen-Bauer, I., Førland, E. J., Hisdal, H., Mayer, S., Sandø, A. B., & Sorteberg, A. (2019). Climate in Svalbard 2100. *A knowledge base for climate adaptation*.

Harrell Jr, F. E. (2021). Hmisc: Harrell Miscellaneous. R package version 4.6-0. Retrieved from https://CRAN.R-project.org/package=Hmisc

Hegseth, E. N., Assmy, P., Wiktor, J. M., Wiktor, J., Kristiansen, S., Leu, E., . . . Cottier, F. (2019). Phytoplankton Seasonal Dynamics in Kongsfjorden, Svalbard and the Adjacent Shelf. In H. Hop & C. Wiencke (Eds.), *The Ecosystem of Kongsfjorden, Svalbard* (pp. 173-227). Cham: Springer International Publishing.

Hodal, H., Falk-Petersen, S., Hop, H., Kristiansen, S., & Reigstad, M. (2012). Spring bloom dynamics in Kongsfjorden, Svalbard: nutrients, phytoplankton, protozoans and primary production. *Polar Biology, 35*(2), 191-203. doi:10.1007/s00300-011-1053-7

Hodal, H., & Kristiansen, S. (2008). The importance of small-celled phytoplankton in spring blooms at the marginal ice zone in the northern Barents Sea. *Deep Sea Research Part II: Topical Studies in Oceanography, 55*(20), 2176-2185. doi:https://doi.org/10.1016/j.dsr2.2008.05.012

Hodson, A., Nowak, A., & Christiansen, H. (2016). Glacial and periglacial floodplain sediments regulate hydrologic transfer of reactive iron to a high arctic fjord. *Hydrological Processes, 30*(8), 1219-1229. doi:https://doi.org/10.1002/hyp.10701

Holding, J. M., Duarte, C. M., Arrieta, J. M., Vaquer-Sunyer, R., Coello-Camba, A., Wassmann, P., & Agustí, S. (2013). Experimentally determined temperature thresholds for Arctic plankton community metabolism. *Biogeosciences, 10*(1), 357-370. doi:10.5194/bg-10-357-2013

Holding, J. M., Duarte, C. M., Delgado-Huertas, A., Soetaert, K., Vonk, J. E., Agustí, S., . . . Middelburg, J. J. (2017). Autochthonous and allochthonous contributions of organic carbon to microbial food webs in Svalbard fjords. *Limnology and Oceanography, 62*(3), 1307-1323. doi:https://doi.org/10.1002/lno.10526

Holding, J. M., Markager, S., Juul-Pedersen, T., Paulsen, M. L., Møller, E. F., Meire, L., & Sejr, M. K. (2019). Seasonal and spatial patterns of primary production in a high-latitude fjord affected by Greenland Ice Sheet run-off. *Biogeosciences, 16*(19), 3777-3792. doi:10.5194/bg-16-3777-2019

Holmes, D. T., & Buhr, K. A. (2007). Error propagation in calculated ratios. *Clinical Biochemistry, 40*(9), 728-734. doi:https://doi.org/10.1016/j.clinbiochem.2006.12.014

Huang, W.-J., Cai, W.-J., Castelao, R. M., Wang, Y., & Lohrenz, S. E. (2013). Effects of a wind-driven cross-shelf large river plume on biological production and CO2 uptake on the Gulf of Mexico during spring. *Limnology and Oceanography, 58*(5), 1727-1735. doi:10.4319/lo.2013.58.5.1727

Kaiser, K., Canedo-Oropeza, M., McMahon, R., & Amon, R. M. W. (2017). Origins and transformations of dissolved organic matter in large Arctic rivers. *Scientific Reports, 7*(1), 13064. doi:10.1038/s41598-017-12729-1

Kaste, Ø., Gundersen, C. B., Poste, A., Sample, J., & Hjermann, D. Ø. (2022). *The Norwegian river monitoring programme 2020 – water quality status and trends* (7738-2022). Retrieved from Miljødirektoratet, Norge:

Kelley, D., & Richards, C. (2022). oce: Analysis of Oceanographic Data. R package version 1.6-1. Retrieved from https://CRAN.R-project.org/package=oce

Kirchman, D. L., Malmstrom, R. R., & Cottrell, M. T. (2005). Control of bacterial growth by temperature and organic matter in the Western Arctic. *Deep Sea Research Part II: Topical Studies in Oceanography, 52*(24), 3386-3395. doi:https://doi.org/10.1016/j.dsr2.2005.09.005

Klein, K. P., Lantuit, H., Heim, B., Doxaran, D., Juhls, B., Nitze, I., . . . Søreide, J. E. (2021). The Arctic Nearshore Turbidity Algorithm (ANTA) - A multi sensor turbidity algorithm for Arctic nearshore environments. *Science of Remote Sensing, 4*, 100036. doi:https://doi.org/10.1016/j.srs.2021.100036

Kritzberg, E. S., Duarte, C. M., & Wassmann, P. (2010). Changes in Arctic marine bacterial carbon metabolism in response to increasing temperature. *Polar Biology, 33*(12), 1673-1682. doi:10.1007/s00300-010-0799-7

Lantuit, H., Overduin, P. P., Couture, N., Wetterich, S., Aré, F., Atkinson, D., . . . Vasiliev, A. (2012). The Arctic Coastal Dynamics Database: A New Classification Scheme and Statistics on Arctic Permafrost Coastlines. *Estuaries and Coasts, 35*(2), 383-400. doi:10.1007/s12237-010-9362-6

Lavoie, D., Macdonald, R. W., & Denman, K. L. (2009). Primary productivity and export fluxes on the Canadian shelf of the Beaufort Sea: A modelling study. *Journal of Marine Systems, 75*(1), 17-32. doi:https://doi.org/10.1016/j.jmarsys.2008.07.007

Leu, E., Mundy, C. J., Assmy, P., Campbell, K., Gabrielsen, T. M., Gosselin, M., . . . Gradinger, R. (2015). Arctic spring awakening – Steering principles behind the phenology of vernal ice algal blooms. *Progress in Oceanography, 139*, 151-170. doi:https://doi.org/10.1016/j.pocean.2015.07.012

Lique, C., Holland, M. M., Dibike, Y. B., Lawrence, D. M., & Screen, J. A. (2016). Modeling the Arctic freshwater system and its integration in the global system: Lessons learned and future challenges. *Journal of Geophysical Research: Biogeosciences, 121*(3), 540-566. doi:https://doi.org/10.1002/2015JG003120

Lund-Hansen, L. C., Andersen, T. J., Nielsen, M. H., & Pejrup, M. (2010). Suspended Matter, Chl-a, CDOM, Grain Sizes, and Optical Properties in the Arctic Fjord-Type Estuary, Kangerlussuaq, West Greenland During Summer. *Estuaries and Coasts, 33*(6), 1442-1451. doi:10.1007/s12237-010-9300-7

Maerz, J., Hofmeister, R., van der Lee, E. M., Gräwe, U., Riethmüller, R., & Wirtz, K. W. (2016). Maximum sinking velocities of suspended particulate matter in a coastal transition zone. *Biogeosciences, 13*(17), 4863-4876. doi:10.5194/bg-13-4863-2016

Marquardt, M., Vader, A., Stübner, E. I., Reigstad, M., Gabrielsen, T. M., & Stams, A. J. M. (2016). Strong Seasonality of Marine Microbial Eukaryotes in a High-Arctic Fjord (Isfjorden, in West Spitsbergen, Norway). *Applied and Environmental Microbiology, 82*(6), 1868-1880. doi:doi:10.1128/AEM.03208-15

Martínez, M. L., Intralawan, A., Vázquez, G., Pérez-Maqueo, O., Sutton, P., & Landgrave, R. (2007). The coasts of our world: Ecological, economic and social importance. *Ecological Economics, 63*(2), 254-272. doi:https://doi.org/10.1016/j.ecolecon.2006.10.022

McClelland, J. W., Holmes, R. M., Dunton, K. H., & Macdonald, R. W. (2012). The Arctic Ocean Estuary. *Estuaries and Coasts, 35*(2), 353-368. doi:10.1007/s12237-010-9357-3

McGovern, M., Pavlov, A. K., Deininger, A., Granskog, M. A., Leu, E., Søreide, J. E., & Poste, A. E. (2020). Terrestrial Inputs Drive Seasonality in Organic Matter and Nutrient Biogeochemistry in a High Arctic Fjord System (Isfjorden, Svalbard). *Frontiers in Marine Science, 7*. doi:10.3389/fmars.2020.542563

Meredith, M., Sommerkorn, M., Cassotta, S., Derksen, C., Ekaykin, A., Hollowed, A., . . . Schuur, E. A. G. (2019). Polar Regions. *IPCC Special Report on the Ocean and Cryosphere in a Changing Climate*.

Meslard, F., Bourrin, F., Many, G., & Kerhervé, P. (2018). Suspended particle dynamics and fluxes in an Arctic fjord (Kongsfjorden, Svalbard). *Estuarine, Coastal and Shelf Science, 204*, 212-224. doi:https://doi.org/10.1016/j.ecss.2018.02.020

Middelboe, M., Glud, R., & Sejr, M. (2012). Bacterial carbon cycling in a subarctic fjord: A seasonal study on microbial activity, growth efficiency, and virus-induced mortality in Kobbefjord, Greenland. *Limnology and Oceanography, 57*, 1732-1742. doi:10.4319/lo.2012.57.6.1732

Mock, T., & Gradinger, R. (1999). Determination of Arctic ice algal production with a new in situ incubation technique. *Marine Ecology Progress Series, 177*, 15-26. Retrieved from https://www.int-res.com/abstracts/meps/v177/p15-26/

Mulligan, R. P., & Perrie, W. (2019). Circulation and structure of the Mackenzie River plume in the coastal Arctic Ocean. *Continental Shelf Research, 177*, 59-68. doi:https://doi.org/10.1016/j.csr.2019.03.006

Müller, O., Seuthe, L., Bratbak, G., & Paulsen, M. L. (2018). Bacterial response to permafrost derived organic matter input in an Arctic fjord. *Frontiers in Marine Science, 5*, 263.

Nilsen, F., Cottier, F., Skogseth, R., & Mattsson, S. (2008). Fjord–shelf exchanges controlled by ice and brine production: The interannual variation of Atlantic Water in Isfjorden, Svalbard. *Continental Shelf Research, 28*(14), 1838-1853. doi:https://doi.org/10.1016/j.csr.2008.04.015

Nowak, A., & Hodson, A. (2015). On the biogeochemical response of a glacierized High Arctic watershed to climate change: revealing patterns, processes and heterogeneity among micro-catchments. *Hydrological Processes, 29*(6), 1588-1603. doi:https://doi.org/10.1002/hyp.10263

NOAA. (1999a). Chapter 19. Primary Production by 14 C. Retrieved from https://www.nodc.noaa.gov/archive/arc0001/9900162/2.2/data/0-data/jgofscd/Files/protocols/chap19.html.

NOAA. (1999b). Chapter 20. Determination of Bacterial Production using Methyl-tritiated Thymidine. Retrieved from https://www.nodc.noaa.gov/archive/arc0001/9900162/2.2/data/0-data/jgofscd/Files/protocols/chap20.html.

OGSL. (2014). Unit Convertions. Retrieved from https://ogsl.ca/wp-content/uploads/Unit_conversions_en_0.pdf. from St. Lawrence Global Observatory https://ogsl.ca/wp-content/uploads/Unit_conversions_en_0.pdf

Oksanen, J., Blanchet, F. G., Friendly, M., Kindt, R., Legendre, P., McGlinn, D., . . . Wagner, H. (2020 ). vegan: Community Ecology Package. R package version 2.5-7. Retrieved from https://CRAN.R-project.org/package=vegan

Osadchiev, A., Medvedev, I., Shchuka, S., Kulikov, M., Spivak, E., Pisareva, M., & Semiletov, I. (2020). Influence of estuarine tidal mixing on structure and spatial scales of large river plumes. *Ocean Sci., 16*(4), 781-798. doi:10.5194/os-16-781-2020

Osterholz, H., Dittmar, T., & Niggemann, J. (2014). Molecular evidence for rapid dissolved organic matter turnover in Arctic fjords. *Marine Chemistry, 160*, 1-10. doi:https://doi.org/10.1016/j.marchem.2014.01.002

Parsons, T. R., Maita, Y., & Lalli, C. M. (1984a). 4.3 - Fluorometric Determination of Chlorophylls. In T. R. Parsons, Y. Maita, & C. M. Lalli (Eds.), *A Manual of Chemical & Biological Methods for Seawater Analysis* (pp. 107-109). Amsterdam: Pergamon.

Parsons, T. R., Maita, Y., & Lalli, C. M. (1984b). 4.4 - Fluorometric Determination of Phaeo-pigments. In T. R. Parsons, Y. Maita, & C. M. Lalli (Eds.), *A Manual of Chemical & Biological Methods for Seawater Analysis* (pp. 109-110). Amsterdam: Pergamon.

Paulsen, M., Müller, O., Larsen, A., Møller, E., Middelboe, M., Sejr, M., & Stedmon, C. (2018). Biological transformation of Arctic dissolved organic matter in a NE Greenland fjord. *Limnology and Oceanography, 64*. doi:10.1002/lno.11091

Paulsen, M. L., Nielsen, S. E. B., Müller, O., Møller, E. F., Stedmon, C. A., Juul-Pedersen, T., . . . Middelboe, M. (2017). Carbon Bioavailability in a High Arctic Fjord Influenced by Glacial Meltwater, NE Greenland. *Frontiers in Marine Science, 4*. Retrieved from https://www.frontiersin.org/article/10.3389/fmars.2017.00176

Pavlov, A. K., Leu, E., Hanelt, D., Bartsch, I., Karsten, U., Hudson, S. R., . . . Granskog, M. A. (2019). The Underwater Light Climate in Kongsfjorden and Its Ecological Implications. In H. Hop & C. Wiencke (Eds.), *The Ecosystem of Kongsfjorden, Svalbard* (pp. 137-170). Cham: Springer International Publishing.

Peterson, B. G., & Carl, P. (2020). PerformanceAnalytics: Econometric Tools for Performance and Risk Analysis. R package version 2.0.4. Retrieved from https://CRAN.R-project.org/package=PerformanceAnalytics

Piontek, J., Galgani, L., Nöthig, E.-M., Peeken, I., & Engel, A. (2021). Organic matter composition and heterotrophic bacterial activity at declining summer sea ice in the central Arctic Ocean. *Limnology and Oceanography, 66*(S1), S343-S362. doi:https://doi.org/10.1002/lno.11639

R Core Team (2021). R: A language and environment for statistical computing. (Version 1.14.1717): R Foundation for Statistical Computing, Vienna, Austria. Retrieved from https://www.R-project.org/

Rachold, V., Are, F. E., Atkinson, D. E., Cherkashov, G., & Solomon, S. M. (2005). Arctic Coastal Dynamics (ACD): an introduction. *Geo-Marine Letters, 25*(2), 63-68. doi:10.1007/s00367-004-0187-9

Randelhoff, A., Holding, J., Janout, M., Sejr, M. K., Babin, M., Tremblay, J.-É., & Alkire, M. B. (2020). Pan-Arctic Ocean Primary Production Constrained by Turbulent Nitrate Fluxes. *Frontiers in Marine Science, 7*. Retrieved from https://www.frontiersin.org/article/10.3389/fmars.2020.00150

Rich, J., Gosselin, M., Sherr, E., Sherr, B., & Kirchman, D. L. (1997). High bacterial production, uptake and concentrations of dissolved organic matter in the Central Arctic Ocean. *Deep Sea Research Part II: Topical Studies in Oceanography, 44*(8), 1645-1663. doi:https://doi.org/10.1016/S0967-0645(97)00058-1

Robinson, D., Hayes, A., & Couch, S. (2022). broom: Convert Statistical Objects into Tidy Tibbles. R package version 0.7.12. Retrieved from https://CRAN.R-project.org/package=broom

Rysgaard, S., Nielsen, T. G., & Hansen, B. W. (1999). Seasonal variation in nutrients, pelagic primary production and grazing in a high-Arctic coastal marine ecosystem, Young Sound, Northeast Greenland. *Marine Ecology Progress Series, 179*, 13-25. Retrieved from https://www.int-res.com/abstracts/meps/v179/p13-25/

Scully, M. E., Friedrichs, C., & Brubaker, J. (2005). Control of estuarine stratification and mixing by wind-induced straining of the estuarine density field. *Estuaries, 28*(3), 321-326. doi:10.1007/BF02693915

Smith, E. M., & Benner, R. (2005). Photochemical transformations of riverine dissolved organic matter: effects on estuarine bacterial metabolism and nutrient demand. *Aquatic Microbial Ecology, 40*(1), 37-50. Retrieved from https://www.int-res.com/abstracts/ame/v40/n1/p37-50/

Smoła, Z. T., Tatarek, A., Wiktor, J. M., Wiktor, J. M. W., Kubiszyn, A., & Węsławski, J. M. (2017). Primary producers and production in Hornsund and Kongsfjorden – comparison of two fjord systems. *Polish Polar Research, vol. 38*(No 3), 351-373. doi:10.1515/popore-2017-0013

Steemann, N. E. (1952). The use of radioactive carbon (C14) for measurement organic production in the sea. *Jour. du Conseil pour l'exploration de la mer, 13*(2), 117.

Sutherland, R. A. (1998). Loss-on-ignition estimates of organic matter and relationships to organic carbon in fluvial bed sediments. *Hydrobiologia, 389*(1), 153-167. doi:10.1023/A:1003570219018

Szeligowska, M., Trudnowska, E., Boehnke, R., Dąbrowska, A. M., Dragańska-Deja, K., Deja, K., . . . Błachowiak-Samołyk, K. (2021). The interplay between plankton and particles in the Isfjorden waters influenced by marine- and land-terminating glaciers. *Science of The Total Environment, 780*, 146491. doi:https://doi.org/10.1016/j.scitotenv.2021.146491

Søgaard, D. H., Kristensen, M., Rysgaard, S., Glud, R. N., Hansen, P. J., & Hilligsøe, K. M. (2010). Autotrophic and heterotrophic activity in Arctic first-year sea ice: seasonal study from Malene Bight, SW Greenland. *Marine Ecology Progress Series, 419*, 31-45. Retrieved from https://www.int-res.com/abstracts/meps/v419/p31-45/

Søreide, J. E., Pitusi, V., Vader, A., Damsgård, B., Nilsen, F., Skogseth, R., . . . Węsławski, J. M. (2021). *Environmental status of Svalbard coastal waters: coastscapes and focal ecosystem components (SvalCoast)*. Retrieved from

Terhaar, J., Lauerwald, R., Regnier, P., Gruber, N., & Bopp, L. (2021). Around one third of current Arctic Ocean primary production sustained by rivers and coastal erosion. *Nature Communications, 12*(1), 169. doi:10.1038/s41467-020-20470-z

Testa, J. M., Kemp, W. M., Hopkinson Jr., C. S., & Smith, S. V. (2012). Ecosystem Metabolism. In *Estuarine Ecology* (pp. 381-416).

The Nansen Legacy (2021). Sampling Protocols: Version 7. *The Nansen Legacy Report Series*. 90-94. doi:https://doi.org/10.7557/nlrs.5793

Thimijan, R., & Heins, R. (1983). Photometric, radiometric, and quantum light units of measure: a review of procedures for interconversion. *Hortic Sci, 18*, 818-822.

USGS. (2011). Office of Water Quality Technical Memorandum 2011.03. Retrieved from https://water.usgs.gov/water-resources/memos/documents/WQ.2011.03.pdf. from U.S. Geological Survey https://water.usgs.gov/water-resources/memos/documents/WQ.2011.03.pdf

Vallières, C., Retamal, L., Ramlal, P., Osburn, C. L., & Vincent, W. F. (2008). Bacterial production and microbial food web structure in a large arctic river and the coastal Arctic Ocean. *Journal of Marine Systems, 74*(3), 756-773. doi:https://doi.org/10.1016/j.jmarsys.2007.12.002

Vihtakari, M. (2020). PlotSvalbard: PlotSvalbard - Plot research data from Svalbard on maps. R package version 0.9.2. Retrieved from https://github.com/MikkoVihtakari/PlotSvalbard

Vonnahme, T. R., Persson, E., Dietrich, U., Hejdukova, E., Dybwad, C., Elster, J., . . . Gradinger, R. (2021). Early spring subglacial discharge plumes fuel under-ice primary production at a Svalbard tidewater glacier. *The Cryosphere, 15*(4), 2083-2107. doi:10.5194/tc-15-2083-2021

Wainright, S. C. (1990). Sediment-to-water fluxes of particulate material and microbes by resuspension and their contribution to the planktonic food web. *Marine Ecology Progress Series, 62*(3), 271-281. Retrieved from http://www.jstor.org/stable/24842155

Wang, Q., Li, Y., & Wang, Y. (2011). Optimizing the weight loss-on-ignition methodology to quantify organic and carbonate carbon of sediments from diverse sources. *Environmental Monitoring and Assessment, 174*(1), 241-257. doi:10.1007/s10661-010-1454-z

Ward, N. D., Bianchi, T. S., Medeiros, P. M., Seidel, M., Richey, J. E., Keil, R. G., & Sawakuchi, H. O. (2017). Where Carbon Goes When Water Flows: Carbon Cycling across the Aquatic Continuum. *Frontiers in Marine Science, 4*. Retrieved from https://www.frontiersin.org/article/10.3389/fmars.2017.00007

Wassmann, P., Carmack, E. C., Bluhm, B. A., Duarte, C. M., Berge, J., Brown, K., . . . Huntington, H. P. (2020). Towards a unifying pan-arctic perspective: A conceptual modelling toolkit. *Progress in Oceanography, 189*, 102455. doi:https://doi.org/10.1016/j.pocean.2020.102455

Wei, T., & Simko, V. (2021). R package 'corrplot': Visualization of a Correlation Matrix (Version 0.92). Retrieved from https://github.com/taiyun/corrplot

Weslawski, J., Gluchowska, M., Kotwicki, L., Szczuciński, W., Tatarek, A., Wiktor, J., . . . Zajączkowski, M. (2011). *Adventfjorden: Arctic sea in the backyard*.

Wickham, H. (2007). Reshaping Data with the reshape Package. *Journal of Statistical Software, 21*(12), 1 - 20. doi:10.18637/jss.v021.i12

Wickham, H. (2016). Elegant Graphics for Data Analysis.: Springer-Verlag New York. Retrieved from https://ggplot2.tidyverse.org.

Wickham, H., Averick, M., Bryan, J., Chang, W., McGowan, L. D. A., François, R., . . . Yutani, H. (2019). Welcome to the tidyverse., *4(43), 1686*. doi:https://doi.org/10.21105/joss.01686

Wilke, C. O. (2020). cowplot: Streamlined Plot Theme and Plot Annotations for 'ggplot2'. R package version 1.1.1. Retrieved from https://CRAN.R-project.org/package=cowplot

Winkler, L. W. (1888). Die Bestimmung des im Wasser gelösten Sauerstoffes. *Berichte der deutschen chemischen Gesellschaft, 21*(2), 2843-2854. doi:https://doi.org/10.1002/cber.188802102122

Wood, S. N. (2017). *Generalized Additive Models: An Introduction with R (2nd edition)*: Chapman and Hall/CRC.

Wrona, F. J., Johansson, M., Culp, J. M., Jenkins, A., Mård, J., Myers-Smith, I. H., . . . Wookey, P. A. (2016). Transitions in Arctic ecosystems: Ecological implications of a changing hydrological regime. *Journal of Geophysical Research: Biogeosciences, 121*(3), 650-674. doi:https://doi.org/10.1002/2015JG003133

Zajączkowski, M., Nygård, H., Hegseth, E. N., & Berge, J. (2010). Vertical flux of particulate matter in an Arctic fjord: the case of lack of the sea-ice cover in Adventfjorden 2006–2007. *Polar Biology, 33*(2), 223-239. doi:10.1007/s00300-009-0699-x

Zajączkowski, M., & Włodarska-Kowalczuk, M. (2007). Dynamic sedimentary environments of an Arctic glacier-fed river estuary (Adventfjorden, Svalbard). I. Flux, deposition, and sediment dynamics. *Estuarine, Coastal and Shelf Science, 74*(1), 285-296. doi:https://doi.org/10.1016/j.ecss.2007.04.015

# 8 Appendix

**Table A1:** Measuring protocol for LSC for BP and PP. Both made in collaboration with the Hidex/MikroWin developers.

| | **Bacterial production ($^{3}$H)** | **Primary Production ($^{14}$C)** |
|---|---|---|
| **Target Isotope** | Free | Free |
| **Activity type** | Low Energy Beta Radiation | Low Energy Beta Radiation |
| **Tray delay** | 8h | 1h |
| **Ionizing delay** | 20s | 5s |
| **Chamber delay** | 20s | 20s |
| **Counting time** | 600sec | 1800s |
| **Repeats** | 3 | 1 |
| **Maximum counts** | 10000 | 3999999 |
| **Coincidence time** | 35ns | 35ns |
| **ROI 1** | 5-250 Type Beta | 5-550 Type Beta |
| **ROI 2** | | 5-550 Type BTriple |

*Tray delay: Delay before protocol start*
*Ionizing delay: Time in front of ionizing air (removing static electricity)*
*Chamber delay: Delay in measurement chamber before measurement start*
*Coincidence time: Time between measurements*
*ROI: Region Of Interest. Range is measured in channels of the detector.*

The use of 2 ROI's for 14C was to be able to distinguish between triple coincidences only (BTriple) and all coincidences (Beta). This was necessary to get the chemiluminescence counts for later correction, which was detected in Beta but filtered out in BTriple.

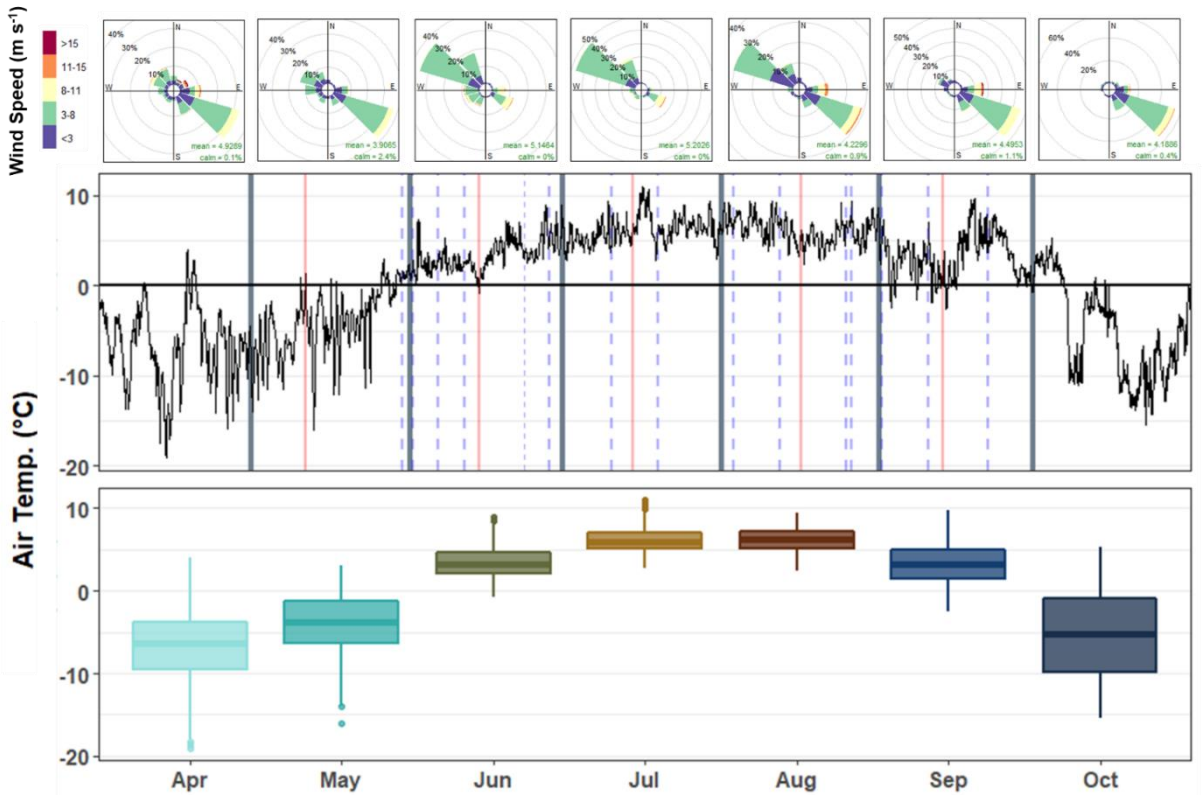


**Fig. A1:** Weather data from the Svalbard Airport weather station from 1st of April to 31st of October 2021. **A)** Wind direction and speed plotted as wind roses using hourly averages but plotted for the full month. **B)** Hourly means of air temperature. Red line signifies main campaigns while blue stapled lines indicate river monitoring sampling. Grey lines indicate the 1st day of each month. **C)** Boxplot of hourly temperature data plotted per month. *(Source: weather station Svalbard Lufthavn (SN99840), Norsk Klimaservicesenter*)

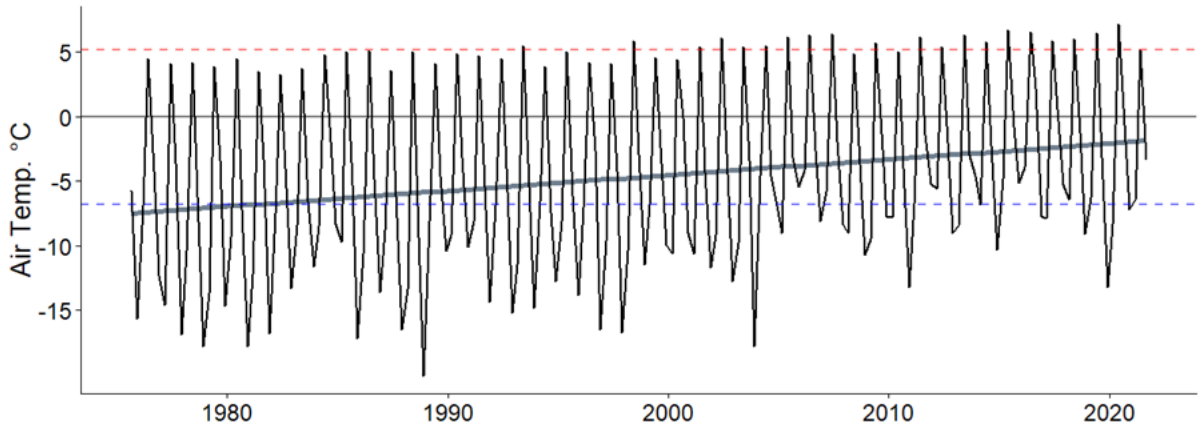


**Fig. A2:** Seasonal air temperature data from the Svalbard Lufthand Weather station since it's comisson in 1975. Each time point is quaterly average. Red stapled line is placed at the 2021 Q3 average (June 1st to August 31st) of 2021, while the blue line is placed at the Q1+Q2 average from December 1st 2020 to May 31st 2021. The grey line shows the trend in temperature over the monitoring period based on seasonal means (Source: weather station Svalbard Lufthavn (SN99840), Norsk Klimaservicesenter)

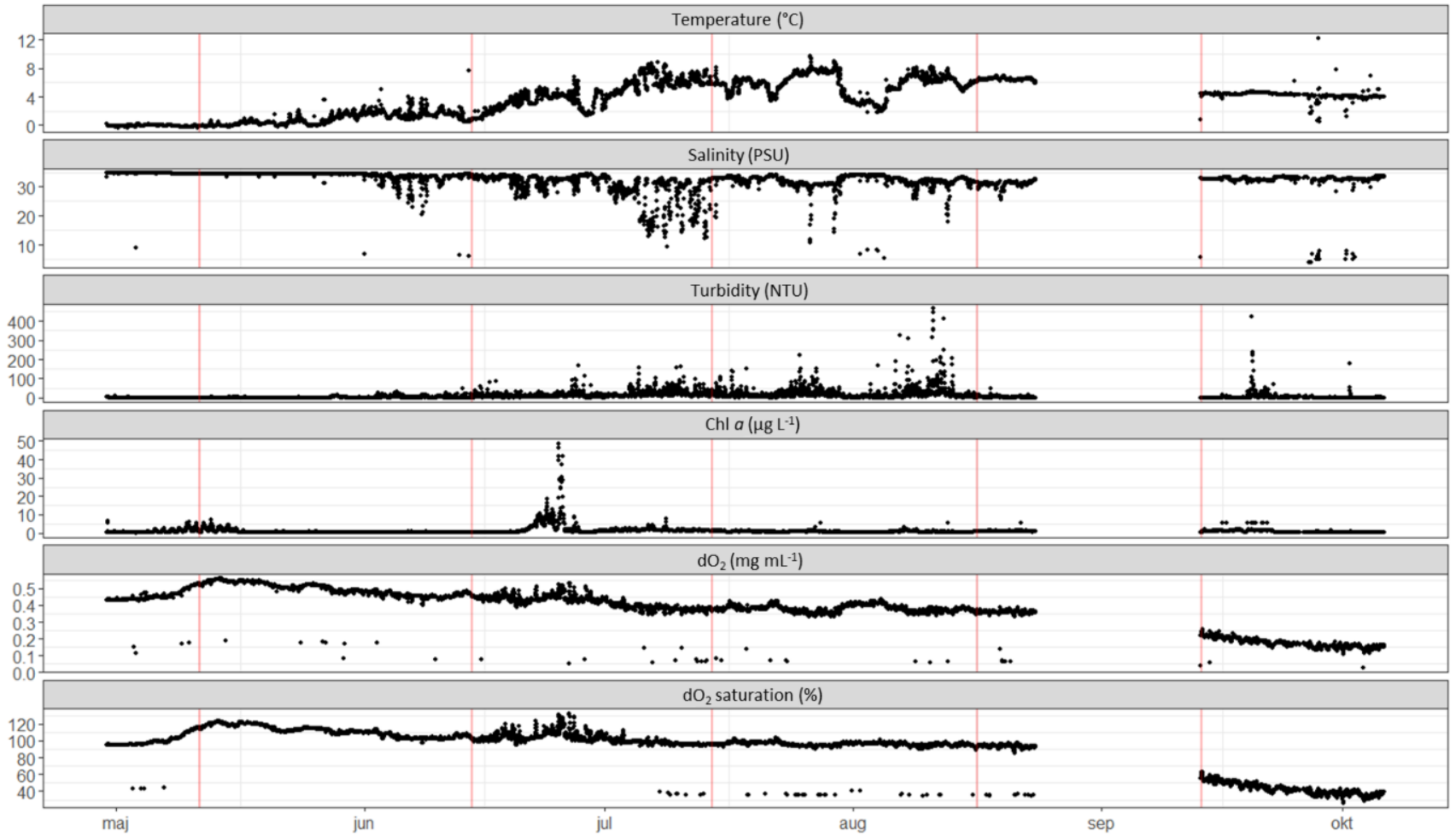


**Fig. A3:** Fjord NIVA buoy sensor data, with sensors sitting at a depth of 2m. Logging interval at every full hour. Data is from the full deployment period of 2021. The missing data in august was due to power failure, which was restored during September sampling. Red lines indicate main campaign samplings. Data is not validated by NIVA.

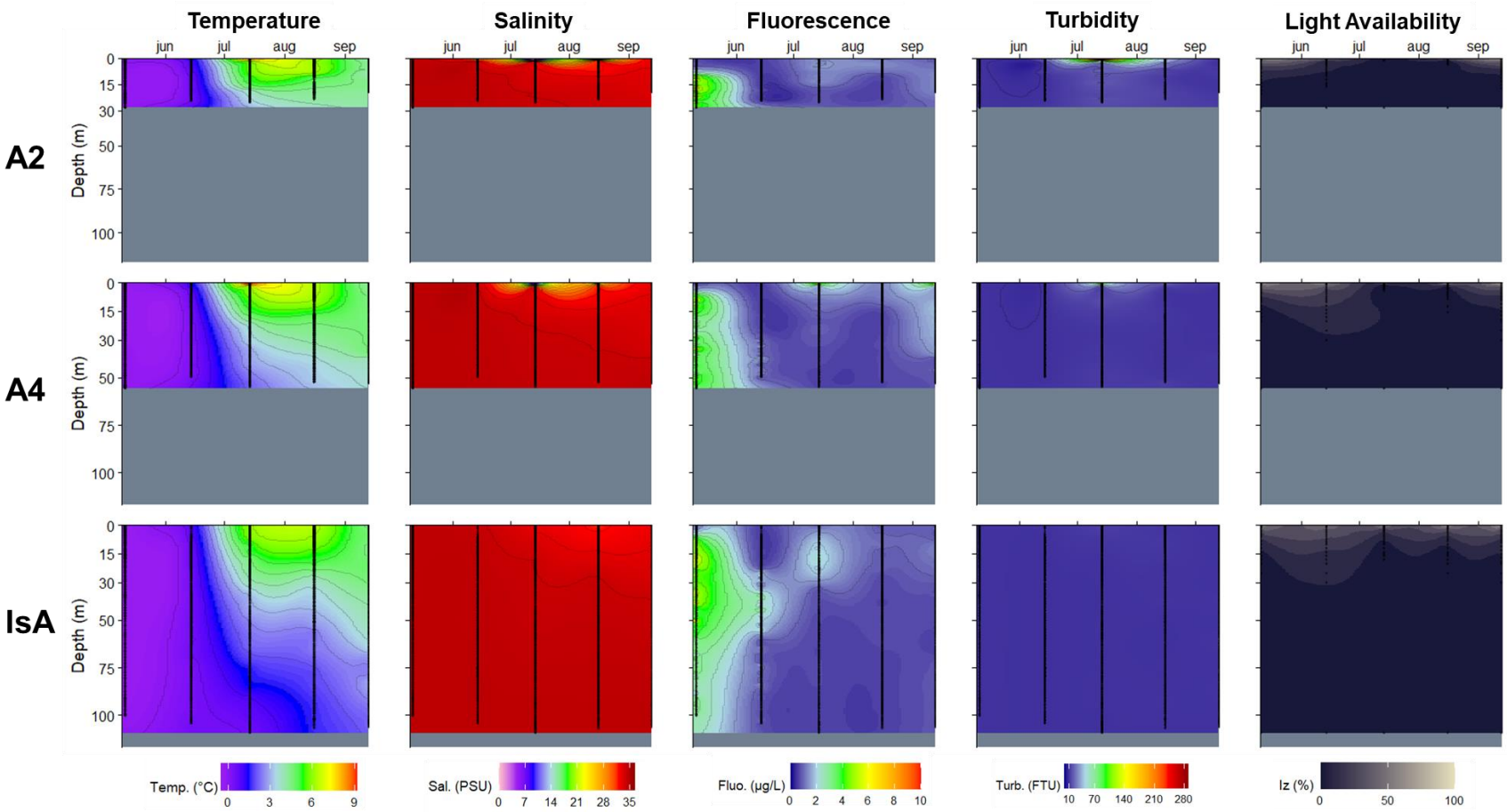


**Fig. A4:** Modelled contour plots based on monthly CTD and LiCor data (black dots) from fjord stations. Top row: A2, mid row: A4, bottom row: IsA. Fluorescence is measured as chlorophyll a fluorescence. Light availability (Iz) is measured in % PAR (µmol photons $m^{-2}s^{-1}$)

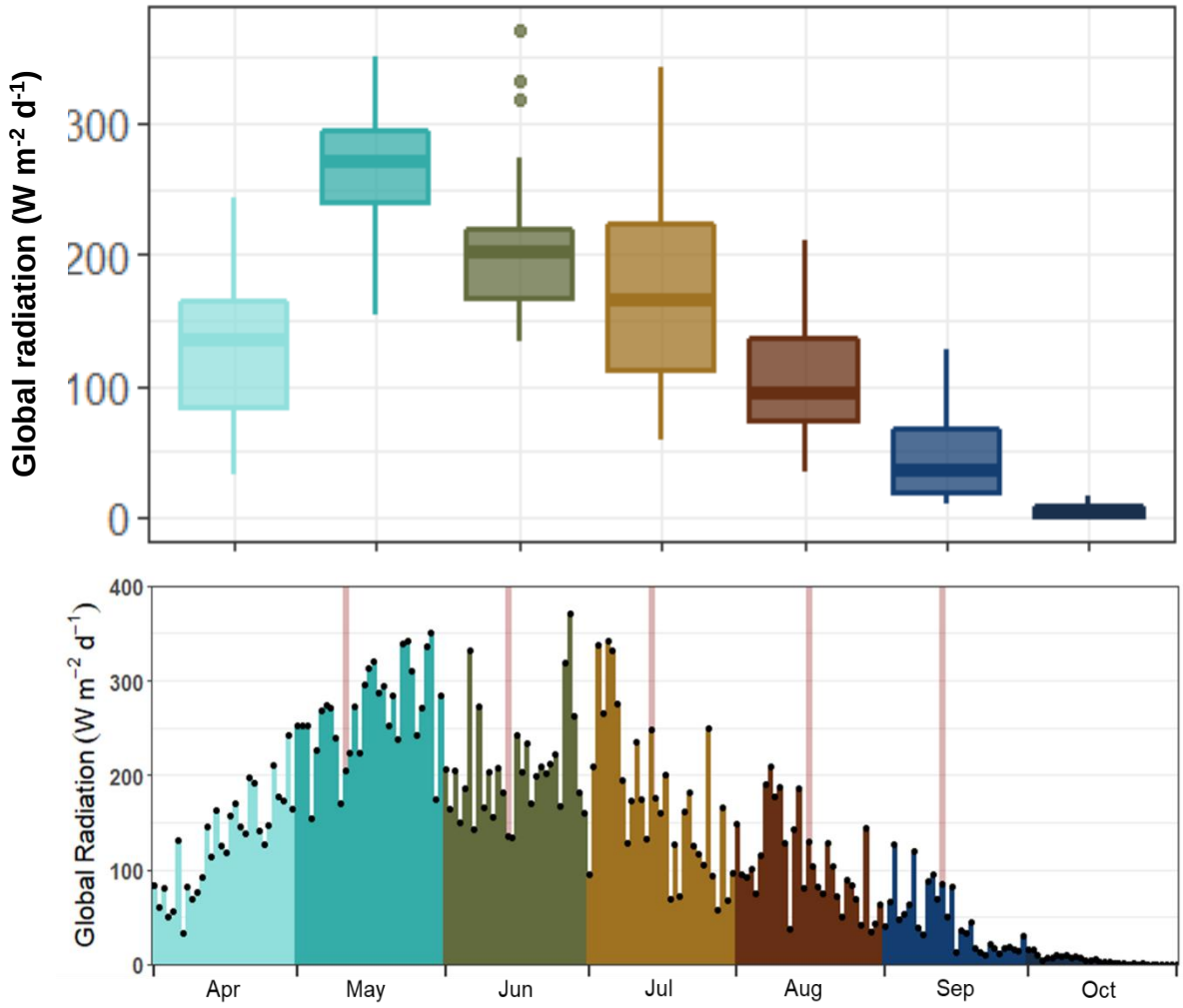


**Fig. A5: Top)** average daily measurements summed up per month as boxplots. **Bottom)** Daily average solar radiation, 1st of May to 31st of November. Red lines indicate sampling days for the main campaign. (*Source: weather station Janssonhaugen Vest (SN99874), Norsk Klimaservicesenter*)

**Table A2**: Data on environmental variables from main campaigns sampling.

| General Info | | | | | Basic Environment | | | Particulate Matter | | | | Dissolved Matter | | | | | Biomass | |
|---|---|---|---|---|---|---|---|---|---|---|---|---|---|---|---|---|---|---|
| Month | Station | Depth | Region | Period | Sal. | Temp. | Turb. | SPM | SPM_inorg. | SPM_Org | SPM_Org | DOC | N_inorg | P_Inorg | SI_Inorg | NH4 | Chl *a* | Phaeopig. |
| | | | | | PSU | °C | NTU | mg/L | mg/L | mg/L | % | µM | µM | µM | µM | µM | µg/L | % |
| May | A2 | 0 | FS | PR-M | 35.3 | 0.0 | 2.1 | 25.3 | 20.7 | 4.6 | 18.2 | 264 | 2.28 | 0.32 | 1.74 | 0.79 | 2.1 | 24.9 |
| May | A2 | 15 | FD | PR-M | 35.6 | -0.2 | 3.1 | 4.3 | 2.1 | 2.2 | 51.2 | 256 | 1.64 | 0.29 | 1.42 | 0.35 | 6.3 | 24.6 |
| May | A4 | 0 | FS | PR-M | 35.4 | -0.3 | 1.6 | 6.0 | 4.5 | 1.5 | 25.0 | 372 | 3.86 | 0.16 | 1.60 | 0.50 | 2.8 | 18.2 |
| May | A4 | 15 | FD | PR-M | 35.4 | -0.3 | 1.6 | 28.6 | 22.8 | 5.8 | 20.3 | 249 | 2.78 | 0.32 | 1.46 | 0.30 | 8.2 | 11.8 |
| May | IsA | 0 | FS | PR-M | 35.3 | -0.3 | 1.1 | 2.9 | 1.7 | 1.2 | 41.4 | 167 | 1.21 | 0.26 | 1.17 | 0.31 | 4.3 | 18.1 |
| May | IsA | 15 | FD | PR-M | 34.5 | -0.3 | 1.2 | 30.6 | 24.1 | 6.5 | 21.2 | 213 | 2.07 | 0.29 | 1.32 | 0.43 | 5.6 | 19.3 |
| May | IsA | 50 | FD | PR-M | 35.4 | -0.3 | 0.9 | 2.0 | 1.0 | 1.0 | 50.0 | 254 | 3.14 | 0.32 | 1.25 | 0.43 | 7.6 | 18.8 |
| June | A2 | 0 | FS | M | 34.7 | 1.2 | 5.6 | 34.1 | 28.7 | 5.4 | 15.8 | 222 | 1.29 | 0.26 | 4.27 | 1.64 | 0.1 | 50.7 |
| June | A2 | 15 | FD | M | 33.1 | 0.5 | 2.1 | 15.0 | NA | NA | NA | 222 | 1.29 | 0.26 | 1.53 | 1.86 | 0.1 | 42.6 |
| June | A4 | 0 | FS | M | 35.7 | 1.1 | 1.2 | 21.5 | 17.7 | 3.8 | 17.9 | 219 | 1.00 | 0.26 | 1.53 | 1.64 | 0.1 | 46.8 |
| June | A4 | 15 | FD | M | 34.7 | 0.3 | 1.0 | 15.1 | NA | NA | NA | 189 | 1.21 | 0.26 | 1.00 | 1.29 | 0.1 | 38.4 |
| June | IsA | 0 | FS | M | 35.9 | 0.8 | 1.0 | 14.4 | 12.1 | 2.4 | 16.3 | 103 | 1.00 | 0.26 | 1.14 | 1.43 | 0.2 | 33.2 |
| June | IsA | 15 | FD | M | 36.0 | 0.5 | 0.6 | 15.0 | NA | NA | NA | 100 | 1.14 | 0.29 | 0.89 | 2.07 | 0.1 | 36.7 |
| June | IsA | 50 | FD | M | 36.0 | 0.4 | 0.6 | 22.6 | 16.8 | 5.8 | 25.5 | 100 | 1.36 | 0.29 | 0.93 | 1.78 | 2.0 | 24.7 |
| June | River | 0 | R | M | 0.2 | NA | 40.5 | 52.9 | 50.5 | 2.4 | 4.5 | 107 | 6.00 | 0.03 | 67.29 | 1.07 | 0.1 | 51.2 |
| July | A2 | 0 | FS | M | 2.7 | 8.0 | 193.7 | 135.8 | 129.4 | 6.4 | 4.7 | 23 | 2.57 | 0.06 | 40.95 | 0.32 | 3.3 | 28.6 |
| July | A2 | 15 | FD | M | 34.3 | 4.8 | 9.7 | 26.1 | 22.6 | 3.6 | 13.6 | 91 | 0.07 | 0.19 | 2.28 | 0.64 | 0.7 | 35.8 |
| July | A4 | 0 | FS | M | 8.7 | 8.7 | 76.2 | 70.0 | 64.0 | 6.0 | 8.6 | 46 | 0.57 | 0.10 | 35.25 | 0.17 | 10.0 | 32.4 |
| July | A4 | 15 | FD | M | 34.7 | 4.9 | 4.5 | 22.8 | 18.7 | 4.1 | 17.8 | 84 | 0.07 | 0.23 | 2.07 | 0.79 | 0.4 | 34.2 |
| July | IsA | 0 | FS | M | 16.6 | 5.8 | 2.5 | 27.9 | 22.6 | 5.3 | 19.0 | 199 | 0.04 | 0.16 | 3.28 | 0.24 | 0.8 | 33.6 |
| July | IsA | 15 | FD | M | 34.1 | 5.0 | 3.5 | 28.2 | 23.1 | 5.1 | 18.1 | 217 | 0.07 | 0.19 | 1.78 | 0.33 | 1.3 | 25.2 |
| July | IsA | 50 | FD | M | 35.1 | 2.5 | 2.2 | 20.6 | 17.9 | 2.7 | 13.3 | 206 | 0.43 | 0.26 | 1.39 | 1.36 | NA | NA |
| July | River | 0 | R | M | 0.3 | 9.0 | 379.0 | 329.8 | 314.4 | 15.4 | 4.7 | 281 | 5.14 | 0.06 | 55.90 | 0.57 | 0.5 | 53.4 |
| August | A2 | 0 | FS | M | 16.3 | 6.4 | 12.7 | 22.0 | 19.3 | 2.7 | 12.4 | 76 | 4.85 | 0.10 | 33.11 | 1.07 | 1.4 | 21.0 |
| August | A2 | 15 | FD | M | 34.5 | 4.7 | 4.3 | 25.6 | 21.5 | 4.1 | 15.9 | 172 | 0.43 | 0.23 | 3.06 | 1.21 | 0.2 | 40.2 |
| August | A4 | 0 | FS | M | 24.4 | 6.2 | 14.6 | 28.8 | 25.1 | 3.7 | 12.8 | 117 | 2.78 | 0.16 | 18.51 | 1.00 | 0.7 | 17.6 |
| August | A4 | 15 | FD | M | 33.5 | 5.2 | 2.0 | 28.9 | 24.4 | 4.5 | 15.6 | 142 | 0.43 | 0.23 | 2.96 | 1.07 | 0.2 | 37.2 |
| August | IsA | 0 | FS | M | 33.4 | 6.1 | 1.6 | 19.9 | 16.3 | 3.6 | 18.1 | 128 | 0.14 | 0.16 | 3.45 | 0.36 | 0.7 | 27.9 |
| August | IsA | 15 | FD | M | 33.6 | 5.2 | 1.8 | 20.4 | 16.5 | 3.9 | 19.0 | 137 | 0.36 | 0.19 | 3.13 | 0.86 | 0.5 | 35.9 |
| August | IsA | 50 | FD | M | 34.9 | 2.7 | 1.1 | 20.5 | 17.7 | 2.8 | 13.7 | 137 | 1.00 | 0.32 | 2.24 | 1.64 | 0.2 | 46.9 |
| August | River | 0 | R | M | 0.2 | 7.0 | 258.0 | 187.2 | 178.0 | 9.2 | 4.9 | 36 | 11.42 | 0.06 | 80.11 | 0.93 | 0.4 | 46.9 |
| September | A2 | 0 | FS | Po-M | 34.5 | 4.1 | 2.0 | 18.9 | 16.3 | 2.6 | 13.7 | 97 | 0.29 | 0.16 | 2.14 | 0.57 | 0.8 | 26.7 |
| September | A2 | 15 | FD | Po-M | 34.9 | 4.4 | 1.5 | 14.3 | 12.2 | 2.1 | 14.7 | 95 | 0.29 | 0.19 | 1.74 | 0.79 | 0.8 | 27.7 |
| September | A4 | 0 | FS | Po-M | 34.3 | 4.3 | 1.6 | 13.7 | 11.4 | 2.3 | 16.8 | 95 | 0.21 | 0.16 | 1.60 | 2.86 | 0.9 | 23.3 |
| September | A4 | 15 | FD | Po-M | 34.7 | 4.5 | 0.8 | 14.1 | 11.8 | 2.3 | 16.4 | 96 | 0.29 | 0.19 | 1.57 | 0.93 | 0.7 | 28.3 |
| September | IsA | 0 | FS | Po-M | 33.7 | 4.4 | 0.7 | 14.0 | 11.9 | 2.1 | 15.0 | 89 | 0.21 | 0.16 | 1.82 | 0.57 | 0.6 | 28.4 |
| September | IsA | 15 | FD | Po-M | 34.3 | 4.4 | 1.1 | 15.9 | 13.5 | 2.5 | 15.4 | 88 | 0.36 | 0.19 | 1.53 | 7.00 | 0.7 | 29.1 |
| September | IsA | 50 | FD | Po-M | 35.3 | 3.8 | 1.0 | 14.5 | 12.4 | 2.1 | 14.5 | 94 | 1.07 | 0.32 | 2.35 | 2.00 | 0.2 | 39.7 |
| September | River | 0 | R | Po-M | 0.7 | 0.0 | 43.7 | 41.6 | 38.6 | 3.0 | 7.2 | 51 | 11.78 | 0.06 | 99.70 | 1.00 | 0.2 | 59.9 |

**Table A3:** Data from *in vitro* incubations with biomass (Chl a) for reference.

| General Info | | | | | Basic Environment | | | Bacterial Production | | Biomass | Primary Production | | | Balance |
|---|---|---|---|---|---|---|---|---|---|---|---|---|---|---|
| Month | Station | Depth | Region | Period | Sal. PSU | Temp. °C | Turb. NTU | BP µgC/L/d | SD (BP) µgC/L/d | Chl *a* µg/L | NPP µgC/L/d | SD (NPP) µgC/L/d | NPP_biomass µgC/L/d /Chl *a* | NPP:BP |
| May | A2 | 0 | FS | PR-M | 35.3 | 0.0 | 2.1 | 0.14 | 0.09 | 2.13 | NA | NA | NA | NA |
| May | A2 | 15 | FD | PR-M | 35.6 | -0.2 | 3.1 | 0.17 | 0.04 | 6.30 | NA | NA | NA | NA |
| May | A4 | 0 | FS | PR-M | 35.4 | -0.3 | 1.6 | 0.15 | 0.04 | 2.78 | NA | NA | NA | NA |
| May | A4 | 15 | FD | PR-M | 35.4 | -0.3 | 1.6 | 0.23 | 0.04 | 8.15 | NA | NA | NA | NA |
| May | IsA | 0 | FS | PR-M | 35.3 | -0.3 | 1.1 | 0.03 | 0.09 | 4.27 | NA | NA | NA | NA |
| May | IsA | 15 | FD | PR-M | 34.5 | -0.3 | 1.2 | 0.09 | 0.06 | 5.58 | NA | NA | NA | NA |
| May | IsA | 50 | FD | PR-M | 35.4 | -0.3 | 0.9 | 0.11 | 0.08 | 7.57 | NA | NA | NA | NA |
| June | A2 | 0 | FS | M | 34.7 | 1.2 | 5.6 | 0.06 | 0.03 | 0.07 | 0.11 | 0.05 | 1.60 | 1.80 |
| June | A2 | 15 | FD | M | 33.1 | 0.5 | 2.1 | 0.09 | 0.07 | 0.09 | 0.28 | 0.07 | 3.18 | 2.93 |
| June | A4 | 0 | FS | M | 35.7 | 1.1 | 1.2 | 0.04 | 0.01 | 0.07 | 0.15 | 0.05 | 2.01 | 3.35 |
| June | A4 | 15 | FD | M | 34.7 | 0.3 | 1.0 | 0.05 | 0.07 | 0.09 | 0.25 | 0.05 | 2.75 | 5.14 |
| June | IsA | 0 | FS | M | 35.9 | 0.8 | 1.0 | 0.06 | 0.18 | 0.16 | 0.32 | 0.14 | 1.96 | 5.54 |
| June | IsA | 15 | FD | M | 36.0 | 0.5 | 0.6 | 0.01 | NA | 0.13 | 0.33 | 0.08 | 2.59 | 50.33 |
| June | IsA | 50 | FD | M | 36.0 | 0.4 | 0.6 | 0.03 | 0.00 | 1.97 | 11.07 | 0.43 | 5.61 | 408.17 |
| June | River | 0 | R | M | 0.2 | NA | 40.5 | 0.30 | 0.15 | 0.09 | 0.46 | 0.08 | 5.05 | 1.55 |
| July | A2 | 0 | FS | M | 2.7 | 8.0 | 193.7 | 0.29 | 0.48 | 3.30 | 38.99 | 5.43 | 11.81 | 132.74 |
| July | A2 | 15 | FD | M | 34.3 | 4.8 | 9.7 | 0.12 | 0.11 | 0.69 | 2.04 | 0.93 | 2.97 | 17.26 |
| July | A4 | 0 | FS | M | 8.7 | 8.7 | 76.2 | 0.18 | 0.13 | 10.01 | 299.42 | 50.72 | 29.90 | 1692.54 |
| July | A4 | 15 | FD | M | 34.7 | 4.9 | 4.5 | 0.20 | 0.06 | 0.39 | 2.90 | 0.95 | 7.48 | 14.55 |
| July | IsA | 0 | FS | M | 16.6 | 5.8 | 2.5 | 0.16 | 0.05 | 0.77 | 0.91 | 0.19 | 1.18 | 5.54 |
| July | IsA | 15 | FD | M | 34.1 | 5.0 | 3.5 | 0.01 | 0.07 | 1.26 | 2.35 | 0.22 | 1.87 | 323.92 |
| July | IsA | 50 | FD | M | 35.1 | 2.5 | 2.2 | 0.11 | 0.09 | NA | 0.98 | 0.19 | NA | 8.67 |
| July | River | 0 | R | M | 0.3 | 9.0 | 379.0 | 0.29 | 0.27 | 0.48 | 1.12 | 0.26 | 2.31 | 3.90 |
| August | A2 | 0 | FS | M | 16.3 | 6.4 | 12.7 | 0.01 | 0.06 | 1.40 | 19.81 | 1.13 | 14.12 | 2810.05 |
| August | A2 | 15 | FD | M | 34.5 | 4.7 | 4.3 | 0.09 | 0.05 | 0.21 | 1.22 | 0.36 | 5.66 | 13.32 |
| August | A4 | 0 | FS | M | 24.4 | 6.2 | 14.6 | 0.01 | 0.10 | 0.74 | 11.24 | 3.22 | 15.27 | 1072.94 |
| August | A4 | 15 | FD | M | 33.5 | 5.2 | 2.0 | 0.10 | 0.05 | 0.24 | 1.24 | 0.27 | 5.11 | 12.27 |
| August | IsA | 0 | FS | M | 33.4 | 6.1 | 1.6 | 0.06 | 0.16 | 0.69 | 2.67 | 1.06 | 3.88 | 47.20 |
| August | IsA | 15 | FD | M | 33.6 | 5.2 | 1.8 | 0.14 | 0.07 | 0.46 | 1.23 | 0.32 | 2.70 | 8.53 |
| August | IsA | 50 | FD | M | 34.9 | 2.7 | 1.1 | 0.07 | 0.04 | 0.21 | 0.38 | 0.05 | 1.81 | 5.24 |
| August | River | 0 | R | M | 0.2 | 7.0 | 258.0 | 0.52 | 0.23 | 0.39 | 0.99 | 0.08 | 2.54 | 1.88 |
| September | A2 | 0 | FS | Po-M | 34.5 | 4.1 | 2.0 | 1.15 | 0.09 | 0.77 | 3.33 | 0.27 | 4.34 | 2.89 |
| September | A2 | 15 | FD | Po-M | 34.9 | 4.4 | 1.5 | 0.60 | 0.20 | 0.78 | 4.22 | 0.59 | 5.40 | 7.04 |
| September | A4 | 0 | FS | Po-M | 34.3 | 4.3 | 1.6 | 0.79 | 0.14 | 0.88 | 4.08 | 0.39 | 4.62 | 5.18 |
| September | A4 | 15 | FD | Po-M | 34.7 | 4.5 | 0.8 | 0.48 | 0.17 | 0.74 | 4.49 | 0.62 | 6.09 | 9.30 |
| September | IsA | 0 | FS | Po-M | 33.7 | 4.4 | 0.7 | 0.61 | 0.16 | 0.60 | 2.46 | 0.24 | 4.07 | 4.02 |
| September | IsA | 15 | FD | Po-M | 34.3 | 4.4 | 1.1 | 0.64 | 0.18 | 0.70 | 3.34 | 0.39 | 4.75 | 5.18 |
| September | IsA | 50 | FD | Po-M | 35.3 | 3.8 | 1.0 | 0.16 | 0.08 | 0.18 | 1.26 | 0.17 | 7.21 | 8.14 |
| September | River | 0 | R | Po-M | 0.7 | 0.0 | 43.7 | 0.26 | 0.10 | 0.15 | 0.18 | 0.05 | 1.19 | 0.70 |

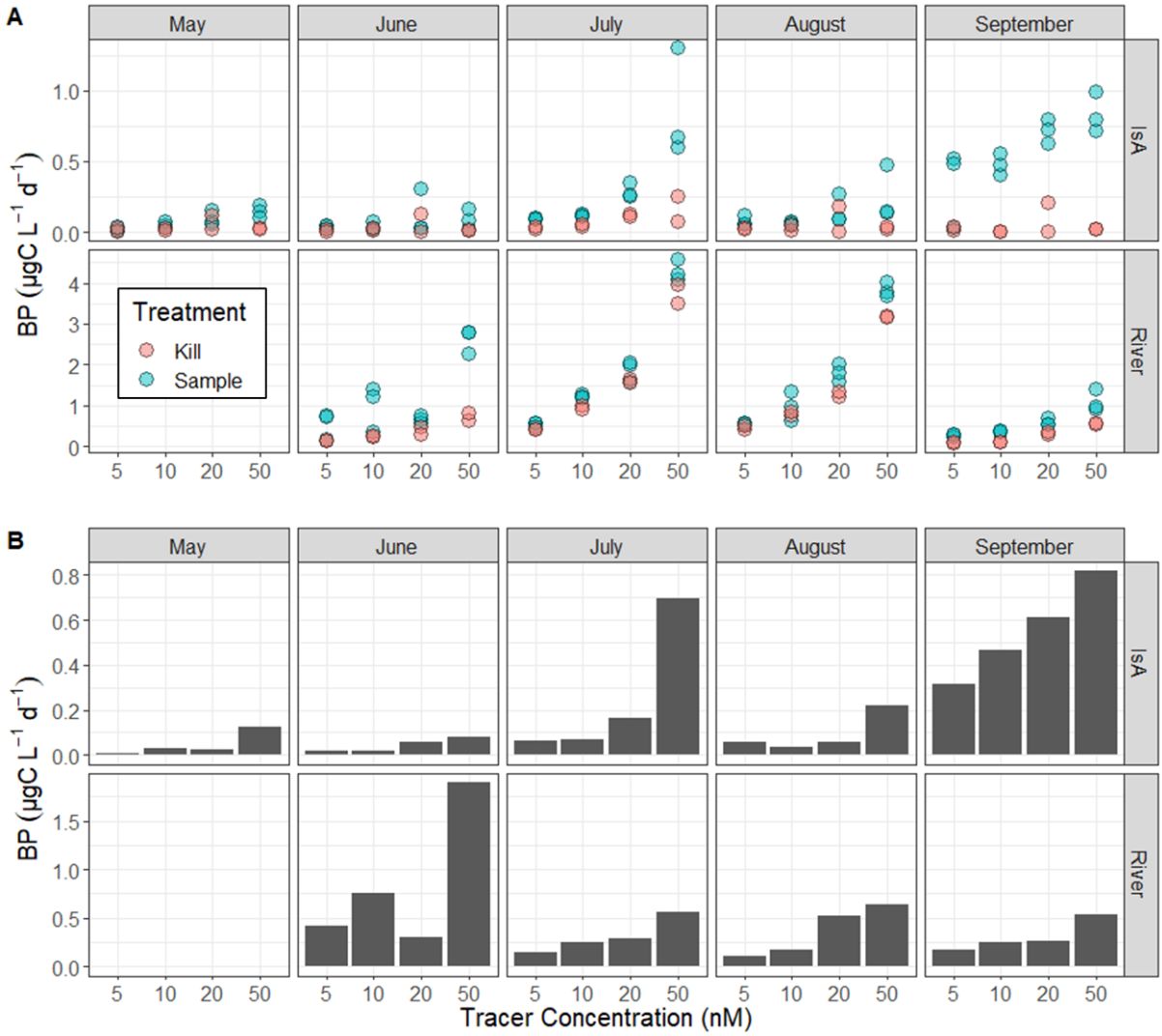


**Fig. A6:** Saturation experiments from BP incubations. **A)** Live sample (Sample) and kill control (kill) measurements, showing the grouping of the datapoints. The experimental concentration (20nM) shows that the samples are not saturated at this concentration. The differences in kill control values between IsA and River indicates increased binding of tracer to sediments in the River samples. Since kill controls also increase with saturation, I see that binding potential is relative rather than constant. **B)** The final uptake (Kill control average subtracted from live sample average).

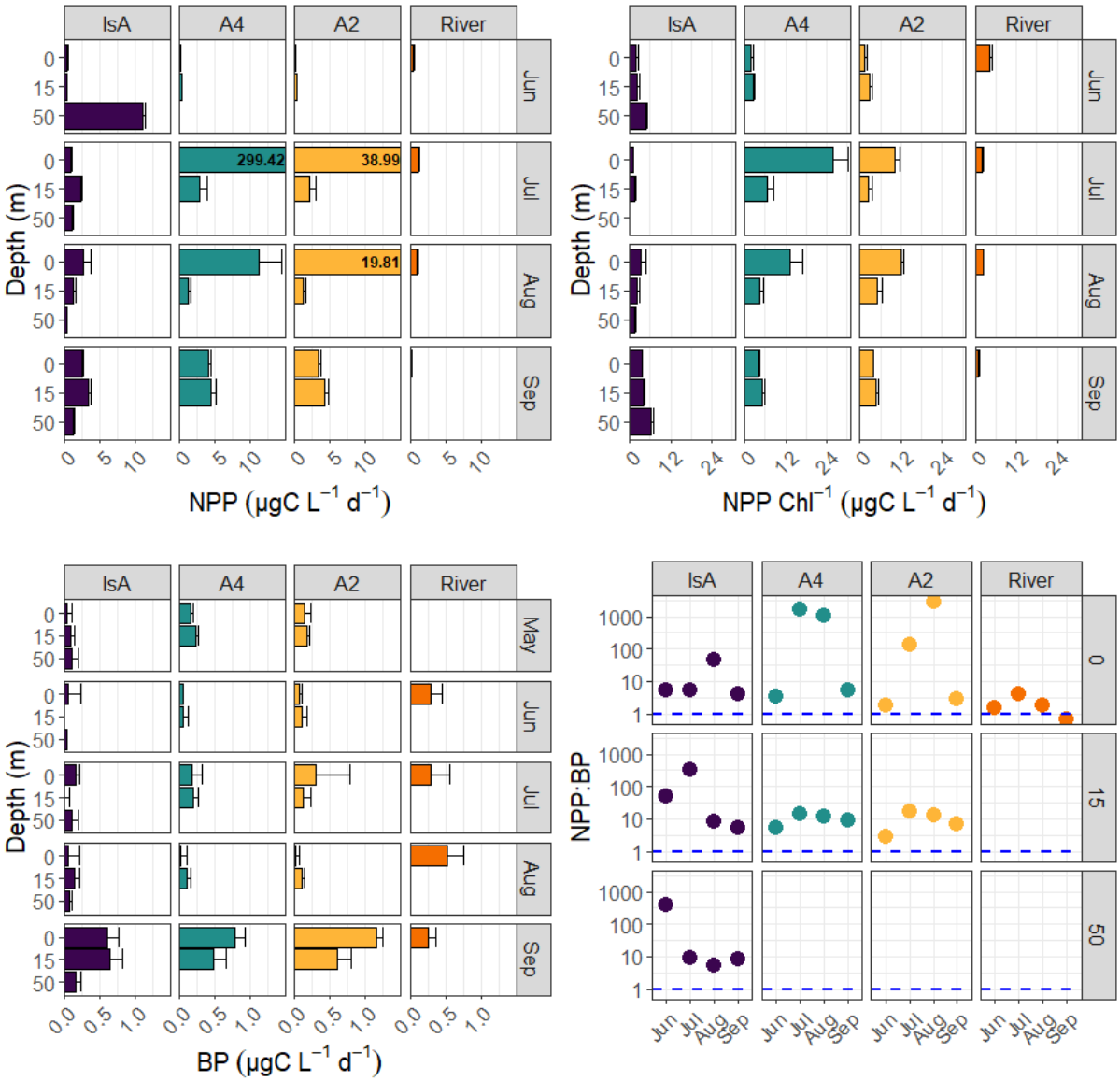


**Fig. A7: A)** NPP across depths and times. Numbers insede columns are for measurements where NPP > 15. **B)** Bomass specific NPP across depths and times. **C)** BP across depths and times. **D)** Ratio of NPP to BP across depth and times. Notice different x-axis scales on A-C.

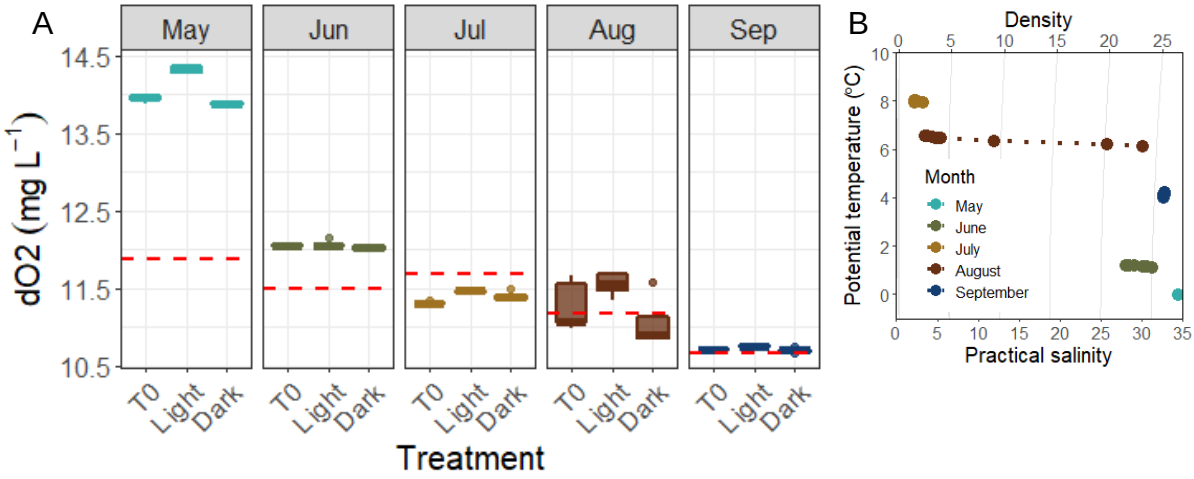


**Figure A8: A)** Dissolved oxygen measured from in situ incubations. Each box consists of five data points. Red dashed lines indicate 100% saturation based on temperature and salinity based on Garcia & Gordon, 1992, **B)** T/S plot of incubated water, clearly showing stratified water sampled in august.

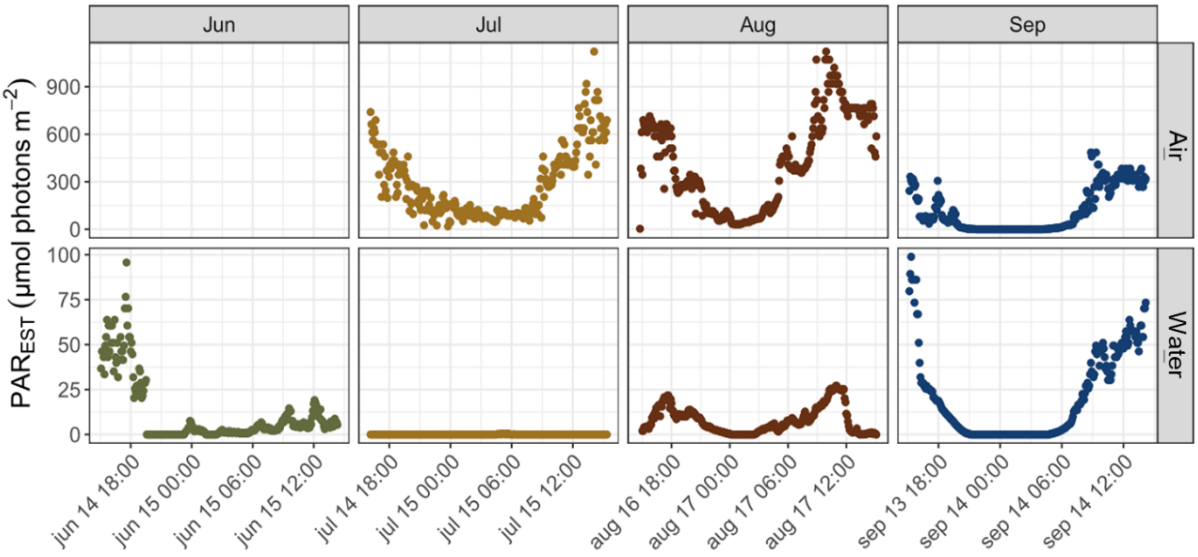


**Figure A9:** Light data from HOBO loggers during incubation for metabolic balance. **Top:** in Air sensor, **Bottom:** on-incubation rig sensor (Water). PAR estimated based on Thimijan & Heins 1983, (conversion value from LUX to PAR = 54). Notice different y-scales.

# Winkler Titration Protocol

*Translated from Falck, 2007 (personal protocol), with slight modifications for using the analysis on incubated samples, rather than freshly collected (relates to fixation step)*

**Preparation of stock solutions (all stored dark at room temperature):**
$MnCl_2$ solution: Dissolve 200g $MnCl_2 \cdot 4H_2O$ in 500ml DI water. Add 2ml conc. HCl for conservation.
NaOH + KI solution: Dissolve 180g NaOH in ~300ml DI water. Add 50ml of a KI solution. Dilute to a final concentration of 500ml using DI.
HCl solution: 3 parts conc. HCl to 1 part DI water (75% solution).
$Na_2S_2O_3xH_2O$: Use a Titrisol® volumetric solution for 1000 ml, $c(Na_2S_2O_3) = 0.1$ mol/l (0.1 N). Prepare a 1000ml solution using the manufacturers guideline. Dilute the stock with DI to a final volume of 5000ml.
$KH(IO_3)_2$: Dissolve 1.2998g $KH(IO_3)_2$ in 1000ml of water.

**Sample analysis**

- **$dO_2$ Fixation (oxidation):** Remove flask stopper (careful not to cause air mixing) and add 1ml $MnCl_2$ solution, followed by 1ml of NaOH + KI solution. Place stopper back and let it settle by gravity, letting excess displaced sample water (2ml) flow out. Shake bottle well for 1min. Wrap stopper and neck in parafilm and let the sample precipitate overnight, dark, at room temperature.
- **Reduction using acid:** Remove the parafilm and the stopper. Extract 10-20ml sampled water (when using ~100ml bottles) from just below the surface using a syringe. Be careful not to remove any precipitate. Add 2ml of 75% HCl solution. Add a magnetic stir-bar and place the sample on a stir plate.
- **Titration:** Add the auto-dispenser tip for the thiosulfate solution below the surface of the sample, making sure no bubbles are in the tubing (flush prior to titration). Add thiosulfate until the sample is bright yellow. Add ~0.5ml of starch indicator solution using a syringe. Carefully continue the titration, lowering the dispensing rate until the solution turns clear (one drop at the end). Note down the titration volume.

  Colour steps: Orange → yellow → green/black (after indicator addition) → dark purple → magenta → slight violet → clear

**Calibration test (done within 48h of sample analysis):**

- Dissolve 2g KI (accuracy of 0.0001g) in ~150-20ml DI water. Add 2ml of 75% HCl solution.
- Shake $KH(IO_3)_2$ well and add exactly 15ml of the $KH(IO_3)_2$ solution using a dedicated 15ml volumetric glass pipette
- Titrate using $Na_2S_2O_3xH_2O$ solution following the titration step in the sample analysis.
- 3 tests are conducted and the average titrated volume of the closest 2-3 (error acceptance of 2%) is used to calculate the calibration factor F, as $F = 3358.80 / V_{titrated}$

*“I have thought of a nice ending for it: and he lived happily ever after to the end of his days.”*

***Bilbo Baggins***